Mo isotope variations in molybdenites at single-crystal, ore deposit, and global scales: Implications for Mo source fluid, transport, fractionation mechanisms, and molybdenite mineralization

by

Alysa Segato

A thesis
presented to the University of Waterloo
in fulfilment of the
thesis requirement for the degree of
Master of Science
in
Earth Sciences

Waterloo, Ontario, Canada, 2018

Authors Declaration:

I hereby declare that I am the sole author of this thesis. This is a true copy of the thesis, including any required final revisions, as accepted by my examiners.

I understand that my thesis may be made electronically available to the public.

Abstract

In this study, the Mo isotopic composition (δ^{98}Mo) of molybdenite from 29 hand samples from various ore deposit types was analyzed. This data was compiled with data from the literature and all data (n = 420) was reported relative to international standard NIST SRM 3134 = 0.25‰ for comparison. Using this larger dataset, the range of δ^{98}Mo in porphyry deposits is greater, and it was determined that the δ^{98}Mo of molybdenite cannot be used to fingerprint the age of a deposit or the deposit type. Higher temperature deposit types (granite = 0.10‰, n = 25, 2SD = 1.03‰; porphyry = 0.20‰, n = 243, 2SD = 1.01‰; skarn = 0.36‰, n = 42, 2SD = 0.70‰) have generally lower δ^{98}Mo than lower temperature deposit types (pegmatites = 0.48‰, n = 80, 2SD = 1.05‰; perigranitic = 0.75‰, n = 10, 2SD = 1.12‰; greisen = 0.79‰, n = 6, 2SD = 1.93‰), consistent with findings from earlier molybdenite δ^{98}Mo compilations. Therefore, temperature can be considered as one control on Mo isotopic composition. The average δ^{98}Mo of molybdenite is 0.37‰ (n = 479; 2SD = 1.30‰), which is similar to a recently estimated maximum δ^{98}Mo for the upper continental crust of 0.40‰ and likely represents a maximum for the average bulk continental crust δ^{98}Mo.

The δ^{98}Mo of the molybdenite samples from various deposits was compared with Re concentrations and S isotope compositions (δ^{34}S). Consistent with earlier compilations based on a smaller dataset, an overall negative correlation was found between δ^{98}Mo and Re concentration, which implies that the Mo source fluid is another important control on the Mo isotopic composition. Samples with a high Re concentration and a low δ^{98}Mo suggest a mantle-derived source fluid whereas samples with high δ^{98}Mo (>1.5‰) had uniformly low Re concentrations that suggests a crustal-sourced fluid. The relationship between δ^{98}Mo and δ^{34}S was also investigated as a positive correlation between these isotope systems in ore-forming systems with limited S and Mo availability would indicate Rayleigh distillation as a main mechanism of Mo isotope fractionation. No such relationship was observed, indicating that other fractionation mechanisms such as redox changes are important.

To test the hypothesis of small scale zoning, molybdenite grains were cut parallel and/or across cleavage planes and analyzed. The variation observed at the single-crystal scale was within the long-term reproducibility of Mo isotope analyses (~0.1‰; 2SD = 0.2‰). Several hand samples were collected from the Berg epithermal-porphyry deposit (British Columbia) and the Hemlo disseminated Au deposit (Ontario) to quantify Mo isotopic variation at the deposit scale. At the Berg deposit, modest variation in δ^{98}Mo was observed (~1‰). At the

Hemlo deposit, Mo isotope fractionation exceeded 5‰, which is greater than the range previously reported for any other deposit type and indicates significant Mo remobilization. The mineral assemblages, trace element composition, and the abundance of pyrite in the Hemlo hand samples do not correlate with the Mo isotopic composition of bulk samples. The observed Mo isotope fractionation is likely due to alteration of the host rocks by S-rich reducing fluids.

Acknowledgements

My supervisor Dr. Brian Kendall is thanked immensely for his patience, mentorship, and support over the course of this project. Dr. Jacob Hanley is thanked for supplying the samples used in this project and for his involvement as a committee member. Committee member Dr. Chris Yakymchuk is also thanked for his comments and involvement in the project. Dr. Gwyneth Gordon and Dr. Stephen Romaniello of the W.M. Keck Foundation Laboratory for Environmental Biogeochemistry at Arizona State University are thanked immensely for their assistance in isotopic analysis. Dr. Shuhuan Li is thanked for her assistance with the X-ray diffraction analysis. Liyan Xing is thanked for her help with digesting and purifying some samples in the Metal Isotope Geochemistry Laboratory at the University of Waterloo. This research was financially supported by a NSERC Discovery Grant to Dr. Brian Kendall.

Finally, I would like to thank my parents, family, and especially my husband Valentino. Your support over the past several years has propelled me to achieve not only this goal but so much more than I thought possible.

.

Table of Contents

List of Figures

List of Tables

Chapter 1: Introduction

1.1 Main Research Goal

Metal isotope systems are rapidly emerging as useful tools for constraining processes during ore mineralization and for ore exploration. Determining the metal isotope composition is a unique geochemical tool because it allows for direct study of the ore metal of interest. Early successes in the study of some metal isotope systems, most notably Cu isotopes in porphyry deposits and Zn isotopes in various hydrothermal deposits have provided motivation to explore the usefulness of other metal isotope systems. The Mo isotope system is one of the newer systems of interest. Molybdenite (MoS_2) is an ideal mineral for Mo isotope studies because it is roughly 60% molybdenum by weight and in most cases, it is the main Mo ore mineral of interest in porphyry Mo and Cu-Mo deposits and an accessory mineral in many Au deposits. The Mo isotope composition of molybdenite may yield direct information about ore mineralization processes and the internal workings of the ore-forming system. We can also gain new insights into the processes that contribute to Mo cycling within the Earth's surface by taking a closer look at the mechanisms behind Mo isotope fractionation. Studying fractionation mechanisms can also uncover how Mo interacts with different fluids, partitions between melt versus fluid and brine versus vapor, and fractionates at different temperatures and between different chemical species. Ultimately, Mo isotopes have the potential to be refined into a useful geochemical tool, but as yet there are relatively few detailed studies exploring Mo isotope fractionation in ore-forming systems (Hannah et al., 2007; Mathur et al., 2010a; Greber et al., 2011, 2014; Breillat et al., 2016; Shafiei et al., 2015; Wang et al., 2016; Yao et al., 2016). The main goal of this thesis is to further our understanding of Mo isotope cycling in ore deposits and assess the possibility of utilizing Mo isotopes as a geochemical exploration tool.

1.2 Background on Mo Isotopes in Mineralizing Systems

The invention of the multi-collector inductively coupled plasma mass spectrometer (MC-ICP-MS) in the early 1990s (Halliday et al., 1995) provided geochemists with a tool to study isotope fractionation of metals. Before that time, it was mostly the isotope variations of "traditional" light elements (such as hydrogen, carbon, nitrogen, oxygen, and sulfur) that were studied. The low mass of these elements results in a large mass difference between their isotopes. Heavier "non-traditional" elements (such as iron, copper, zinc, molybdenum,

mercury, nickel, and uranium) have a smaller mass difference between their isotopes, and hence isotopic variations of these metals were historically very difficult to measure precisely. Despite the advent of MC-ICP-MS technology more than 20 years ago, the study of Mo isotope fractionation in ore-forming systems is still in its infancy. To date, only a handful of studies pertaining to Mo isotope fractionation in ore deposits have been conducted, including for porphyry systems (Wieser and De Laeter, 2003; Hannah et al., 2007; Klemm et al., 2008; Mathur et al., 2010a; Greber et al., 2011; Song et al., 2011; Greber et al., 2014; Shafiei et al., 2015; Brellait et al., 2016; Wang et al., 2016; Yao et al., 2016).

Molybdenum has seven stable isotopes (each with an abundance of 10-25%) that span a mass range of approximately 8%: ^{92}Mo, ^{94}Mo, ^{95}Mo, ^{96}Mo, ^{97}Mo, ^{98}Mo, and ^{100}Mo (Mayer and Wieser, 2014). The fractionation of Mo isotopes is mass dependent and is known to be highly responsive to changes in redox conditions (Anbar 2004; Kendall et al., 2017). These factors make Mo an ideal candidate for studying geological systems characterized by redox reactions. In most ore deposit studies, Mo isotope data is collected from molybdenite. The Mo isotopic composition of molybdenite (and other geological materials) is reported as per mil (‰) deviations relative to the NIST SRM 3134 standard (set to 0.25‰) using the following delta notation (Nägler et al., 2014):

$$\delta^{98}\mathrm{Mo}_{\,\mathrm{sample}}\,(‰) = 1000 \times [(^{98}\mathrm{Mo}/^{95}\mathrm{Mo})_{\,\mathrm{sample}}/(^{98}\mathrm{Mo}/^{95}\mathrm{Mo})_{\,\mathrm{NIST\ SRM\ 3134}}) - 1] + 0.25$$

The total range of Mo isotope variation in molybdenites is ~4‰, and ranges between –1.37‰ to +2.52‰ relative to NIST SRM 3134 = 0.25‰ (Breillat et al., 2016). Molybdenites from porphyry deposits have the greatest potential for studying the mechanisms behind Mo isotope fractionation because these deposits are the most important source of molybdenum. A variation of 2‰ has been observed in molybdenites from porphyry deposits (Breillat et al., 2016). By comparison, the largest degree of variation (2.6‰) is found in granite and greisen deposits (Breillat et al. 2016).

Preliminary studies have shown that there are several mechanisms that can influence Mo isotope fractionation, but their relative importance in ore-forming systems is still not well understood. The temperature of the deposit can influence Mo isotope partitioning between the melt-fluid and vapour-brine phases (Shafiei et al., 2015). In high temperature deposits (400-600°C), Rayleigh distillation can cause fractionation of Mo isotopes (Hannah et al., 2007). Redox conditions play an important role in fractionation of Mo isotopes, although the

magnitude of isotope fractionation decreases at higher temperature (Greber et al., 2011, 2014; Shafiei et al., 2015). Fluid boiling may cause Mo isotope fractionation between vapour and brine phases (Shafiei et al., 2015). Greber et al. (2014) suggest that during molybdenite crystallization, hydrothermal fluids prefer to retain the heavy Mo isotopes and the light Mo isotopes will be preferentially incorporated in the molybdenite crystals. In addition, Greber et al. (2014) noted that Mo isotope fractionation occurs during fractional crystallization of a magma and during exsolution of a magmatic-hydrothermal fluid, with both processes resulting in an isotopically heavier fluid compared to the source magma. The isotopic composition of the Mo source (i.e., crustal- versus mantle-derived magmas) can also influence the molybdenite δ^{98}Mo signature (Wang et al., 2016).

1.3 Thesis Objectives

Preliminary studies of Mo isotopes in ore deposits have shown great potential and motivate further research to increase the effectiveness of Mo isotopes as a process tracer for mineralizing systems. One goal of this thesis is to build upon the work of Breillat et al. (2016) and infer the major differences in Mo isotope composition between different types of ore deposits using a global suite of molybdenites. This study reports Mo isotope data for 29 hand samples from 14 unique ore deposits. The deposits vary in size, age, climate region, grade, tonnage, temperature of ore deposition, deposit type, late stage alteration, and number of mineralization events. The deposits analyzed in this study include nine porphyry deposits (1 - Moly Hill, Quebec; 2 and 3 - Lake George and Trout Lake, New Brunswick; 4 and 5 - Santo Nino Mine and Childs-Adwinkle Mine, Arizona; 6 - Sach's Mine, NSW, Australia; 7 - Wolfram, Queensland, Australia; 8 - Altenberg, Saxony, Germany; 9 - Strzegom, Poland), two epithermal deposits (Berg and Logan Lake, British Columbia), two greisen deposits (Beura, Ossa Valley, Italy; New Ross, Nova Scotia), and one disseminated gold deposit (Hemlo C Zone, Ontario). The molybdenites were handpicked and have a wide distribution of grain sizes and molybdenite concentrations. The new data produced by this thesis combined with new data measured by Wang et al. (2016) and Yao et al. (2016) will be used to expand on the Mo isotope compilation of Breillat et al. (2016). The compilation includes Mo isotope data from skarn deposits, porphyry-type deposits, iron oxide copper-gold deposits, large epithermal deposits, gold deposits, and carbonate deposits. By re-normalizing the δ^{98}Mo data to the newly defined international standard NIST SRM 3134 = 0.25‰, the compilation can be used to make large scale comparisons, define an overall range of Mo isotope values for

molybdenite, and further constrain the average isotopic composition for crustal Mo. The current suggested maximum Mo isotopic composition for the upper crustal average is 0.40‰ relative to NIST SRM 3134 = 0.25‰ (Willbold and Elliot, 2017). The larger dataset of molybdenites also yielded a similar average (0.29‰ relative to NIST SRM 3134 = 0.25‰) but with 2σ variability exceeding 1‰ (Breillat et al., 2016).

Several studies have shown that significant variability in the Mo isotope composition of molybdenites can occur for specific categories of ore deposits (> 2‰) and even within single deposits (> 1‰), including at the cm-scale (Hannah et al., 2007; Mathur et al., 2010a; Greber et al., 2011, 2014; Shafiei et al., 2015; Breillat et al., 2016). Isotopic variability within single molybdenite crystal grains has not been previously assessed.

Previous studies indicated that Rayleigh distillation may be a mechanism for Mo isotope fractionation (Hannah et al., 2007; Greber et al., 2011; Greber et al., 2014) but further work is still needed. Measuring the degree of covariation between Mo and S isotope compositions in molybdenites from a single deposit represents one test of this hypothesis since molybdenite is roughly 40% S by weight. In an ore-forming system with limited Mo and S availability, the isotopic signatures of both elements should be positively correlated if Rayleigh distillation is the main mechanism of isotope fractionation (Hannah et al., 2007).

By studying trace elements, the depositional environment and mineralization events can be categorized, and geochemical patterns can be identified. The trace element concentration of Re has received the most attention in molybdenites (Mathur et al., 2010a; Wang et al., 2016) because Re^{4+} can substitute for Mo^{4+} in the molybdenite structure (Stein et al., 2001). Mathur et al. (2010a) suggests that there may be a negative correlation between Mo isotopic signature and Re concentration. This negative correlation may be directly related to the source of the mineralizing fluid (Mathur et al., 2010a; Wang et al. 2016). Samples with a crustal source will generally have a higher δ^{98}Mo signature (Wang et al., 2016), but a lower Re concentration (Mao et al., 1999). Samples with a mantle source have a generally lower δ^{98}Mo signature, but a higher Re concentration (Wang et al., 2016). This study will add to the above work and determine how other fractionation processes (e.g., fluid boiling, redox conditions) may affect this relationship.

This project also looks closely at two cases of Mo isotope fractionation within a single deposit. Six samples from different regions of the Eocene epithermal-porphyry deposit in

Berg, British Columbia, have been analyzed in this study. Nine hand samples from the Late Archean disseminated gold deposit in Hemlo, Ontario, were also studied. This type of deposit has not previously been studied using the Mo isotope system.

Looking closely at a single deposit has its advantages. At the epithermal Berg deposit in British Columbia and disseminated gold Hemlo deposit in Ontario, we explore the possibility of identifying distinct isotopic reservoirs like those outlined for Cu isotopes in porphyry deposits by Mathur et al. (2009). We also determine if the Mo isotopic signature increases or decreases moving further away from the source area. If this is the case, Mo isotopes may be used as a vector to find the source region. This is comparable to Zn isotopes in sphalerite, which can be used to trace the origin of hydrothermal deposits by following a trail of progressively lighter Zn isotope compositions back to the source area (Kelley et al., 2009). Song et al. (2011) have shown the potential of Mo isotopes as a tracer of fluid migration. By looking at multiple samples from within a deposit, we can isolate the dominant fractionation mechanisms and determine how the late-stage alteration affects Mo isotopes. Study of other isotope systems such as Cu and Zn indicate low temperature alteration has a more significant impact on the degree of isotope fractionation when compared to high temperature alteration (Rouxel et al., 2004, Braxton and Mathur 2011). Undoubtedly there is still much to be uncovered through the study of Mo isotopes and heavy metal isotopes in general. Future work in this promising field is still needed to further decipher geochemical processes and refine metal isotopes into a useful geochemical exploration tool.

In summary, the specific thesis objectives are:

1. Generate a literature review of existing knowledge on heavy metal stable isotope systems in ore deposits to create a foundation for our study and aid in our understanding of the Mo isotope system. A comprehensive literature review on this topic has not been published.
2. Produce an updated compilation of Mo isotope data from molybdenites that can be used to test the hypothesis by Mathur et al. (2010a) and Breillat et al. (2016) that some types of ore deposits have a Mo isotope signature distinctive from other types of ore deposits and assess temperature as a control on Mo isotope fractionation.
3. Determine if Mo isotopic variability occurs at the single grain scale in molybdenite.
4. Test the hypotheses that positive correlations occur between Mo and S isotope compositions (expected in the case of Rayleigh distillation), and that negative

correlations occur between Mo isotope compositions and Re concentrations in molybdenites (expected if the Mo source is an important controlling factor).

5. Examine within-deposit Mo isotopic variations in the Berg epithermal-porphyry deposit and the Hemlo disseminated gold deposit, with the goal of determining the effect of alteration, inferring causes of Mo isotope variation, and evaluating spatial trends.

1.4 Organization of the Thesis

This thesis began with this introductory chapter outlining the motivation for this study and the research objectives. Chapter 2 is a literature review of heavy metal stable isotopes in ore deposits. This chapter fulfills objective 1 and provides a strong foundational framework for causes of metal isotope fractionation in mineralizing systems, which will help guide interpretation of the Mo isotope data reported in chapter 3. Chapter 3 will feature new data collected during this study and addresses objectives 2-5. Chapter 4 concludes the thesis and will summarize the findings of this study and outline directions for future work.

Chapter 2: Heavy Metal Stable Isotope Geochemistry Literature Review

2.1 Introduction

As early as the 1940s, studies of ore deposit geology utilized stable isotope geochemistry as an important research tool. Until recently, stable isotope geochemistry in ore deposits focused on the "traditional" light elements, namely hydrogen, carbon, nitrogen, oxygen, and sulfur (Thode, 1991). Study of heavy metals such as copper, zinc, and iron historically posed a challenge due to their high mass, which resulted in a small mass difference between isotopes. The low mass of “traditional” elements and the large mass difference between isotopes, made it relatively easier to measure their isotopic composition and explore isotope fractionation and cycling in nature. Thanks to improvements in analytical methods, especially the introduction of multi-collector inductively coupled plasma mass spectrometers (MC-ICP-MS) in the 1990s, we now have the necessary tools to study "non-traditional" heavy element isotope fractionation (Halliday et al., 2000).

Because the field of heavy metal isotope geochemistry is relatively young, its application to ore geology is still actively being explored. In recent years, ore deposit geochemists expanded their study of isotopes to include heavy metals and metalloids such as zinc, iron, uranium, molybdenum, selenium, and copper. These and other non-traditional elements are depicted in Figure 1. Studying heavy metal isotope fractionation has clear advantages with respect to understanding the processes contributing to ore formation. Compared with light stable isotopes, heavy metal isotopes can provide more direct information about ore genesis because isotope data is collected for the metal(s) of economic importance. Insight can also be gained on the processes contributing to metal cycling within the Earth’s surface by taking a closer look at the mechanisms behind isotope fractionation (Mason et al., 2005; Hannah et al., 2007; Mathur et al., 2009). Key mechanisms include oxidation and reduction of metals, precipitation of ore minerals, fluid boiling, magmatic evolution and fluid exsolution, and Rayleigh distillation (Hannah et al., 2007; Kelly et al., 2009; Mathur et al., 2009; Greber et al., 2011; 2014; Uvarova et al., 2014). Spatiotemporal variations in metal isotopic compositions can be used to identify trends and patterns within the deposit that may be useful for ore exploration (Kelly et al., 2009; Braxton and Mathur, 2011). This literature review will examine data presently available regarding heavy metal isotope fractionation in ore deposits, and aims to further the understanding of ore deposit formation, isotope fractionation mechanisms, and applications to exploration.

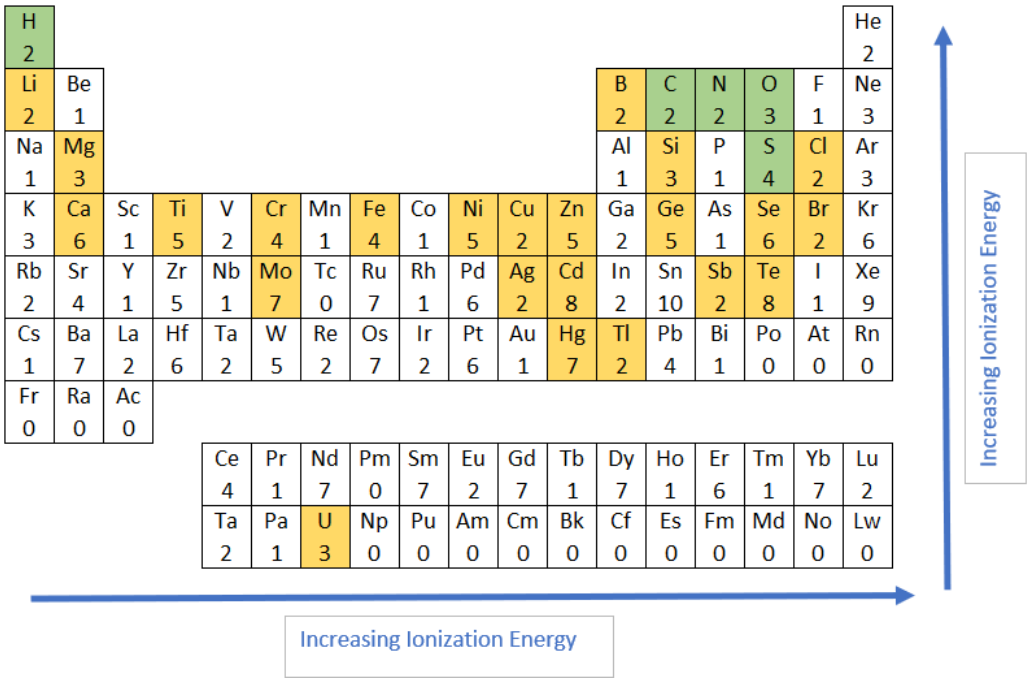

Figure 1: Periodic Table of Elements. The green elements are considered traditional elements studied in stable isotope geochemistry, whereas non-traditional elements are in orange. Ionization energy increases towards the top right of the table. The number associated with each element is the number of isotopes.

Of the heavy metals, Cu isotopes have received the most attention. Studies of Cu isotope fractionation have included volcanic massive sulfide deposits (Mason et al., 2005; Housh and Ciftci, 2008), modern "black smoker" chimneys (Berkenbosch et al., 2015), sediment-hosted deposits (Asael et al., 2009), porphyry deposits (Li et al., 2009; Mathur et al., 2009; Mathur et al., 2010b; Mirnejad et al., 2010; Braxton and Mathur, 2011; Palacios et al., 2011; Asadi et al., 2015), Ni-Cu-PGE sulfide mineralization (Ripley et al., 2015), and hydrothermal deposits (Larson et al., 2003; Maher et al., 2007). Molybdenum isotopes have been measured in skarn deposits, polymetallic epithermal veins, porphyry deposits, alpine-type fissure veins, greisens, perigranitic veins, pegmatites, and granites (Barling et al., 2001; Siebert et al., 2001; Wieser and de Laeter, 2003; Malinovsky et al., 2005; 2007; Hannah et al., 2007; Mathur et al., 2010a; Greber et al., 2011; 2014; Shafiei et al., 2015; Breillat et al., 2016; Wang et al., 2016; Yao et al., 2016). Zinc isotopes have also received attention for sphalerites from shale-hosted massive sulfides and hydrothermal deposits (Mason et al., 2005; Wilkinson et al., 2005; John et al., 2008; Kelley et al., 2009; Chen et al., 2014; Zhuo et al., 2014; Duan et al., 2016) as well as carbonate-hosted deposits (Pasava et al., 2014). Zinc isotope fractionation coupled with Fe isotope fractionation has been studied in large hydrothermal deposits by Gagnevin et al. (2012). Fe isotopes are also of relevance in skarn

deposits (Wang et al., 2011) and banded iron formations (Johnson et al., 2008; Hou et al., 2014; Debret et al., 2016). U isotope fractionation in uranium ore deposits has also been studied in detail (Brennecka et al., 2010; Murphy et al., 2014; Uvarova et al., 2014; Placzek et al., 2016). Other heavy metal isotopes that have potential for investigation include Se (Wen and Carignan, 2011; Layton-Matthews et al., 2013), Hg (Sherman et al., 2009), Ni (Gueguen et al., 2014; Hofmann et al., 2014), Ge (Escoube et al., 2011), Cd (Zhu et al., 2016), and V (Prytulak et al., 2013).

2.2 Analytical Techniques

Heavy element isotope fractionation is commonly measured by a multi-collector inductively coupled plasma mass spectrometer (MC-ICP-MS) and/or a thermal ionization mass spectrometer (TIMS). Both systems utilize an ionization source to ionize and focus ions into a beam. Ions are then precisely separated based on their mass to charge ratio by the magnet, and the intensity of the ion beam is measured by a detector. The difference between the two instruments comes down to the ionization source. The TIMS utilizes a hot filament to ionize the sample. Since the filament can only reach a maximum ionization temperature of 2200ºC (Smith, 2000), TIMS is less effective for samples with high ionization energies. The MC-ICP-MS can analyze nearly all elements on the periodic table due to the high ionization efficiency of the plasma source, which reaches temperatures of 6000-10000K (Wieser et al., 2012). The MC-ICP-MS can achieve higher accuracy and precision for elements with high ionization compared to TIMS (Huemann et al., 1998; Albarede et al., 2004; Wieser and Schwieters 2005; Yang 2009; Wieser et al., 2012). To ensure precision for MC-ICP-MS measurements, solutions must be purified and careful corrections must be applied to the data to correct for mass biases and interferences such as isobaric and polyatomic species, doubly-charged oxides, and argides created in the Ar plasma (Yang, 2009; Wieser et al., 2012).

For many metal isotope systems, international standards exist to allow for cross lab comparison. Using the measured metal isotope ratios in samples and standards, the difference in abundance between the heavy and light isotopes in a sample, expressed as per mil deviations relative to a standard, can be calculated using the following equation:

$$\delta\ (‰) = \left[\frac{abundance\ of\ heavy\ isotope\ in\ sample \div abundance\ of\ light\ isotope\ in\ sample}{abundance\ of\ heavy\ isotope\ in\ standard \div abundance\ of\ light\ isotope\ in\ standard} - 1\right] \text{x}1000$$

The isotopic signature (δ) can be used to indicate the degree of enrichment or depletion of the heavy isotope in the sample. Samples with a positive isotope composition indicate enrichment in the heavy isotope relative to the standard, whereas samples with a negative isotope composition indicate heavy isotope depletion.

If the sample contains significant concentrations of other elements besides the metal of interest, then it is typically necessary to dissolve the sample and perform ion-exchange column chromatography to isolate and purify the metal for isotopic analysis (Albarede et al., 2004). This step will avoid matrix effects (i.e., isobaric interferences) during mass spectrometry. In rare cases, it is possible to analyze minerals without ion exchange chromatography if the metal is the most abundant constituent of the mineral and the other elements are not expected to cause significant isobaric or polyatomic interferences (e.g., molybdenite; Barling et al., 2001).

The most precise method commonly used for MC-ICP-MS and TIMS measurements is the double spike method, which can be used to correct for instrumental and column chromatography mass fractionation when the metal has four or more isotopes (Rudge et al., 2009). The double spike comprises a solution artificially enriched in two different isotopes and has a known isotopic composition. The most important step is determining the optimal double spike composition and mixing proportions of sample and double spike in such a way as to maximize the precision of isotope analyses. Tables are available in Rudge et al. (2009) to assist in determining the optimal measurements for the element of interest. If calibrated correctly, the double spike method can be a more precise tool than sample-standard bracketing and the element spike method for correcting instrumental mass fractionation and measuring isotopic compositions (e.g., Mo; Kendall et al., 2017).

2.3 Cu Isotopes

With regards to metal isotope geochemistry, Cu is the most widely studied metal for ore deposits. Copper has only two isotopes, heavy ^{65}Cu and light ^{63}Cu. The Cu isotopic composition is reported relative to standard NIST SRM 976 and signatures range from -16.49‰ to 20.04‰ in ore deposits (Wang et al., 2017). Cu samples are primarily collected from the minerals chalcopyrite, chalcocite, and bornite. Cu isotope fractionation is mass-dependent and has been studied in porphyries, skarn deposits, volcanogenic massive sulfide deposits, magmatic sulfide deposits, and sediment-hosted Cu deposits. Cu isotopes have been

used to define Cu reservoirs, determine the processes of Cu transport, shed light on the mechanisms that govern Cu isotope fractionation in ore-forming systems, and provide a vectoring tool for ore exploration.

2.3.1 Cu Reservoirs

Porphyry deposits are the largest source of Cu worldwide. The isotopic signature, δ^{65}Cu, of Cu minerals in porphyry systems has been used to define three Cu reservoirs that each have a characteristic Cu signature: 1) the hypogene zone, 2) the enriched (supergene) zone, and 3) the leach cap. In the hypogene zone, minerals are precipitated by high temperature (400-600°C) magmatic fluids, whereas in the supergene zone and leach cap, the minerals are altered and precipitated by low temperature (T < 300°C) hydrothermal fluids (Sinclair, 2007). Primary hypogene Cu sulfide minerals generally show minimal Cu isotope fractionation ranging from -1.1‰ to +1.0‰ (Haest et al., 2009; Mathur et al., 2009; Palacios et al., 2010; Mirnejad et al., 2010; Braxton and Mathur 2011; Asadi et al., 2015). The minimal isotope fractionation relative to average crust in the hypogene zone is attributed to precipitation from high temperature magmatic fluids (Mathur et al., 2009). This explains why hypogene minerals exposed to high temperature primary alteration experience little isotope fractionation compared to the enriched zone and leach cap, both of which reflect alteration by secondary low temperature fluids.

Unlike the hypogene zone, the leach cap and enriched zones show evidence of significant Cu isotope fractionation. The enriched zone shows preferential enrichment in the heavier ^{65}Cu isotope and the δ^{65}Cu is commonly higher than 3‰ (Mathur et al., 2009; 2010b; Palacios et al., 2010; Mirnejad et al., 2010; Braxton and Mathur 2011; Asadi et al., 2015). Since the enriched zone is where the highest grade of Cu is found, identifying heavy Cu isotope enrichment is potentially an important pathfinder for ore exploration. The leach cap has the greatest extent of Cu isotope fractionation with a range of -13.5‰ to +2.7‰ (Haest et al., 2009; Mathur et al., 2009; Li et al., 2009; Palacios et al., 2010; Mirnejad et al., 2010; Braxton and Mathur 2011; Asadi et al., 2015). In most cases, δ^{65}Cu values are negative and depict an environment that is depleted in the heavy ^{65}Cu isotope. This would indicate that ^{65}Cu has been preferentially removed from the leach cap compared to ^{63}Cu during the process of low temperature supergene alteration. Evidence from most studies (Haest et al., 2009; Mathur et al., 2009, 2010b; Palacios et al., 2010; Asadi et al., 2015) suggests that the heavy Cu isotope has leached downwards and precipitated in the enriched zone (Figure 2).

Therefore, the isotopic signature of Cu can be used to trace paleo-fluid pathways and Cu movement during supergene alteration.

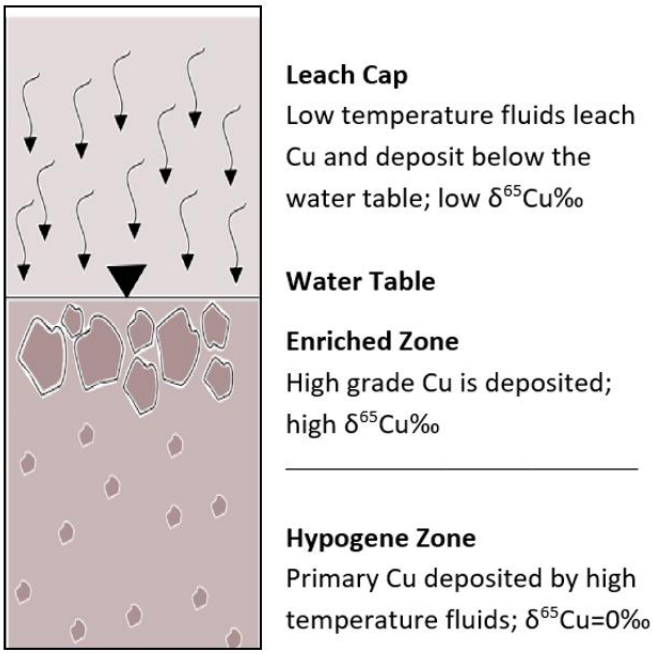

Figure 2: Cross section of Cu porphyry deposit experiencing single stage leaching and supergene alteration (modified from Mathur et al., 2009).

Compared to most porphyry deposits, a very wide range of δ^{65}Cu values was observed by Duan et al. (2016) at the Tiegelongnan high sulfidation Cu deposit in Tibet (-4.76‰ to 2.84‰). This wide range and a trend towards increasing δ^{65}Cu with depth is related to supergene alteration and then further leaching and transport of heavy Cu downwards (Duan et al., 2016). In magmatic sulfide deposits and volcanogenic massive sulfide deposits, very little fractionation of Cu isotopes is observed and δ^{65}Cu is near 0‰ (Larson et al., 2003; Rouxel et al., 2004; Mason et al., 2005). The same is true for modern volcanic arc chimneys where δ^{65}Cu is ~0‰ to 0.5‰, which is equivalent to the δ^{65}Cu of mantle rocks (Berkenbosch et al., 2015). Skarn deposits originate from high temperature fluids and have a range of Cu isotope compositions (-1.29‰ < δ^{65}Cu < 2.98‰) (Maher and Larson, 2007). Although less Cu isotope fractionation occurs in skarn deposits compared to porphyry deposits, Cu reservoirs can be observed. The heavy Cu isotope tends to be concentrated farther from the skarn intrusion, whereas the lighter Cu isotope is more concentrated near the intrusive body. Copper isotope fractionation in high temperature deposits is most likely related to late-stage, low temperature secondary processes causing Cu to mobilize and precipitate elsewhere in the deposit (Rouxel et al., 2004). Other processes contributing to Cu isotope fractionation include

significant Cu leaching, precipitation of Cu sulfides, and hydrothermal reworking of the deposit. The potential mechanisms for Cu transport are discussed in Section 2.3.3.

2.3.2 Cu Minerals

Exploring Cu isotope fractionation between different minerals can provide insight into geochemical processes in ore-forming systems. In porphyry deposits, specific Cu-bearing sulfide minerals are abundant in each zone. In the hypogene zone, the primary Cu sulfide mineral chalcopyrite exhibits little to no isotope fractionation relative to the crust. In the enriched zone of the porphyry deposit where the highest grades of Cu are observed, the mineral of interest is chalcocite. Chalcocite commonly is enriched in heavy ^{65}Cu. Chalcopyrite and bornite are also found in the enriched zone. In the leach cap, minerals such as goethite, jarosite, bornite, and hematite are commonly found. These minerals are often depleted in the heavy Cu isotope (Figure 2). To understand the variations in δ^{65}Cu signatures between the minerals and between different porphyry deposits, the fluid-mineral Cu isotope fractionation factor must be considered. The fluid-solid fractionation factor depends on the minerals present, the physicochemical conditions, and the fluid compositions.

The two most abundant Cu sulfides in skarn deposits are chalcopyrite and bornite. These two sulfides are cogenetic and commonly found spatially close together within a skarn deposit (Maher and Larson, 2007). Although these two minerals are cogenetic, they each have a different isotopic signature. Chalcopyrite contains more of the heavy isotope ^{65}Cu compared to bornite. Their isotopic signature typically differs by 0.30‰ to 0.48‰ (Maher and Larson, 2007). Since the two minerals were determined to be cogenetic, the isotopic difference between them likely occurred under equilibrium conditions (Maher and Larson, 2007). The cause of isotope fractionation between minerals is attributed to bond length and strength (Maher and Larson, 2007). Because bornite has a much longer and weaker Cu-S bond than chalcopyrite, a mass fractionation effect will take place, causing the lighter isotope ^{63}Cu to be preferentially included to a greater extent in bornite. This trend is also evident in bornite and chalcopyrite from volcanogenic massive sulfide deposits (Housh and Ciftci, 2008).

In magmatic sulfide deposits, there are two important mineral groups to consider, primary and secondary Cu sulfide minerals. Primary Cu sulfides, mainly chalcopyrite, exhibit little to no isotope fractionation. The δ^{65}Cu of chalcopyrite from modern high temperature

hydrothermal ‘black smoker’ chimneys that have not experienced metamorphism also have little isotope fractionation relative to mantle rocks, which is comparable to what is observed in the hypogene zone in a porphyry deposit (Berkenbosch et al., 2015). In VMS deposits, secondary Cu sulfide minerals such as bornite, covellite, and digenite, are highly enriched in the heavy isotope ^{65}Cu (Larson et al., 2003). Possible mechanisms of Cu isotope fractionation associated with secondary Cu sulfide minerals were explored, including the effects of boiling or salinity on the system. These factors were determined to have no effect on Cu isotope fractionation (Rouxel et al., 2004). In modern intraoceanic arc/backarc volcanoes, the minor amount of Cu isotope fractionation observed was attributed to partitioning of Cu isotopes between vapour and fluid phases in the vent fluids (Berkenbosch et al., 2015).

2.3.3 Fractionation of Cu Isotopes During Transport

2.3.3.1 Redox Reactions

There are many mechanisms that can cause fractionation of Cu isotopes during transport. As seen in section 2.3.1, low temperature secondary processes can introduce significant Cu isotope fractionation in high temperature deposits. Redox reactions are an important mechanism for fractionation during low temperature alteration such as serpentinization (Ehrlich et al., 2004; Ikehata and Hirata, 2012). In porphyry systems, the preferential mobilization of heavy ^{65}Cu during supergene alteration is directly related to oxidation of Cu minerals in the leach cap and subsequent reduction of Cu(II) in the enriched zone (Mathur et al., 2009; Haest et al., 2009; Palacios et al., 2011; Asadi et al., 2015). Above the water table exists an oxidizing environment and below the water table is a reducing environment. The oxidizing shallow surface waters interacting with the reducing supergene zone also have a heavy δ^{65}Cu signature compared to more distal waters, which have a lighter isotopic signature (Mathur et al., 2013). When uplift occurs, the water table is lowered and oxidative weathering of rocks now situated above the water table will occur and create a new leached zone. In hypogene zones of high temperature alteration (e.g., potassic, sodic-potassic), little isotope fractionation is observed or slightly negative δ^{65}Cu signatures are observed, indicating alteration is controlled by variations in pH and/or temperature rather than redox reactions (Mathur et al., 2013).

The extent of Cu isotope fractionation during redox reactions will vary depending on whether it is an open or closed system. Study of these reactions was performed using isotope analysis of Cu(I) and Cu(II) minerals within the same hand sample and is outlined below

(Asael et al., 2007). In a closed system, hand samples will show evidence of reduced Cu(I) minerals (in most cases chalcopyrite) and precipitated Cu(II) oxides. The observed difference in δ^{65}Cu between Cu(II) and Cu(I) minerals is 1.7‰, which means Cu(II) minerals are enriched in the heavy isotope. As the water table was lowered due to regional uplift, primary Cu(I) minerals were oxidized and then quickly reduced due to fluctuations in the water table. During the brief oxidation of Cu(I) minerals, aqueous Cu(II) is produced, which is then precipitated nearby as Cu(II) oxides. Overall, the hand sample will show little to no evidence of isotope fractionation since there has been minimal transport of the Cu isotopes. In an open system, however, there will be no mass balance at the hand sample scale. Study of the Cu isotopic compositions will yield different results. In open system samples, the difference in δ^{65}Cu between Cu(II) and Cu(I) minerals is -1.2‰, which means Cu(II) minerals are depleted in ^{65}Cu (Asael et al., 2007). Similar to the closed system, as the water table is lowered, Cu(I) is oxidized producing aqueous Cu(II). Since this is an open system, the water table will remain lowered, thus enabling some of the isotopically heavy aqueous Cu(II) to escape and travel downwards. The remaining Cu will have lighter δ^{65}Cu, and hence precipitation of isotopically light Cu oxides can occur in the leach cap. The isotopically heavy Cu(II) will precipitate in the supergene enriched zone (Asael et al., 2007).

This information can be used to indicate the degree of Cu mobility in any low temperature system and has been applied to porphyry systems (Mathur et al., 2009; Asadi et al., 2015), sediment hosted Cu (Asael et al., 2007), magmatic sulfides (Rouxel et al., 2004), and volcanogenic massive sulfide deposits (Housh and Ciftci, 2008). If the oxidized Cu(II) mineral has a higher δ^{65}Cu signature than the Cu(I) mineral, then there has been little to no transport of heavy Cu(II) ions, and therefore little to no net Cu isotope fractionation has occurred in the system. If the oxidized Cu(II) mineral has a lower δ^{65}Cu than the Cu(I) mineral, then there has been significant transport of heavy Cu(II) ions downwards, followed by reduction and Cu(I) precipitation in a deeper zone of enrichment (Asael et al., 2007). This is useful for exploration geology because if there has been significant Cu transport, it is likely that there exists an enriched zone at depth.

In the oceanic crust, native Cu has been measured in both basaltic basement rock and overlying sedimentary layers (Dekov et al., 2013). The observed Cu is suggested to be derived from hydrothermal sources as well as seawater. The CuO found along veins in the basaltic basement rock exhibit minimal isotope fractionation and is thought to have

precipitated under low temperature conditions following the dissolution of igneous and hydrothermal Cu-sulfides under anoxic conditions, thus preventing redox-related isotope fractionation from occurring (Dekov et al., 2013). Conversely, the overlying sedimentary layers have positive δ^{65}Cu, indicating redox fractionation during CuO precipitation from seawater.

2.3.3.2 Rayleigh Distillation

Rayleigh distillation has been used to explain the transport of Cu laterally down the hydraulic gradient to produce "exotic" Cu deposits, as seen in porphyry deposits (Braxton and Mathur, 2011). When redox reactions occur, such as those described in section 2.3.3.1, the resulting groundwater will be very acidic and Cu-rich (Mathur et al., 2009). This groundwater could result in heavy aqueous Cu depositing directly below in the enrichment zone or Cu may move laterally down-gradient and precipitate as an exotic deposit. An "exotic deposit" is defined as a portion of the supergene Cu mineralization in an area that does not show evidence of previous hypogene Cu mineralization (Braxton and Mathur, 2011). The δ^{65}Cu in the exotic zone has a very wide range (-2.0‰ to +6.3‰), with higher values found closer to the main part of the deposit and lower values at more distal locations (Braxton and Mathur, 2011).

To explain this phenomenon, simplified models for Rayleigh fractionation have been developed that consider equilibrium distillation and redox reactions involved in Cu transport. Rayleigh equations can be used to describe isotope fractionation between the leaching fluid and the residual solid phase (Figure 3A) as well as between the Cu-rich fluid and the precipitated Cu mineral using a fluid-solid isotope fractionation factor (Figure 3B). Leaching causes the δ^{65}Cu in the leach cap chalcopyrite to become lower with further leaching (Figure 3A). Subsequently, as Cu(II) minerals are precipitated, the δ^{65}Cu of the leach solution also decreases. Since the δ^{65}Cu of the fluid is becoming progressively lower, the precipitated chalcocite will also progressively exhibit a spatiotemporal trend towards lighter δ^{65}Cu (Figure 3B). This basic model can also be modified to incorporate multi-cycle processes and explain the isotopic response of successive leach cycles or regional uplift events as seen in Braxton and Mathur (2011).

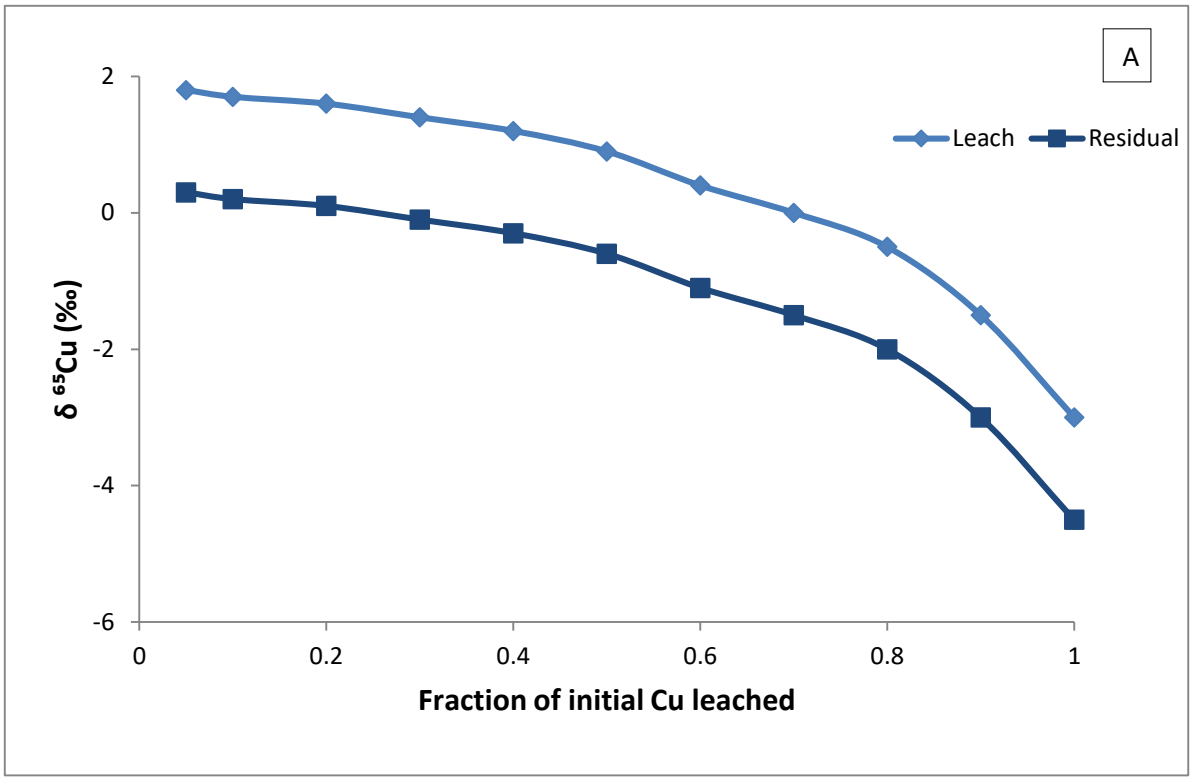

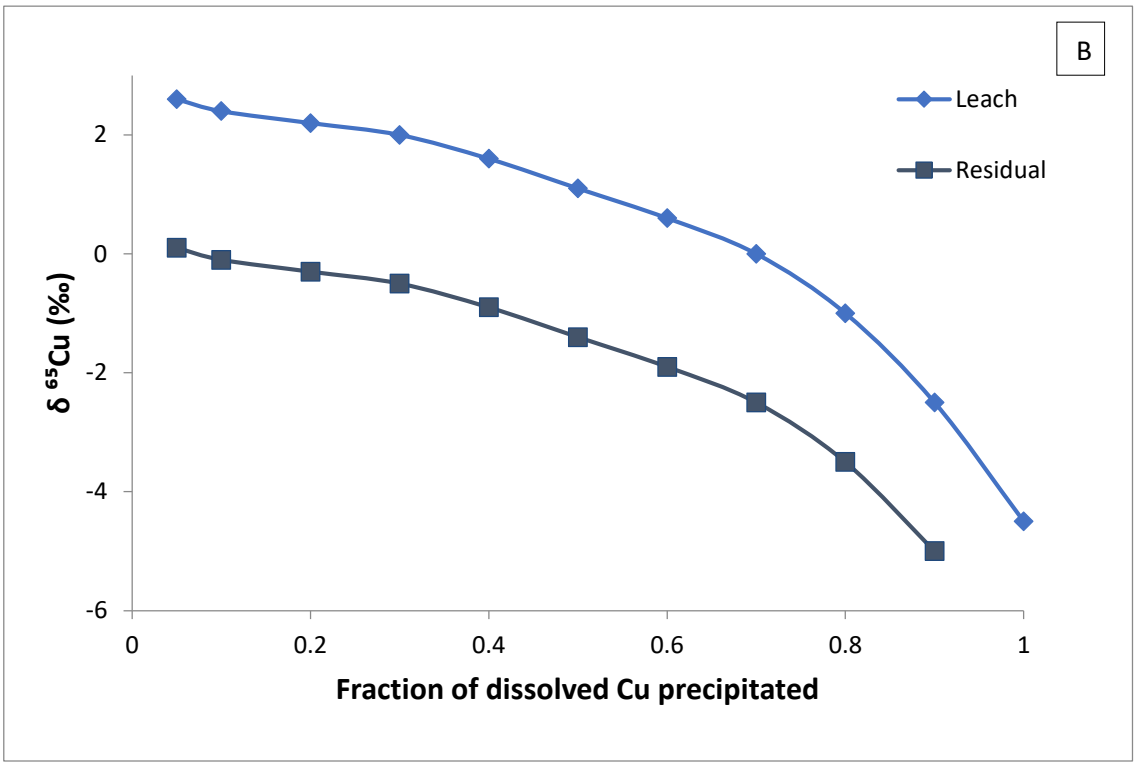

Figure 3: A. Rayleigh fractionation model showing decreasing δ^{65}Cu over time in leach fluid and residual solid chalcopyrite with a fluid-solid fractionation factor of +1.5‰. B. Rayleigh fractionation model showing decreasing δ^{65}Cu over time in leach fluid and precipitated chalcocite with a fluid-solid fractionation factor of +2.5‰ (modified from Braxton and Mathur, 2011).

Rayleigh distillation has also been proposed as the mechanism behind Cu isotope fractionation in skarn deposits. In most systems, Cu isotope fractionation is attributed to low temperature redox reactions. However, in skarn deposits, there is no evidence of oxidation or reduction of Cu due to low temperature alteration (Maher and Larson, 2007). Maher et al. (2011) suggest that Cu will be partitioned between vapour and brine phases, causing the vapour to have an isotopically light signature and the residual brine to have a heavier isotopic signature. The importance of phase separation between the vapour and liquid has been highlighted in experiments by Maher et al. (2011) and quantum mechanics calculations by Seo et al. (2007). However, studies by Seo et al. (2007) indicate that phase separation will cause the vapour to become enriched in the heavy isotope, not the light isotope. It has also been proposed that vapour transport of Cu may occur in modern volcanic chimney systems due to the periodic release of magmatic volatiles causing fractionation between aqueous and vapourous species (Berkenbosch et al., 2015). Copper isotope fractionation during magmatic activity may also be a possibility due to partial melting and/or fractional crystallization from a sulfide liquid (Ripley et al., 2015).

2.4 Mo Isotopes

The application of Mo isotopes from ore deposits as a process tracer is rapidly emerging. Major goals of the initial Mo isotope studies were to look for systematic variations between different deposit types, infer the fractionation mechanisms, and more recently to decipher the connection between observed Mo isotope variations and Mo mineralization processes within an individual deposit. Predictably, much of this work has focused on molybdenite, MoS_2, which is approximately 60% Mo by weight and often dominates the Mo mass balance in mineralizing systems. Rhenium concentrations in molybdenites may range from a few ppm to several weight percent due to the tendency for Re^{4+} to substitute for Mo^{4+} (Stein et al., 2001; Golden et al., 2013), which raises the possibility of paired Mo and Re isotope analyses of molybdenites, now that the analytical methodology for measurement of non-radioactive Re isotope variations in geological samples is rapidly improving (Miller et al., 2009; 2015). Molybdenites are commonly associated with Sn, Cu, W, As, Au, Fe, and Bi mineralization, and can be found as a trace mineral phase in many different types of ore deposit (King, 2004).

The total range of Mo isotope variation in molybdenites is ~4‰, and ranges between –1.37‰ to +2.52‰ relative to NIST SRM 3134 = 0.25‰. Significant variability in the Mo

isotope composition of molybdenites can occur for specific categories of ore deposits (> 2‰) and even within single deposits (> 1‰), including at the cm-scale (Hannah et al., 2007; Mathur et al., 2010a; Greber et al., 2011, 2014; Shafiei et al., 2015; Breillat et al., 2016). The average Mo isotope composition of molybdenite is 0.29 ± 1.04‰ (2SD, n =391) relative to NIST SRM 3134 = 0.25‰ (Breillat et al., 2016). Since the two standard deviation of this dataset is quite large at 1.04‰, the average molybdenite Mo isotopic signature cannot be used to precisely define the average crustal Mo isotope composition (Breillat et al., 2016).

The type and age of deposit do not appear to exert any systematic control on the Mo isotopic signature of molybdenites, indicating that Mo isotopes cannot be reliably used to fingerprint ore deposit type (Hannah et al., 2007; Breillat et al., 2016). There is a general correlation between the temperature of molybdenite deposition and isotopic composition. Molybdenite deposited by high temperature fluids, such as those found in porphyry deposits (mean of 0.08±0.79‰, 2SD, n =180), have a tendency towards low Mo isotope compositions (Breillat et al., 2016). By contrast, molybdenites deposited by low temperature fluids, such as in greisen deposits (mean of 1.25±2.62‰, 2SD, n=3) have higher overall Mo isotope compositions (Breillat et al., 2016). However, temperature is not the only control on the Mo isotope composition of molybdenite. Preliminary studies indicate that the isotopic fractionation of Mo is also influenced by Rayleigh distillation, fluid boiling, variations in redox conditions, source isotopic composition, and molybdenite crystal structure (Hannah et al., 2007; Mathur et al., 2010a; Greber et al., 2011, 2014; Shafiei et al., 2015; Wang et al., 2016).

2.4.1 Fractionation Mechanisms and Transport

Preliminary studies indicate that the isotopic fractionation of Mo is influenced by Rayleigh distillation, melt-fluid and brine-vapor partitioning, variations in redox conditions, molybdenite crystal structure, and the isotopic composition of the original Mo source (i.e., crustal- versus mantle-derived magmas) (Hannah et al., 2007; Mathur et al., 2010a; Greber et al., 2011, 2014; Shafiei et al., 2015; Wang et al., 2016; Yao et al., 2016). Based on experimental, petrographic, and geochemical evidence, Mo may be transported by species such as MoO_3, $MoO_3 \cdot nH_2O$, MoO_4^{2-}, $HMoO_4^-$, H_2MoO_4, $MoO(OH)Cl_2$, MoO_2Cl_2, K_2MoO_4, $KHMoO_4$, Na_2MoO_4, $NaHMoO_4$, and $NaHMoO_2S_2$ (e.g., Candella and Holland, 1984; Stein, 1985; Cao, 1989; Farges et al., 2006; Rempel et al., 2006, 2009; Zhang et al., 2012, Shafiei et al., 2015).

To date, little work has been done to experimentally determine fractionation factors between the different Mo species in ore forming systems (Tossell, 2005). The dominant species involved and their associated isotope fractionations are poorly understood, although Zhang et al. (2012) recently suggested transport as $NaHMoO_2S_2$ in reducing S-containing fluids. Molybdenum may be transported in the vapor state as $MoO_3 \cdot nH_2O$ (Rempel et al., 2006, 2009; Shafiei et al., 2015) and precipitate from the vapor upon reaction with H_2S. It is possible that a small amount of fractionation occurs between molybdate and the hydrated $MoO_3 \cdot nH_2O$. If Mo crystallizes from vapor upon reaction with H_2S, this means Mo isotope fractionation is possible at high temperatures and that the amount of Mo isotope fractionation by Rayleigh distillation may be proportional to the sulfur content of the fluid. The theoretical isotope fractionation factor between dithiomolybdate and trithiomolybdate is about 3‰ at 25ºC which would be smaller at higher temperature (Tossell, 2005). At 25ºC, the amount of fractionation between molybdate and tetrathiomolybdate is approximately 5.4‰ which again would be less in high temperature systems (Tossell, 2005). If Mo is transported in a vapor state, then Rayleigh fractionation could account for Mo isotope fractionation of approximately 1‰ per amu (Hannah et al., 2007). By comparison, natural observations of Mo isotope fractionation during fractional crystallization from a magma are about 0.4‰ to 0.6‰ (see review by Kendall et al., 2017). Zajacz et al. (2017) also found Mo to partition strongly into the fluid phase, however, in the presence of HCl, they experimentally observed increased Mo partitioning into the vapor phase.

Fluid boiling may explain Mo isotopic variability in high-temperature vein deposits in porphyry systems. At high temperatures (400-600°C), the mineralizing fluid can boil, leading to separation of the fluid phase into brine and vapor. Lighter Mo isotopes will preferentially partition into the vapor phase (as $MoO_3 \cdot nH_2O$) whereas heavier Mo isotopes will remain in the brine (as $NaHMoO_2S_2$) because of mass dependent isotope fractionation (Rempel et al., 2006, 2009; Zhang et al., 2012; Shafiei et al., 2015). The chemical species existing in the vapor and brine phases also support Mo movement into the brine phase (Zhang et al., 2012; Greber et al., 2014). In the Cu porphyry system from the Kerman area (Iran), the brine phase transported and deposited Mo in the early stages of mineralization, whereas the vapor phase rose and ultimately deposited molybdenite in "transitional" veins in the hydrothermal system (Shafiei et al., 2015). Specifically, an early brine phase produced oxidizing, saline, and high temperature (400-600°C) conditions for precipitation of isotopically heavier molybdenite. By contrast, a transitional H_2O-rich vapor phase was associated with crystallization of

isotopically lighter molybdenite at lower pressure, salinity, pH, and temperature (300-400°C) (Shafiei et al., 2015). In addition to the brine and vapour phases described by Shafiei et al. (2015), a late stage fluid was also observed at the Kerman Cu porphyry system. The late-stage, H_2S-rich, acidic, and low-temperature (T < 300°C) liquid phase also crystallized isotopically light molybdenite under more reducing conditions.

As Mo is precipitated out of these three fluid phases, the Mo isotopic composition of the fluid can evolve by Rayleigh fractionation (Hannah et al., 2007; Mathur et al., 2010a; Greber et al., 2014; Shafiei et al., 2015) and add to the Mo isotopic variability observed at individual mineralization stages (Shafiei et al., 2015). These three fluid phases thus represent different physicochemical environments for molybdenite precipitation and thus may lead to distinctive isotopic compositions. The Mo isotope signature of molybdenite precipitated from the brine phase was the highest (0.94±0.54‰), followed by the vapour phase (0.37±0.55‰) and late-stage low temperature fluids (0.27±0.41‰) (Shafiei et al., 2015). This observation suggests the Mo isotopic composition of molybdenites in a porphyry system will evolve to lower values over time and with distance from the mineralizing source. The crystal structure of the molybdenite may exert some control on the Mo isotope composition, with heavier Mo isotopes preferentially taken up by the denser 2H polytype (earlier, high-temperature fluid) compared with the less dense 3R polytype (later, low-temperature fluid) (Shafiei et al., 2015).

Greber et al. (2014) observed the opposite trend at the porphyry-type Questa deposit in New Mexico. As the fluid source gradually evolved over time, the Mo isotope signature of the molybdenite precipitates gradually increased. The first and lightest molybdenites were precipitated from magmatic fluids (median = -0.29‰). As the system was infiltrated by hydrothermal fluids, the molybdenite signature progressively increased (median = -0.05‰). The heaviest Mo isotope signature was observed in molybdenites precipitated by late-stage stockwork veins (median = 0.22‰). Greber et al. (2014) suggest progressive fractional crystallization of a magma will preferentially remove the lighter Mo isotopes first, leaving behind a residual melt that is enriched in the heavy Mo isotopes. Melt-fluid interactions may also explain this trend as isotopically heavy aqueous fluid is exsolved from the magma leaving behind an isotopically light melt (Greber et al., 2014). Greber et al. (2014) also suggested that precipitation of the molybdenite itself is associated with preferential incorporation of lighter Mo isotopes into the molybdenite, causing heavier Mo isotopes to become progressively more concentrated into the remaining hydrothermal fluid.

Alternatively, variations in the redox conditions of mineralizing fluids may exert a major control on Mo isotope fractionation in ore-forming systems. Greber et al. (2011) examined molybdenites from high temperature (300-600°C) Late Paleozoic mineralization events in Switzerland and found a bimodal distribution in Mo isotope compositions, centering on 0.2‰ and 1.1‰. Hence, single-stage Rayleigh distillation is probably not the main mechanism responsible for Mo isotope fractionation. Greber et al. (2011) observed isotopic variability in the molybdenites at both small (cm apart) and large (different hand samples) scales. To explain these observations, Greber et al. (2011) suggested that Mo isotope fractionation was influenced by redox conditions during precipitation of molybdenite during two major episodes of fluid expulsion from an evolving magma or from molybdenite precipitation from vapor and brine phases.

The low-temperature systems studied thus far for Mo isotopes point to the importance of redox reactions on the Mo isotope signature of Mo-bearing mineral phases. In a low-temperature mineralizing system (100-160°C) in Switzerland, molybdate transport by oxidizing surface waters into brecciated rocks, followed by Mo reduction and precipitation, resulted in large variations in the Mo isotope composition of Mo-bearing sulfide phases (Greber et al., 2011; the mineralogy could not be identified by the authors). Subsequent dissolution and re-precipitation of Mo may also have contributed to the observed Mo isotope variation of ~3‰ in the brecciated rocks.

Song et al. (2011) demonstrate the effective use of Mo isotopes to indicate the type of metallogenic environment at the Dajiangping pyrite deposit, China. Two orebodies in the Song et al. (2011) study region (Orebody III and Orebody IV) exhibit very different Mo isotopic signatures. Orebody III was deposited in an open system, reducing marine environment by submarine exhalative hydrothermal fluids and has a higher average Mo isotope signature but less isotopic variability (0.22‰ to 0.69‰, mean δ^{98}Mo=0.52‰, relative to NIST SRM 3134 = 0.25‰). Orebody IV was deposited in an oxic-suboxic semi-closed marine depositional environment and has a very wide range of observed Mo isotopic compositions (-0.80‰ to 1.18‰, mean δ^{98}Mo=0.07‰). In Orebody IV, the main ore bed was observed to have a negative Mo isotope signature that gradually increased upward through the ore beds, thus indicating significant Mo isotope fractionation is possible in an oxic-suboxic restricted setting (Song et al., 2011).

Finally, the Mo source may also influence the Mo isotopic composition of molybdenite (Mathur et al., 2010a; Wang et al., 2016). Study of the trace element concentration of Re in molybdenites has supported this hypothesis. Comparison of Re concentrations in molybdenite with the Mo isotopic composition revealed a negative correlation (Mathur et al., 2010a; Wang et al., 2016). Since molybdenites precipitated from mantle-derived magmas have generally higher Re concentrations when compared to crustal-derived magmas and mixing of crustal- and mantle-derived magmas (Mao et al., 1999), the observed negative correlation may be directly related to the source of the mineralizing fluid (Mathur et al., 2010a; Wang et al., 2016). The study by Wang et al. (2016) compared Mo isotopic signature to Re concentration in molybdenites from five porphyry Mo deposits from the Gangdese metallogenic belt, Tibetan plateau. Molybdenites from mantle-derived magmas exhibit a generally low Mo isotope signature (<0.00‰) and a high Re concentration (>1000 ppm). Molybdenites precipitated by mixing of crustal- and mantle-derived magmas have a more positive Mo isotope signature than mantle-derived magmas and a lower Re concentration. Molybdenites precipitated from crustal-magmas were observed to have the most positive Mo isotope signatures and lowest Re concentration. The trend observed in these molybdenites indicates that the source fluid can be identified using Mo isotopic composition and that the effects of other Mo isotope fractionation processes in ore-forming systems do not fully eradicate this relationship.

2.5 Zn Isotopes

Zinc is another heavy metal whose isotopes have been studied to gain further insight into the mechanisms leading to ore deposition. Zinc has 5 stable isotopes: ^{64}Zn, ^{66}Zn, ^{67}Zn, ^{68}Zn, and ^{70}Zn. Zinc isotope data is commonly collected from the sulfide mineral sphalerite (ZnS). The isotopic composition of Zn is commonly reported as $\delta^{66/64}$Zn relative to the international standard BCR-1 (Chen et al., 2014). Zinc sulfides have been found to experience a smaller magnitude of isotope fractionation during precipitation from hydrothermal fluids compared to Cu sulfides (Fujii et al., 2011). The total range of Zn isotopic signatures in ore deposits spans from -0.40‰ to 1.33‰ (Duan et al., 2016). It has been proposed that Zn isotopes may be a useful tool for determining the mineralizing fluid pathways and interpreting how metals are transported and deposited within hydrothermal systems (Mason et al., 2005; Kelley et al., 2009; Chen et al., 2014; Duan et al., 2016).

Most Zn isotope studies in ore geology have focused on massive sulfide and hydrothermal deposits (Mason et al., 2005; Wilkinson et al., 2005; John et al., 2008; Kelley et al., 2009; Chen et al., 2014; Zhuo et al., 2014, Duan et al., 2016). At the Alexandrinka volcanic-hosted massive sulfide deposit, Mason et al. (2005) found that although the extent of isotope fractionation was small, trends can still be observed in the Zn isotopic composition. They found that close to the rim of the vent chimney, a heavier Zn isotope signature was observed compared to the core of the chimney (Figure 4). Zhou et al. (2014) had similar findings from their study of Pb-Zn hydrothermal sulfide deposits in southwest China. They observed an increase in the Zn isotope composition moving from the center or bottom of the deposit towards the periphery or top of the deposit. Zhou et al. (2014) also observed that Zn sulfides precipitated earlier have a lower isotope composition than Zn sulfides precipitated by more evolved fluids. Studies of the Irish ore field hydrothermal system by Wilkinson et al. (2005) concluded that the main ore bodies had a much heavier Zn isotopic signature than the deeper veins. A study of active fumaroles and thermal springs by Chen et al. (2014) showed that the fluids are enriched in the heavy Zn isotope relative to the host rock. These findings are summarized in Figure 4.

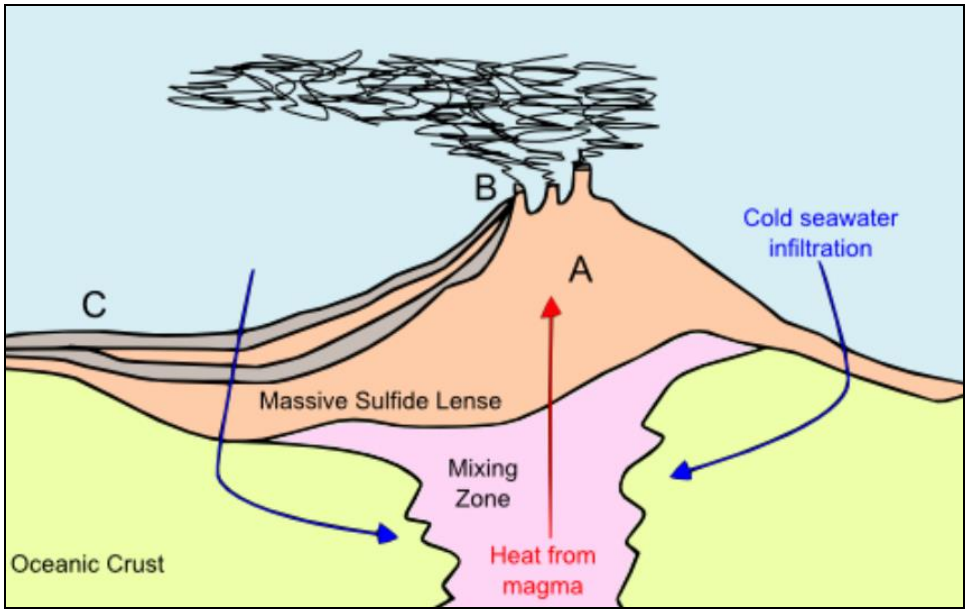

Figure 4: Cross section of an active Zn "black smoker" chimney. In zone A, Zn first begins to precipitate. Due to kinetic isotope fractionation, the lighter Zn isotopes will become incorporated into the mineral precipitate. As precipitation continues towards zone B, mineral precipitates will gradually have an increasingly higher Zn isotopic signature. Zn sulfides precipitated furthest away from the deposit in zone C lenses will have the heaviest Zn isotope signature and create a heavy isotope halo around the deposit (modified from Mason et al., 2005).

The above studies identify similar Zn isotopic trends and the data can be used to infer possible mechanisms of isotope fractionation. Chen et al. (2014) attributes isotope fractionation directly to water-mineral interactions. As sphalerite is precipitated out of solution, Zn isotopes are partitioned between liquid and mineral phases. Wilkinson et al. (2005) identify kinetic isotope fractionation as the mechanism causing the light Zn isotopes to be preferentially included in the first Zn sulfide precipitates. As the fluids diffuse outward through the hydrothermal system precipitating sulfides, the fluids will continue to evolve through Rayleigh fractionation to a heavy Zn isotopic composition and will precipitate progressively heavier Zn sulfides (Mason et al., 2005; Wilkinson et al., 2005; Kelley et al., 2009). Therefore, it may be possible to use Zn isotopes as a vector to trace the fluid pathways back to the source (Kelley et al., 2014; Chen et al., 2014). However, a study by Gagnevin et al. (2012) of the Navan Zn-Pb orebody suggests that Zn isotopes may not be a good tracer to use when looking at a single deposit. If a deposit has experienced multiple pulses of hydrothermal fluid flow, rapid precipitation of sphalerite could induce significant kinetic isotope fractionation at short spatiotemporal scales, thus limiting the use of Zn isotopes as a vector within a deposit (Gagnevin et al., 2012). Zn isotopes may still be a useful vector for new deposits, which could be found by identifying isotopically heavy Zn haloes (Gagnevin et al., 2012).

Duan et al. (2016) studied Zn isotope fractionation at the Zhaxikang Pb-Zn deposit in south Tibet and found the heaviest isotopic signature in the more evolved porphyritic monzogranite (0.49‰), compared to the metamorphosed basement rocks (0.36‰, 2SD = 0.03‰), and the lighter Fe-Mn carbonatites precipitated in veins (0.27‰, 2SD = 0.05‰). Primary sphalerite and galena also have isotopically lighter Zn than the basement rock. From these observations, Duan et al. (2016) suggested Zn isotopes may be used to trace the source of the ore forming metals. Using the Zn isotope fractionation factor between sphalerite and fluid, Duan et al. (2016) inferred that magmatic-hydrothermal fluids likely lead to precipitation of Zn in basement rock and Fe-Mn carbonatites.

To shed light on isotope fractionation between primary and secondary Zn mineralization, Ducher et al. (2016) defined a set of mass dependent equilibrium fractionation factors for Zn using first-principles calculations. In general, secondary minerals formed by supergene alteration (adamite, gahnite, gunnigite, hemimorphite, hydrozincite, zincite) were found to have an isotopically heavier signature than primary Zn sulfide minerals (sphalerite,

wurtzite). This agrees with natural observations where heavy isotope enrichment has been observed in minerals with the largest bond strength. Ducher et al. (2016) indicate a linear relationship between Zn interatomic forces and Zn reduced partition functional ratios (β-factors) and showed an increase in β-factors with increased bond strength.

John et al. (2008) and Mason et al. (2005) suggest that changing temperature may play an important role on Zn isotope fractionation because temperature can influence the sphalerite-fluid fractionation factor. If high temperature fluids are cooled within the subsurface, fluids may precipitate Zn sulfides that are enriched in the lighter Zn isotopes due to kinetic isotope fractionation (John et al., 2008). This would explain why low temperature hydrothermal fluids have a distinctly heavy Zn isotopic composition. Studies of thermal springs by Chen et al. (2014) found that high temperature hydrothermal alteration resulted in more Zn isotope fractionation than low temperature chemical weathering. John et al. (2008) estimated high temperature hydrothermal alteration could cause Zn isotope fractionation of up to 1‰. These enriched waters can be a major source for heavy Zn to the oceans (Pons et al., 2013). Alternatively, an experimental study of Zn metal-silicate partitioning indicated temperature had no influence on Zn isotope fractionation (Mahan et al., 2017). Other possible opportunities for Zn isotope fractionation noted by Chen et al. (2014) are the formation of hydrothermal clays and the removal of organic bound Zn by chemical weathering. Chen et al. (2014) also postulated that if Zn is scavenged due to secondary co-precipitation of Zn into Fe oxides-hydroxides, the heavier Zn isotopes could become enriched in the solids.

Jamieson-Hanes et al. (2017) assessed the effects of redox conditions on Zn isotope fractionation. Experimentally under sulfate-reducing conditions, ZnS was precipitated from aqueous fluids. The amount of Zn precipitation was directly related to the extent of sulfate reduction. As ZnS was precipitated, the remaining fluid evolved to higher δ^{66}Zn as the lighter Zn isotopes were preferentially incorporated into the mineral phase (Jamieson-Hanes et al., 2017). This experimental data is consistent with observations from natural systems (Mason et al., 2005; Wilkinson et al., 2005; John et al., 2008; Kelley et al., 2009; Chen et al., 2014; Zhuo et al., 2014). Experimentally it was also observed that Zn isotope fractionation may occur at fluid-solid interfaces during adsorption as well as through precipitation (Veeramani et al., 2015; Dong et al., 2016). The Zn adsorbed to calcite was measured to have an isotopically heavy signature compared to the surrounding fluid (Dong et al., 2016). This observation is explained by an equilibrium isotope effect between the aqueous species

($Zn(H_2O)_6^{2+}$) and the adsorbed Zn (Dong et al., 2016). This can also be attributed to direct adsorption of $ZnCO_{3(aq)}$, which is isotopically heavy. The type of aqueous Zn species is an important control on Zn precipitation from aqueous fluids (Veeramani et al., 2015). When sphalerite is precipitated, the fluid will evolve to a heavier Zn isotope composition. The opposite trend was observed during the precipitation of hydrozincite and hopeite. Therefore, the extent of Zn isotope fractionation by adsorption and precipitation from aqueous fluids is directly related to the aqueous Zn species present in the fluid and can be used for determining reaction pathways in aqueous environments (Veeramani et al., 2015; Dong et al., 2016).

Zn isotopes are also being used as an indicator of pH in ancient hydrothermal environments (Fujii et al., 2011). Through computational methods, Fujii et al. (2011) determined that there was little Zn isotope fractionation between aqueous sulfide species (-$Zn(HS)_2$, $Zn(HS)^{3-}$, $Zn(HS)_4^{2-}$). They determined that solutions with pH>9 will precipitate sulfides with a negative Zn isotope signature ($\delta^{66}Zn < -0.6‰$). Conversely, Zn sulfides precipitated by more acidic solutions will be influenced by the aqueous sulfide species present in the parent fluid and appear nearly unfractionated for hydrothermal systems with high pCO_2.

2.6 Other Non-Traditional Metal Isotope Systems

2.6.1 Fe Isotopes

Iron isotopes can be used to indicate the fluid history (Debret et al., 2016) and in some cases, the source of iron in an ore deposit (Markl et al., 2006). Iron has 4 stable isotopes: ^{54}Fe, ^{56}Fe, ^{57}Fe, and ^{58}Fe and the isotopic composition is recorded as $\delta^{56/54}Fe$ relative to standard IRMM-014 (Beard et al., 2003; Faure and Mensing, 2005). Redox variations as well as the presence of chlorine and sulfur ions can contribute to further Fe isotope fractionation and Fe mobility within the ore-forming system (Debret et al., 2016).

Fe isotope data is collected from primary Fe sulfides such as pyrite and secondary Fe oxides such as hematite and goethite from skarn deposits (Wang et al., 2011) and banded iron formations (Johnson et al., 2008; Hou et al., 2014; Debret et al., 2016). Little Fe isotopic variation is observed in primary hematite of magmatic or metamorphic origin (Johnson et al., 2004; Rouxel et al., 2004). For hydrothermal Fe mineralization, the typical range of Fe isotopic compositions is 2.5‰ (Markl et al., 2006). The Fe isotopic signature can be affected by late stage alteration. In some Fe ore deposits, the Fe isotopic composition has been found

to vary within a single vein or hand sample (Markl et al., 2006). In these cases, Fe isotopes can be used to trace the fluid history and do not provide a good indication of Fe source (Beard et al., 2002; Graham et al., 2004). Debret et al. (2016) demonstrated the potential use of Fe isotope compositions in subduction-related serpentinites as a tracer for Fe mobility.

Fe isotope fractionation during hydrothermal mineralization occurs when Fe is leached from the basement rock (Rouxel et al., 2004). The composition of the precipitating fluid can be identified using Fe isotopes. Fluids rich in chlorine will form bonds with Fe(II) and precipitate isotopically light Fe (Welch et al., 2003; Markl et al., 2006). Reducing fluids rich in CO_2 will also precipitate isotopically light Fe in the form of siderite (Wiesli et al., 2004; Markl et al., 2006). Conversely, oxidizing fluids will precipitate hematite with an isotopically heavy Fe signature (Skulan et al., 2002; Markl et al., 2006). Therefore, Fe isotopes can be used to trace fluid history and determine depositional mechanisms. Residual fluids can be further oxidized or may experience recharge by Fe-rich fluids, thus causing the small-scale variations in isotopic composition that are observed.

Late stage alteration of primary siderite to form the secondary minerals goethite and hematite can also lead to Fe isotope fractionation. In low temperature systems, the secondary replacement minerals will inherit the isotopic composition of the primary mineral (Markl et al., 2006). Therefore, Fe isotopes can be used to identify precursor minerals. In minerals that experience high temperature alteration, the precipitated replacement minerals are at thermodynamic equilibrium and the isotopic composition differs from the parent mineral by a fractionation factor (Markl et al., 2006). Consequently, in hydrothermal systems, by considering thermodynamics and the Fe isotope fractionation factor, it is possible to trace the fluid history of an Fe deposit.

Fe isotopes can also be used to determine the redox conditions at the time of Fe precipitation in banded iron formations (Johnson et al., 2008; Hou et al., 2014; Debret et al., 2016). When oxidation of Fe^{2+} to Fe^{3+} occurs, isotope fractionation will take place. The Fe^{2+} ions will become enriched in the lighter isotopes, and Fe^{3+} will become enriched in the heavier isotopes (Anbar et al., 2005; Hou et al., 2014). The degree of Fe isotope fractionation will depend on the extent of Fe^{2+} oxidation to Fe^{3+}. If Fe^{2+} is totally oxidized to Fe^{3+}, then the BIF will have the same isotopic signature as seawater. If incomplete oxidation occurs, Rayleigh fractionation will cause the heavy Fe isotopes to be preferentially included in Fe oxides and hydroxides, thus giving the BIF a positive Fe isotope signature (Hou et al., 2014).

2.6.2 Se Isotopes

The study of selenium can be complicated because Se is found in very low concentrations in the Earth's crust (0.05 ppm) compared to other non-traditional elements discussed in this review (Lakin, 1973; Faure and Mensing, 2005). The distribution of Se and its isotopes is also very complex and can be difficult to interpret. Selenium has 6 naturally occurring stable isotopes: ^{74}Se, ^{76}Se, ^{77}Se, ^{78}Se, ^{80}Se, and ^{82}Se (Faure and Mensing, 2005). The isotopic composition is commonly recorded as $\delta^{82/76}$Se relative to proposed international standard NIST SRM 3149 (Layton-Matthews et al., 2013). Se deposition is usually associated with volcanism (Layton-Matthews et al., 2013) and studies also show that Se can be found in high concentrations in some black shale deposits (Wen and Carignan, 2011). The total range of Se isotope fractionation observed in ore deposits is -12.77‰ to 4.93‰ (Wen et al., 2007). This entire range of fractionation was observed at the Yutangba sedimentary-type Se deposit (Wen et al., 2007). Significant Se isotope fractionation was also observed in VHMS deposits -10.2‰ to 1.3‰ (Layton-Matthews et al., 2013). The Se isotopic composition may provide a useful tool for identifying the mechanisms leading to Se isotope fractionation, accumulation, and redistribution.

Similar to the previous metal isotope systems, Se experiences mass dependent kinetic isotope fractionation (Layton-Matthews et al., 2013). Se precipitated directly from hydrothermal fluids was found to have experienced little to no isotopic fractionation (Wen et al., 2007). Fractionation of Se isotopes has been attributed to redox processes caused by secondary hydrothermal alteration or low temperature supergene alteration (Wen and Carignan, 2011). Reducing fluids will break Se-O bonds and cause the product mineral to become enriched in the light Se isotopes (Wen and Carignan, 2011). Depending on the reducing agent and concentration of Se, the breaking of Se-O bonds may be responsible for a Se isotope fractionation of ~7-11‰ (Johnson and Bullen, 2004). Under oxidizing conditions, Se^{6+} ions bond with O^{2-} ions to form SeO_4^{2-}. The formation of new Se-O bonds did not lead to any significant Se isotope fractionation (Wen and Carignan, 2011). Therefore, secondary hydrothermal alteration and supergene alteration are thought to have a greater influence on Se enrichment than initial Se precipitation from seawater or hydrothermal fluids.

It is possible that Se isotopes may also have applications as a tracer for finding the deposit source (Rouxel et al., 2004). During oxidation, Se can be mobilized and transported in the form of H_2Se along with sulfides, then reduction occurs and Se is precipitated directly

in the form of selenides or as a replacement of sulfur in sulfide minerals (Wen and Carignan, 2011). The heavier isotopes of Se are commonly concentrated in these distal Se-sulfides due to mass dependent fractionation causing fluids to evolve to a heavier isotopic composition (Wen and Carignan, 2011). Therefore, Se isotopes can also be used to identify whether significant alteration, remobilization or precipitation has occurred within the deposit (Layton-Matthews et al., 2013).

2.6.3 Hg Isotopes

The Hg isotopic composition is commonly reported as $\delta^{202/198}$Hg (Sherman et al., 2009). No international standard exists for Hg although it is recommended that NIMS-1 be used over NIST SRM 3133, which was intended for quantitative analysis not isotopic measurements (Mejia et al., 2010; Brand et al., 2014). The element Hg has been observed to have an uncharacteristically wide range of isotopic compositions (>5‰) that cannot be explained using only mass dependent fractionation (Smith et al., 2005; Xie et al., 2005; Smith et al., 2008; Sherman et al., 2009). Mercury differs from the previously studied isotope systems because it has a higher atomic number. For heavier metals in general, the large mass of the element will lead to volume dependent fractionation due to the "nuclear volume effect" (Schauble, 2007; Brennecka et al., 2010). This effect will cause variations in the nuclei's ability to attract electrons. In ore deposits, volume dependent isotope fractionation may be responsible for up to 3‰ of Hg isotope fractionation compared to the 0.5-1‰ fractionation that is mass dependent (Schauble, 2007). Mercury has 7 stable isotopes and an abundance of oxidation states (Smith et al., 2005). For most other metals previously reviewed in this chapter, an important mechanism for isotope fractionation is redox reactions. Since metals with more oxidation states tend to experience greater isotope fractionation, the many oxidation states of Hg could be causing the large isotopic variations (Smith et al., 2005).

In hydrothermal systems, little to no isotope fractionation occurs during the initial release of Hg from the source area, but instead Hg isotope fractionation occurs during transportation of Hg (Smith et al., 2008). As the hydrothermal fluids boil, Hg will begin to vaporize (Smith et al., 2005). This will cause Hg isotopes to fractionate between the brine and vapor phases, with the lighter Hg isotopes preferentially partitioning into the vapor phase. The preferential loss of the lighter Hg isotopes to the vapor phase can be modelled using Rayleigh distillation (Sherman et al., 2009). The heavier Hg isotopes will remain in the liquid phase and precipitate deep in the hydrothermal system in sulfide minerals (Smith et al.,

2008). This combination of boiling, vaporization of Hg during low temperature hydrothermal activity, and redox reactions all lead to fractionation of Hg in hydrothermal systems.

The Hg isotope fractionation discussed above is mass dependent. In hydrothermal black smokers, there is also the possibility that volume dependent isotope fractionation can influence Hg isotopic compositions, but is poorly understood (Sherman et al., 2009). It is speculated that photochemical reduction of Hg^{2+} near the Earth's surface could cause volume dependent isotope fractionation during secondary leaching of sediments in vents (Sherman et al., 2009). Further study is required to determine Hg isotope applications in locating the source area and deciphering the migration patterns of this transition metal.

2.6.4 U Isotopes

Uranium is a radioactive element and has no stable isotopes. Isotopes ^{238}U and ^{235}U have a very long half-life and are commonly used for determining the U isotopic composition (Faure and Mensing, 2005). The isotopic composition is recorded as $\delta^{238/235}U$ relative to standard CRM 145 (Kendall et al., 2013). Uranium is the heaviest element discussed in this literature review and its isotopes experience volume dependent fractionation (Brennecka et al., 2010). U isotope fractionation of nearly 5‰ has been observed in mineralized sediment samples (Murphy et al., 2014). In ore-forming systems, the primary mechanism for U isotope fractionation is believed to be redox variation (Schauble, 2007; Stirling et al., 2007; Weyer et al., 2008; Murphy et al., 2014; Uvarova et al., 2014; Placzek et al., 2016).

Using the isotopic composition of U, it is possible to determine the paleo-redox conditions of the deposit (Murphy et al., 2014). If the deposit experienced a lack of redox variation, such as leaching causing aqueous alteration, little to no isotope fractionation will occur (Stirling et al., 2007). If the deposit experienced a change from oxidizing to reducing conditions, U will fractionate causing the heavy isotope to preferentially move into the reduced phase (Brennecka et al., 2010; Murphy et al., 2014; Uvarova et al., 2014). This observation differs from mass dependent fractionation whereby the reduced phase is enriched in the light U isotope. For redox-related U isotopic fractionation, volume dependent fractionation is dominant because of the small relative mass difference between ^{238}U and ^{235}U. As the heavy U isotope is preferentially reduced from U(VI) to U(IV) and precipitated, the remaining fluid will have a gradually lighter U isotope signature as it moves through the hydrothermal system, following a Rayleigh distillation model that results in solid-liquid

fractionation of nearly 1‰ (Murphy et al., 2014). Therefore, U isotopes can also provide a tool to trace U flow paths. Utilizing the U isotopic signature can also have applications in sandstone-hosted U deposit exploration and environmental remediation (Placzek et al., 2016).

In high temperature systems where there are redox changes, the same processes can be observed, however, the degree of U isotope fractionation is much less (Brennecka et al., 2010). Uvarova et al. (2014) observed little U isotope fractionation for U mineralization associated with igneous sources when compared to sedimentary basin-hosted deposits, which generally had higher and more variable U isotope compositions. Therefore, in coherence with the study by Abe et al. (2008), the magnitude of nuclear volume isotope effects will vary inversely with temperature.

2.7 Future Directions

Other isotope systems that are emerging as having significance for ore systems include Ni, Ge, Cd, Tl, and V. Initial work on the Ni isotope system has focused on cosmochemistry, meteorites and sedimentary systems, however, there are also trends observed in ore deposits (Gueguen et al., 2013; Hofmann et al., 2014; Elliot and Steele, 2017). Ni has 5 stable isotopes and fractionation is typically recorded as $\delta^{60/58}$Ni using international standard NIST SRM 986 (Hofmann et al., 2014; Elliott and Steele, 2017). Positive Ni isotope compositions are observed in shales, coal and soil (Gueguen et al., 2013). Conversely, komatiite-hosted Ni deposits have a distinctly negative Ni isotope composition due to high temperature fractionation between metal and silicate phases (Huh et al., 2009; Hofmann et al., 2014). In igneous rocks, little to no isotope fractionation occurs, and the bulk silicate Earth is estimated at +0.05‰ (Gueguen et al., 2013). However, Hofmann et al. (2014) found that some enrichment in the light Ni isotopes is possible in magmatic Ni sulfides up to -0.47‰. The high temperature fractionation mechanisms causing light isotope enrichment of Ni sulfides relative to the silicate melt are still poorly understood (Hofmann et al., 2014).

The Ge isotope system and its application to ore deposits is gaining momentum. Ge has 4 stable isotopes and its isotope composition is typically recorded as $\delta^{74/72}$Ge relative to proposed international standard NIST SRM 3120a (Siebert et al., 2006, Escoube et al., 2011). Due to chemical similarities with Si, Ge isotope fractionation has been used as an ocean tracer for biogenic silica cycling (Rouxel and Luais, 2017). Marine sediments generally displayed a positive Ge isotope signature and likely fractionated due to redox variations

(Escoube et al., 2011). Applications of Ge isotopes also extends to interpreting geothermal springs that were enriched in Ge compared to Si due to Ge exclusion during earlier silicate precipitation (Siebert et al., 2006). These high temperature fluids were found to have a negative Ge isotopic signature, indicating the heavier Ge isotopes were removed during cooling and precipitation (Siebert et al., 2006). In ore deposits, Ge isotope fractionation has potential for use as a geochemical tracer (Escoube et al., 2011). Mantle-derived rocks were found to have little Ge isotope fractionation, with bulk silicate Earth near 0.59±0.18‰ (Escoube et al., 2011). Fractionation during hydrothermal sulfide precipitation caused Ge sulfide minerals and ore deposits in general to have a negative Ge isotope composition (-3.53±0.51‰) (Li et al., 2009; Escoube et al., 2011).

In recent years, application of Cd isotopes in geochemistry has focused on understanding micronutrient cycling in marine environments as well as the potential for Cd isotopes as an anthropogenic tracer (Ripperger et al., 2007; Rekhamper et al., 2011). Cd has 6 stable isotopes and experiences mass dependent fractionation that is typically recorded as $\delta^{114/110}$Cd relative to NIST SRM 3108 although no international standard currently exists (Abouchami et al., 2011; Brand et al., 2014). A recent study by Zhu et al. (2016) demonstrated the potential for Cd isotopes to help classify Pb-Zn deposits by determining the Cd concentration and isotopic signature in the mineral sphalerite. Zhu et al. (2016) found that high temperature systems, such as porphyry deposits, displayed little to no isotope fractionation. Low temperature deposits, such as MVT deposits, were found to have the highest Cd concentration as well as a positive Cd isotopic signature. Exhalative systems, such as SEDEX deposits, overall contained very little Cd and did not exhibit nearly as much isotope fractionation as the MVT deposits (Zhu et al., 2016).

Applications of Tl isotopes to ore deposits is also being explored and significant fractionation has been observed particularly in marine settings (Nielsen et al., 2013; 2017). There are two stable isotopes of Tl, ^{205}Tl and ^{203}Tl, which experience mass dependent fractionation. Isotopic measurements are recorded as ε^{205}Tl relative to standard NIST 997 using the following equation (Nielsen et al., 2017):

$$\varepsilon^{205}\mathrm{Tl}_{\mathrm{sample}} = 10^4 \times (^{205}\mathrm{Tl}/^{203}\mathrm{Tl}_{\mathrm{sample}} - {}^{205}\mathrm{Tl}/^{203}\mathrm{Tl}_{\mathrm{NIST997}}) / (^{205}\mathrm{Tl}/^{203}\mathrm{Tl}_{\mathrm{NIST997}})$$

The total isotopic variability for Tl is 35 ε^{205}Tl-units ranging from +15 units for ferromanganese sediments to -20 units for low temperature altered oceanic crust (Nielsen et

al., 2017). Prytulak et al. (2017) found that the Tl isotopic signature can be used to identify the addition of low temperature altered sediments to the source of mantle-derived melt for oceanic basalts and arc lavas. This is possible because minimal Tl isotope fractionation was found to occur during magmatic processes and Tl isotopes are an excellent tracer of pelagic sediments (Prytulak et al., 2017). Future work should focus on identifying Tl isotope fractionation mechanisms and assess the degree of fractionation by igneous processes.

The V isotope system may also have applications in ore geochemistry due to the precision with which measurements can be achieved using MC-ICP-MS. Isotopic measurements of V can be analytically challenging because V has 1 stable isotope which accounts for >99% of all V and one radioactive isotope with a long half-life (10^{17} years). Isotopic compositions are denoted as $\delta^{51/50}$V and no international standard currently exists (Wu et al., 2016). V is redox sensitive and has been used to assess biogeochemical cycling and anthropogenic impacts (Huang et al., 2015). The cycling of V in the Earth's crust has been assessed though V-rich minerals to determine the effects of magmatism, late-stage weathering, and the V species present (Huang et al., 2015). Prytulak et al. (2013) found minimal isotope fractionation in high temperature samples but seafloor weathering did result in evolution of oceanic crust towards a heavier V isotope signature. Basalts were found to have a negative V isotope signature relative to bulk silicate Earth (Prytulak et al., 2013). Further work is still needed to determine V isotope fractionation factors for interactions between melt and precipitated minerals.

2.8 Conclusions

The scope of heavy metal stable isotope geochemistry applications to ore geology is broad and expanding. These isotope systems have also gained attention for their applications to understanding biogeochemical cycling, marine systems, oxidation events, cosmochemistry, as well as solving anthropogenic and environmental issues. Studying heavy metal isotopes has helped gain insights into the mechanisms that govern isotope fractionation. Temperature, redox conditions, metal speciation, Rayleigh distillation and interactions between fluid-vapor or vapor-brine can all have some effect on the degree of isotope fractionation observed in an ore-forming system. In most ore-forming systems, low temperature alteration by hydrothermal or meteoric fluids was linked to a greater magnitude of metal isotopic fractionation than high temperature magmatic or metamorphic fluids. In this way, heavy metal isotope fractionation could also be used to uncover the geological history of the area by

providing clues about the type of mineralization and alteration that occurred. The nature of the isotope fractionation (mass-dependent or volume-dependent) also plays an important role in the resulting isotopic signature. Applications can also relate directly to exploration geology, where information about the deposit size, grade, and extent can be collected directly from the metal of interest. For example, Cu isotopes in porphyry systems link directly to transport of Cu within the system and were used as a tracer/vector to high grade enriched zones and exotic deposits.

Undoubtedly there is still much to be uncovered through the study of heavy metal isotopes in ore-forming systems. To date, Cu, Zn and Mo isotope systems have received the most attention, and further work is still needed to explore additional isotope systems. In the years to come, this promising field will only continue to grow as geochemical processes are deciphered and metal isotopes are refined into a useful geochemical exploration tool.

Chapter 3: Mo isotope variations in molybdenites at single-crystal, ore deposit, and global scales: Implications for Mo source fluid, transport, fractionation mechanisms, and molybdenite mineralization

3.1 Introduction

The study of heavy metal isotope geochemistry and its application to ore geology has greatly expanded in recent years because of technological advances in Multi-Collector Inductively Coupled Plasma Mass Spectrometry (MC-ICP-MS) as a tool for measuring isotopic composition. The Mo isotope composition of molybdenite is a potentially useful tool for understanding ore-forming processes, but has not been studied as extensively as some other metal isotope systems (e.g., Cu). Many different types of ore deposits have been analyzed for Mo isotope compositions and associated fractionation mechanisms; the most common deposit types include skarn deposits, epithermal veins, and porphyry deposits (Wieser and De Laeter, 2003; Hannah et al., 2007; Klemm et al., 2008; Mathur et al., 2010a; Greber et al., 2011; Song et al., 2011; Greber et al., 2014; Shafiei et al., 2015; Breillat et al., 2016; Wang et al., 2016; Yao et al., 2016).

Molybdenum has seven naturally occurring stable isotopes, ^{92}Mo, ^{94}Mo, ^{95}Mo, ^{96}Mo, ^{97}Mo, ^{98}Mo, and ^{100}Mo. Molybdenite, MoS_2, is a Mo-rich sulfide mineral that is approximately 60% molybdenum and 40% sulfur by weight. Rhenium concentrations in molybdenite may range from a few ppm to several weight percent due to the tendency for Re^{4+} to substitute for Mo^{4+} (Stein et al., 2001). Molybdenites are also commonly associated with Sn, Cu, W, As, Au, Fe, and Bi mineralization and can be found as a trace mineral phase in many different types of ore deposit (King, 2004).

Observing the extent of isotope fractionation and spatiotemporal variations in molybdenite isotope composition could aid in defining the mechanism(s) of fractionation for Mo isotopes in ore deposits. Previous studies have shown that isotopic fractionation of Mo in ore-forming systems could be caused by Rayleigh distillation, redox conditions, magmatic evolution, and/or fluid boiling at the time of formation (Hannah et al. 2007; Mathur et al., 2010a; Greber et al., 2011; 2014; Shafiei et al., 2015). For example, a combination of magmatic evolution (fractional crystallization and fluid exsolution) and redox reactions associated with molybdenite crystallization may cause the Mo isotope composition of hydrothermal fluids to evolve to higher values over time in porphyry systems, resulting in

systematic spatiotemporal variations in molybdenite compositions (Greber et al., 2014). On the other hand, significant fluid boiling in porphyry systems may result in formation of isotopically heavy brine and isotopically light vapor/liquid phases that crystallized at higher (earlier stage) and lower (later stage) temperatures, respectively (Shafiei et al., 2015). The mechanisms or combination of mechanisms that contribute to Mo isotope fractionation at the Berg epithermal-porphyry deposit and the Hemlo disseminated Au deposit will also be explored by analyzing multiple hand samples from each deposit. Finally, the study of Mo isotope fractionation in ore deposits could provide us with insight into the relative importance of different processes contributing to ore genesis and may also have mineral exploration implications if predictive of hydrothermal-magmatic processes favoring high metal tenors.

This study reports the Mo isotopic composition of molybdenite from 14 different deposits varying in deposit type, size, grade, paleoclimate, alteration style, complexity and number of mineralization events. By combining this new data with existing δ^{98}Mo values for molybdenites, it is possible to make large scale comparisons using the newly established international standard NIST SRM 3134 set to 0.25‰ to standardize Mo isotope measurements between different laboratories (Nagler et al., 2014). Merging our new data with the recent molybdenite compilation by Breillat et al. (2016) will enable further testing of a recent hypothesis that suggested Mo isotopes may be used to fingerprint specific ore deposit types (Mathur et al., 2010a). The average isotopic composition for molybdenite derived from this large dataset is useful for inferring the isotopic composition of Mo runoff to the oceans, because molybdenite is an important host of crustal Mo that is easily weathered. The average molybdenite isotope composition may also provide a maximum upper limit for the upper crust Mo isotope composition because mineralizing hydrothermal fluids have higher δ^{98}Mo than the evolved (SiO_2-rich) magmas from which the fluids exsolved (Greber et al., 2014).

Another goal of this study is to explore changes in isotopic composition within a single deposit as well as within a single molybdenite grain. Few studies have interpreted variation within a single deposit. Multiple samples from the Eocene Berg porphyry-epithermal deposit in British Columbia and the Late Archean Hemlo disseminated gold deposit in Ontario were measured in this study. Using samples from different regions of the same deposit can help evaluate the effectiveness of Mo isotopes as a tracer for mineralization or fluid pathways. Study of the Hemlo deposit is particularly interesting because disseminated Au deposits have never been analyzed for Mo isotopic composition. In addition,

analysis of Mo isotopic composition from multiple hand samples from within the same deposit will reveal if Mo deposition was related to fluid boiling or redox reactions.

Unique to this study, both the S and Mo isotopic composition of molybdenite was measured for different ore deposits and for multiple samples from the Berg deposit. Hannah et al. (2007) suggested that analyzing the covariance between S and Mo isotopic composition of molybdenite in an ore-forming system could shed light on fractionation mechanisms for Mo. Since S is roughly 40% of molybdenite by weight, a positive correlation between the two isotopic compositions could indicate that Rayleigh distillation is the main mechanism of Mo isotope fractionation in a system with low S and Mo availability (Hannah et al., 2007).

In addition to S isotope compositions, the Re concentration of the molybdenites was also measured. Re is a common trace element found in molybdenite and can sometimes be found to have concentrations up to several weight percent (Stein et al., 2001). The relationship between Mo isotopic composition and Re concentration could shed light on the molybdenite source (Mathur et al., 2010a; Wang et al., 2016). The Re concentration of molybdenite tends to be higher if the mineralizing fluid has a mantle source (Wang et al., 2016). If the mineralizing fluid has a crustal source, the Re concentration tends to be much lower. Mathur et al. (2010a) and Wang et al. (2016) have observed a negative correlation between Re concentration and Mo isotopic composition. This implies molybdenites precipitated from a mantle fluid will have a more negative isotopic signature than molybdenites precipitated from a crustal fluid. The data from this study will expand on these findings and determine the extent to which additional Mo isotope fractionation mechanisms affect this relationship.

3.2 Geological Setting and Sample Descriptions

Molybdenite samples for this study were collected from a diverse selection of Mo-bearing ore deposits worldwide. Deposit types include nine porphyry deposits, two epithermal-porphyry deposits, one greisen deposit, one pipe-like Mo-W-Bi deposit, and one disseminated Au deposit. A single hand sample was collected from 12 of these deposits (Table 1). For many of these deposits, multiple molybdenite grains and/or fragments of grains were selected from the single hand sample for analysis. A total of 29 analyses were made for these deposits. In addition, two deposits, the Eocene Berg porphyry epithermal deposit (11 analyses from seven hand samples) and the Late Archean Hemlo disseminated gold deposit

(19 analyses from 10 hand samples), were selected for closer investigation through multiple hand samples (Table 2; Table 3). Samples were taken from different alteration zones and depths within the deposits. By observing a single deposit in detail, information about the magnitude and cause(s) of Mo isotope fractionation can be inferred at the scales of individual ore-forming systems, hand samples, and individual molybdenite crystals.

3.2.1 Single Molybdenite Hand Samples from Various Deposits

The Sachs Molybdenite Mine and the Wolfram Mine are both part of a large system of granitic intrusions along eastern Australia (Hess, 1924). These leucogranitic plutons are part of a volcanic arc system ranging in age from Permian to Triassic (Weber et al., 1978). At the Sachs Mine in New South Wales, dissolved Mo was transported in the hydrothermal fluids and then crystallized in quartz veins or pipes extending from mineralized granitic plutons along with bismuth and smaller quantities of arsenopyrite, wolframite, gold and silver (Weber et al., 1978). Molybdenite in this area is found as flakes and as large clumps with one mass of pure molybdenite at the Sach's Mine found to weigh more than 1 ton (Weber et al., 1978). The Wolfram Mine in Queensland is the largest molybdenite producer in Australia (Weber et al., 1978). Like the Sachs mine, the Wolfram deposit is a quartz pipe system stemming from a large granodiorite or leucoadamellite pluton (Plimer, 1974). The granodiorite in this area is highly greisenized and experienced low temperature alteration, therefore, the mineralogy has changed to have more quartz and mica and major element zoning is present around the pipes (Plimer, 1974). The primary minerals yielded from this site are wolframite, molybdenite, and bismuth (Hess, 1924; Plimer, 1974).

The Santo Nino Mine and Childs-Adwinkle Mine in Arizona are both part of a large Cu porphyry system formed by the Laramide orogeny during the Late Cretaceous (Wilt and Keith, 1980). A large granodiorite pluton intruded into the quartz monzonite country rock, resulting in mineral-rich veins. Molybdenite in this area can be found as disseminated grains in the quartz monzonite and as crystals in quartz veins with pyrite (Muntyan, 2012). Chalcopyrite and pyrite can also be found disseminated through the highly feldspathized rock. Both deposits have been described as highly brecciated pipes where molybdenite was the last sulfide mineral to precipitate and is concentrated at the outer edges of the pipe (Wilt and Keith, 1980). The primary minerals mined in this area were copper, silver and molybdenite with grades of 7 wt. %, 1oz/T, and 1 wt. %, respectively (Muntyan, 2012).

The Beura, Altenberg and Strzegom deposits in Europe all experienced some degree of metasomatic activity and alteration leading to the precipitation of molybdenite (Cavallo et al., 2004; Mikulski and Stein, 2005; Hoffmann et al., 2013). Molybdenite from the Beura Deposit in Ossola Valley, Italy, is attributed to a lower Permian system of greisenized veins (Cavallo et al., 2004). These veins formed in alpine fissures intersecting the leucogranitic gneiss in the Southern Alps and were affected by metasomatic and hydrothermal activity. The Altenberg mine in Germany has experienced similar alteration leading to the formation of greisens. This deposit is found in a large intercontinental volcanic porphyry complex where local ignimbrite was intruded by microgranitic dykes (Hoffmann et al., 2013). During the emplacement of the dykes, hypogene alteration led to the formation of metasomatic-hydrothermal greisens similar to the Beura deposit (Rakovan, 2007). The greisenization by fluorine-rich fluids exsolved from evolved magma led to the deposition of tin and accessory molybdenite in this area (Rakovan, 2007). The age of molybdenite was determined to be 318 ± 2 Ma and 324 ± 2 Ma by Re-Os age dating of molybdenite (Romer et al., 2007). Similar to the Altenberg deposit, the Strzegom deposit in Poland is also part of the large volcanic porphyry complex. Molybdenite was deposited along with chalcopyrite and pyrite in quartz veins after an uplift event (Mikulski and Stein, 2005). These veins and veinlets intersect the leucogranite porphyry and are 0.34 wt. % molybdenite on average. Mikulski and Stein (2005) found significant alteration in this area including feldspathization, albitization, silicification, sericitization, and chloritization.

The porphyry Moly Hill Mo-Bi deposit in Quebec is one of many Mo deposits centralized around the large Archean Preissac-Lacorne batholith in the Abitibi greenstone belt. The Moly Hill pluton is a felsic monzogranite with molybdenite-bearing quartz veins (Mulja et al., 1995). The deposition at the Moly Hill deposit can be attributed to exsolution of Mo-bearing brines from the monzogranite magma and fluid-boiling which led to Mo saturation in the vapour phase (Taner et al., 1998). The vapour and brine phases interacted with metavolcanics and metasedimentary rocks, leading to precipitation of deep stockwork veins with economical quantities of molybdenite in fractures (Taner et al., 1998). Other molybdenite occurrences in this area are associated with rare-metal bearing pegmatites, but these are not found at the Moly Hill deposit (Mulja et al., 1995).

Two hand samples have been collected from deposits on the Canadian east coast. The Lake George Sb-Au-W-Mo deposit in New Brunswick is hosted by a quartz-feldspar

porphyry dyke intruding granodiorite (Leonard et al., 2006). The ore mineralizing fluids are determined to be of magmatic-hydrothermal origin and directly related to the intrusion (Yang, 2012). As the fluid cooled, it reacted at depth with earlier magmatic sulfide minerals, enhancing the ore fluid, which then further cooled and precipitated in fractures leading to concentrations of Au as well as molybdenite and W sulfide minerals (Yang, 2012). The New Ross deposits in Nova Scotia are in the South Mountain batholith in a monzogranite and leucogranite pluton (Carruzzo et al., 2004). This late Devonian pluton is peraluminous, and hosts polymetallic pegmatites, greisens, and veins. From fluid inclusions, the genesis of the deposit was determined to begin with early magmatic activity leading to aplites and pegmatites, followed by hydrothermal activity with mixing of metamorphic and meteoric fluids leading to the development of greisens and veins (Carruzzo et al., 2004). Molybdenites at the New Ross deposit exhibit significant greisenization and are found with quartz and muscovite along with trace W sulfides and fluorite (Carruzzo et al., 2004).

Table 1: Deposit name, sample ID, and deposit type for each sample.

Sample ID	Sample Description	Location
	Porphyry Deposit	
1A	Half large grain (11 mm) cut perpendicular to layering	Sach's Mine, NSW, Australia
1B	Other half of 1A	
1C	Medium grained (4 mm)	
1D	Half large grain (9 mm) cut parallel to layering	
1E	Other half of 1D	
2A	Fine grained (2 mm)	Santo Nino Mine, Arizona
2B	Fine grained (2 mm)	
4A	Medium grained (4 mm)	Altenberg, Germany
4B	Fine grained (2 mm)	
5A	Medium grained (4 mm)	Childs-Adwinkle, Arizona
5B	Fine grained (2 mm)	
6A	One large grain (9 mm) with visible cleavage planes	Moly Hill, Quebec
6B	Half of large grain (13 mm) cut parallel to cleavage	
6C	Other half of 6B	
6D	Medium grained (4 mm)	
8A	Fine grained (2 mm)	Strzegom, Poland
8B	Fine grained (2 mm)	
11A	Medium grained (3 mm)	New Ross, Nova Scotia
12A	Medium grained (4 mm)	Lake George, New

		Brunswick
13A	Fine grained (2 mm)	Trout Lake, New Brunswick
Greisen		
3A	Fine grained (2 mm)	Beura, Ossola Valley, Italy
3B	Fine grained (2 mm)	
3C	Fine grained (2 mm)	
Pipe-like Mo-W-Bi		
7A	Half large grain (14 mm) cut perpendicular to cleavage	Wolfram, Queensland, Australia
7B	Other half of 7A, cut again parallel to cleavage	
7C	Other half of 7B	
7D	One large grain (10 mm) with visible cleavage planes	
Epithermal Porphyry		
10A	Fine grained (2 mm)	Logan Lake, British Columbia
10B	Fine grained (2 mm)	

3.2.2 Berg, Eocene Epithermal Porphyry, British Columbia

The Eocene epithermal porphyry deposit in Berg, British Columbia, is considered a "classic" porphyry deposit (Panteleyev, 1995). This deposit has multiple shallow porphyritic intrusions that have been intruded by late stage dykes. The main ore minerals are chalcopyrite and molybdenite precipitated in fractures and quartz veins and are found in zones experiencing potassic and phyllic alteration and localized around a composite quartz monzonite porphyry stock (Panteleyev, 1995). Brecciation by late-stage hydrothermal fluids followed the deposition of molybdenite in quartz veins and these veins are observed to be transported as brecciated fragments. A second molybdenite mineralization is also evident as molybdenite-rich quartz veinlets and can be found cross-cutting the breccias (Panteleyev, 1995). Significant leaching by low temperature acidic groundwater led to the formation of a well-developed supergene enrichment blanket and sulfide-rich zones with high grade Cu and Mo (Heberlein et al., 1983). For this study, seven hand samples were collected from different zones within the deposit and analyzed for Mo isotopic composition. The samples are summarized in Table 2.

Table 2: Description of samples from the Berg epithermal-porphyry deposit.

Sample ID	Description
9 (A, B)	Molybdenite mineral separate previously extracted from a quartz-rich sample

15A	Quartz veins in feldspar rich sample with trace molybdenite and pyrite
16 (A, B)	Quartz and feldspar rich sample with trace molybdenite and pyrite
17A	Quartz rich sample with trace molybdenite
18 (A, B)	Quartz and feldspar rich sample with some small darker bands of biotite, trace molybdenite
19A	Quartz veins with trace molybdenite cross cutting fine grained feldspar and quartz rich sample
20 (A, B)	Trace molybdenite and pyrite in quartz rich sample

For some hand samples, subsamples A and B were collected from different parts of the hand sample (or represents, in the case of sample 9, two analyses of the molybdenite mineral separate); molybdenite collected from all samples was fine grained (<2 mm).

3.2.3 Hemlo, Archean Disseminated Au Deposit, Ontario

The late Archean disseminated Au deposit in Hemlo, Ontario, is located within a shear zone at the contact between quartz ± feldspar volcanic porphyry and metasedimentary rocks or barite. At the contact there exist two ore zones, a main ore zone and a lower ore zone. Molybdenite was precipitated along with gold during a single mineralization event during prograde (greenschist facies) metamorphism. Precipitation of molybdenite and gold from a magmatic-metamorphic fluid may have been associated with a combination of potassic alteration, pyrite precipitation, and barite dissolution. Hence, a decrease in pH and change in redox conditions from oxidizing to reducing for the hydrothermal fluid have been attributed to mineralization (Heiligmann et al., 2008; Phillips and Powell, 2010). Subsequent gold remobilization events at peak metamorphic conditions (amphibolite facies) produced late-stage quartz veins, but these contain volumetrically minor amounts of gold and minimal molybdenite (Lin, 2001; Tomkins et al., 2004; Heigilmann et al., 2008), and hence are not a focus of this study. Gold and molybdenite are resistant to modification during amphibolite facies metamorphism (Stein et al., 2001). Both ore zones contain feldspathic ore and muscovitic ore. The higher-grade feldspathic ore (associated with potassic alteration) contains microcline + quartz + muscovite + biotite + barite + plagioclase + pyrite + molybdenite. The lower-grade muscovitic ore (associated with muscovitic alteration) often surrounds the first formed feldspathic ore and contains quartz + muscovite + pyrite + microcline + biotite + barite + trace molybdenite. The molybdenite is either disseminated or occurs as deformed, foliated seams (Lin, 2001; Muir, 2002; Heiligmann et al., 2008).

All 10 Hemlo hand samples from this study were silicate-rich schists with very fine grained molybdenite disseminated with pyrite. These samples were collected from the B and C zones of the David Bell mine and are summarized in Table 3.

Table 3: Sample description for samples from the Hemlo disseminated Au deposit in Ontario.

Sample ID	Zone	Description
14 (A, B, C)	n/a	Molybdenite mineral separate previously extracted from a mica-rich schist
21-1	C	Mica-rich schist, very fine grained, some quartz and feldspar, trace molybdenite and pyrite
22 (-1, -F)	C	Highly foliated muscovite rich sample with quartz and trace molybdenite
23 (-1, -S)	C	Very fine grained and foliated sample with mica and quartz, trace molybdenite
24 (-1, -F, -S)	C	Feldspar rich sample with weak foliation and some mica, trace molybdenite
25-S	B	Foliated sample with feldspar and mica, trace pyrite and molybdenite
26-S-1	C	Feldspar, muscovite and quartz with some pyrite, clear foliation, trace molybdenite
27 (-S-1, -S-2)	C	Feldspar and quartz dominant, poor foliation, trace pyrite and molybdenite
28 (-S-1, -S-2)	B	Quartz veins running through gently foliated feldspar and mica rich sample with trace pyrite
29 (-S-1, -S-2)	B	Poorly foliated feldspar and quartz rich sample with some muscovite and trace pyrite

Samples with -S notation were separated initially using SELFRAG pulsation, -F indicates Frantz magnetic separation, the remaining samples were separated by hand; molybdenite for all samples was very fine grained (<2mm). Relatively pure molybdenite mineral separates could not achieved for Hemlo samples, except for sample 14.

3.3 Analytical Methods

3.3.1 Sample Preparation and Mineralogical Analysis

In most cases, molybdenite separation was done manually by breaking specimens and isolating molybdenite grains by hand. Molybdenite grains were then crushed using an agate mortar and pestle. Larger molybdenite grains were examined with a table-top Hitachi scanning electron microscope (SEM) TM-3000 using a Brucker QUANTAX 70 Energy Dispersive X-ray Spectrometer (EDS) at the University of Waterloo. The molybdenite grains were observed to be homogeneous with no obvious crystal zoning.

The above approach could not be followed for most Hemlo samples (21-29), except for sample 14. Initially, disaggregation of rock samples was performed using SELFRAG high voltage pulse power fragmentation. However, the molybdenite was too fine-grained to achieve a pure mineral separation by hand. Subsequently, samples were powdered in a ball mill using agate jars. Mineral separation using heavy liquids, Frantz magnetic separation, and flotation in ultrapure water also did not result in a pure mineral separate.

To obtain a semi-quantitative estimate of sample mineralogy, X-ray diffraction (XRD) analysis was performed on bulk powdered samples from the Berg and Hemlo deposits at the University of Waterloo (Environmental Particle Analysis Laboratory of the Ecohydrology Research Group) using a PANanalytical Empyrean II with a Cu-x-ray tube (operated at 45 kV and 40 mA) and a PIXcel^{3D} detector. The detection limit for this method is 1% and samples were scanned for 1 hour with a 2θ angle in Bragg-Bretano geometry from 10° and 70°. Various phases were identified by Search-Mach candidates' spectra using HighScore Plus within both a Crystallography Open Database and PAN-ICSD reference database based on a "whole pattern" approach as described by Smith et al. (1987).

3.3.2 Sample dissolution and Mo purification

For all samples except those from the Hemlo deposit, the Mo isotope and trace element concentration data were collected from 0.1 g of separated and crushed molybdenite. Molybdenite samples were dissolved in reverse aqua regia (4 mL HNO_3 and 2 mL HCl) on a hot plate overnight in the W.M. Keck Foundation Laboratory for Environmental Biogeochemistry at Arizona State University. Subsequently, digested sample solutions were further diluted with 2% HNO_3 to make an 8 mL stock solution.

Molybdenite from the Hemlo deposit samples could not be separated by hand because of the trace molybdenite abundance and fine grain size of the molybdenite. Heavy liquid and Frantz magnetic separation techniques were also unsuccessful. Ultimately, a reverse aqua regia leach of the Hemlo material was performed at the Metal Isotope Geochemistry Laboratory at the University of Waterloo. The Mo was isolated and purified from the digested solution using a two-step column chemistry method (Duan et al., 2010) at the Metal Isotope Geochemistry Laboratory. First anion exchange chromatography using BioRad AG1-X8 resin was conducted to remove all matrix elements except Fe and Mo. Subsequently,

cation exchange chromatography was performed using BioRad AG50W-X8 resin to remove Fe and leave behind purified Mo.

3.3.3. Elemental Analyses

The Re concentration of the molybdenites was measured on a Thermo i-CAP quadrupole inductively coupled plasma mass spectrometer (Q-ICP-MS) at Arizona State University for all samples. Samples were diluted with 2% HNO_3 to a Mo concentration of about 300-400 ppb Mo to avoid excessive Mo contamination in the instruments. Instrumental drift was corrected using an internal standard solution (Sc, Ge, In, Bi) introduced into the Q-ICP-MS along with sample solutions. Instrumental accuracy was verified using secondary standards. For Hemlo samples, elemental analysis was also performed for Na, Mg, Al, K, Ca, Fe, Zn and Mo concentrations by Q-ICP-MS.

3.3.4. Mo Isotope Analyses

Mo isotope compositions and Mo concentrations were measured by MC-ICP-MS at Arizona State University using a Thermo Scientific Neptune instrument and a ^{97}Mo-^{100}Mo double spike to correct for mass fractionation during ion-exchange chromatography and Mo isotope analysis. Molybdenum isotope compositions were measured relative to an in-house standard (RochMo2) and then re-calculated relative to the Mo international standard NIST SRM 3134 (also measured alongside samples) using the following equation (Nägler et al., 2014):

$$\delta^{98}\text{Mo}_{\text{sample}}\ (‰) = 1000 \times [(^{98/95}\text{Mo}_{\text{sample}} / {}^{98/95}\text{Mo}_{\text{NIST SRM 3134}}) - 1] + 0.25$$

Previously, Goldberg et al. (2013) determined the international standard NIST SRM 3134 has a heavier isotopic composition (0.33 ± 0.05‰; 2SD, n = 99) than the in-house standard used at ASU (RochMo2). For this study, the measured value for standard NIST SRM 3134 was 0.33 ± 0.04‰; 2SD, n = 5 relative to RochMo2. Therefore, to report data relative to NIST SRM 3134 = 0.25‰, 0.08‰ was subtracted from each sample Mo isotope composition measured relative to RochMo2. The United States Geological Survey reference material (SDO-1) was measured during this study to verify instrumental accuracy. The average δ^{98}Mo was 1.07 ± 0.02‰ (2SD, n = 5) when normalized to NIST SRM 3134 = 0.25‰. This data is in good agreement with the average δ^{98}Mo reported for SDO-1 at ASU by Goldberg et al. (2013), which is 1.07 ± 0.11‰; 2SD, n = 145 (relative to NIST SRM 3134

= 0.25‰). The 2SD uncertainty of a sample is reported as the 2SD uncertainty of sample replicate measurements or 0.11‰ (the long-term uncertainty of SDO-1), whichever is greater.

3.3.5. S Isotope Analyses

To determine the isotopic composition of sulfur, approximately 0.01-0.05 g of separated and crushed molybdenite for each sample was measured using a Costech Element Analyzer coupled to an Isochrom Continuous Flow Stable Isotope Ratio Mass Spectrometer (EA-IRMS) at the Environmental Isotope Laboratory, University of Waterloo. The S isotopic composition is denoted as $\delta^{34}S$ relative to the standard V-CDT as seen in the following equation:

$$\delta^{34}S_{\text{sample}}\ (‰) = 1000 \times [(^{34/32}S_{\text{sample}} / {}^{34/32}S_{\text{V-CDT}}) - 1]$$

Very finely ground molybdenite separates were placed into tin capsules in a 1000ºC combustion furnace and combusted in the presence of oxygen, which raises the temperature and produces pure SO_2. Gas chromatography creates a SO_2 peak that is then ionized by the IRMS allowing the mass of unique S isotopes to be measured. Data for sulfide samples are corrected using standards such as IAEA-S1, IAEA-S2 and IAEA-S3 (AgS), EIL-40 (CuS), EIL-43 (ZnS), and NBS-123 (ZnS). The uncertainty for these clean sulfide standard materials is ± 0.3‰ (Rees, 1984; Morrison et al., 1996).

3.4 Results

The Mo isotopic composition for this study ranges from -0.60‰ to 5.34‰ (Table 4). The lowest Mo isotope signature came from the Logan Lake epithermal porphyry deposit. The Hemlo disseminated Au deposit was found to have the highest Mo isotope signature. The porphyry deposits in this study were found to have Mo isotopic compositions ranging from -0.29‰ at the Lake George deposit to 2.05‰ at the Trout Lake deposit. Multiple hand samples were collected for the Berg epithermal porphyry deposit and the Hemlo disseminated Au deposit. At the Berg deposit, the overall range for Mo isotopic compositions was nearly 1‰. The Hemlo deposit had a range of >5‰, greatly exceeding the range for any deposit or deposit type in this study.

The weight percent Mo was also determined by MC-ICP-MS double-spike method and the range observed for molybdenite separates (excluding Hemlo samples 21-29) span

from 31% to 73% with most samples close to 60% Mo by weight indicating a relatively pure mineral separate. As expected, Hemlo samples 21-29 had a low Mo concentration (0.36 to 13 weight %), which is why additional purification to isolate Mo was performed by column chemistry before Mo isotopic measurements were made.

The S isotope composition was determined for all samples except samples from the Hemlo deposit. Since pure molybdenite mineral separates were not obtained for Hemlo samples 21-29, S isotopic composition was not determined as it could represent other sulfide minerals (e.g., pyrite) and not just the molybdenite of interest. For several pure molybdenite separates, multiple measurements of S isotopic composition were taken from separate aliquots of the finely ground molybdenite separate (2SD <1‰). The range of S isotopic compositions spanned from -4.30‰ at the Childs-Adwinkle deposit to 7.12‰ at the Trout Lake deposit, both of which are porphyry deposits. The S and Mo isotope analyses were measured on different molybdenite crystals from the same hand sample and show no correlation.

The range of Re concentrations was determined for all samples and ranged from ppb levels to several hundred ppm for numerous porphyry (Santo Nino, Childs-Adwinkle, and Lake George) and epithermal porphyry deposits (Logan Lake and Berg). Molybdenite from the porphyry deposit at Childs-Adwinkle Mine in Arizona was found to have the highest concentrations of Re (>500 ppm). A weak negative correlation was observed between Re concentration and Mo isotopic composition for global porphyry deposit samples ($r^2 = 0.388$), multiple samples from the Berg deposit ($r^2 = 0.0346$), and multiple samples from the Hemlo deposit ($r^2 = 0.233$).

In addition to Re concentration, other elemental data was also collected for Hemlo samples. Elements include Na, Mg, K, Al, Ca, Fe, and Zn and are summarized in Table 5. Major element data could help in identification of possible Mo host phases at the Hemlo deposit. The range of elemental concentrations for the Hemlo deposit are as follows in ppm: Na = 20000 – 30000, Mg = 200 – 10000, Al = 4000 – 30000, K = 4000 – 60000, Ca = 3000 – 60000, Fe = 500 – 60000, and Zn = 500 – 30000. Analysis of mineral assemblages was also performed by XRD on bulk sample powders for the Hemlo and Berg deposits. Results are summarized in Table 6. A handful of samples from both deposits were found by XRD to have 1-2% molybdenite with 2H polytype; other samples had molybdenite abundances below the detection limit. Additional minerals identified by XRD include feldspathic minerals (albite,

anorthite, microcline, orthoclase, sanidine), muscovitic minerals (clinochlore, montmorillonite, muscovite) and other minerals (barite, calcite, clinoclase, dolomite, pyrite, quartz, sylvite). Most samples from the Hemlo deposit (7 out of 9 hand samples) had a greater percentage of feldspathic minerals compared to muscovitic mineral assemblages. At the Hemlo deposit, up to 9% pyrite was observed.

Table 4: Summary of new data from this study including Mo isotope compositions, Mo and Re concentrations, and S isotope compositions.

Deposit Type	Location	Sample ID	Re (ppm)	Mo (wt%)	δ^{98}Mo (‰)	N	2σ	δ^{34}S	n	2σ
Greisen	Beura, Ossa Valley, Italy	3A	7.3	60	0.33	1	n/a	0.52	3	0.36
		3B	6.6	57	0.32	1	n/a			
		3C	6.9	55	0.34	1	n/a			
Porphyry	Sach's Mine, NSW, Australia	1A	0.25	65	0.99	1	n/a	0.68	4	0.37
		1B	0.26	55	0.93	1	n/a			
		1C	0.25	57	0.95	1	n/a			
		1D	0.19	58	0.85	2	0.03			
		1E	0.12	61	0.97	1	n/a			
	Santo Nino Mine, Arizona	2A	205.4	65	0.25	2	0.04	0.81		1.00
		2B	112.5	61	0.24	1	n/a			
	Altenberg, Saxony Germany	4A	0.4	56	1.76	2	0.00	0.47	1	n/a
		4B	0.2	55	1.77	1	n/a			
	Childs-Adwinkle Mine, Arizona	5A	523.1	60	0.33	2	0.01	-4.30	1	n/a
		5B	430.8	53	0.43	2	0.02			
	Moly Hill, Quebec	6A	42.9	58	-0.15	2	0.01	-0.50	4	0.82
		6B	12.5	58	-0.02	1	n/a			
		6C	30.5	63	-0.08	1	n/a			
		6D	12.0	56	-0.03	1	n/a			
	Strzegom, Poland	8A	3.9	67	0.08	1	n/a	0.27	1	n/a
		8B	4.4	66	0.12	1	n/a			
	New Ross, Nova Scotia	11A	1.5	57	0.76	2	0.04	5.56	2	0.06
	Lake George, New Brunswick	12A	207.5	73	-0.19	2	0.00	-3.34	2	0.81
		12B	266.6	41	-0.29	2	0.09			
	Trout Lake, New Brunswick	13A	29.0	50	2.05	2	0.04	7.12	2	0.12
i k e M	Wolfram,	7A	7.3	46	0.10	1	n/a	2.27	3	0.57

	Queensland, Australia	7B	7.4	65	0.04	1	n/a			
		7C	7.7	59	0.07	1	n/a			
		7D	8.0	60	-0.11	2	0.03			
Epithermal Porphyry	Logan Lake, British Columbia	10A	428.2	51	-0.59	1	n/a	2.35	1	n/a
		10B	425.9	54	-0.60	1	n/a			
	Berg, British Columbia	9A	147.2	59	-0.13	1	n/a	1.01	2	0.43
		9B	144.6	58	-0.13	1	n/a			
		15A	72.3	32	-0.05	3	0.12	-1.10	2	0.08
		16A	129.2	70	0.77	3	0.01	1.48	4	0.28
		16B	125.1	54	0.77	3	0.07			
		17A	146.8	50	-0.17	3	0.01	-0.32	1	n/a
		18A	242.6	47	-0.03	3	0.03	-0.10	3	0.10
		18B	253.2	49	-0.06	3	0.10			
		19A	119.0	40	0.10	3	0.09	-0.80	2	0.04
		20A	108.4	43	-0.01	3	0.05	-1.28	2	0.03
		20B	103.4	45	0.00	3	0.04			
Disseminated Au	Hemlo, Ontario	14A	23.1	49	2.05	2	0.03	-3.34	1	n/a
		14B	25.7	31	2.04	1	n/a			
		14C	241.0	64	-0.25	3	0.02			
		21-1	0.08	0.36	2.10	3	0.03	n/a		
		22-1	0.52	0.36	1.47	3	0.03			
		22F	n/a	1.4	1.42	3	0.01			
		23-1	0.95	3.8	1.84	3	0.02			
		23-S	0.45	1.4	1.96	3	0.02			
		24-1	3.7	11	0.51	3	0.04			
		24F	n/a	2.4	0.54	3	0.03			
		24-S	4.1	13	1.38	3	0.04			
		25-S	0.12	n/a	n/a					
		26-S-1	0.12	3.3	1.72	3	0.08			
		27-S-1	0.24	0.61	1.54	3	0.01			
		27-S-2	0.36	0.62	1.42	3	0.02			
		28-S-1	0.05	n/a	n/a					
		28-S-2	0.16	n/a	n/a					
		29-S-1	0.15	0.44	5.32	3	0.05			
		29-S-2	0.24	0.49	5.34	3	0.01			

Table 5: Q-ICP-MS elemental data for all molybdenite mineral separates and reverse aqua regia leaches of Hemlo samples.

Sample ID	Na	Mg	Al	K	Ca	Fe	Zn	Mo
Unit	ppm	ppm	ppm	ppm	ppm	ppm	ppm	ppm
DL	1.7	0.068	0.47	1.3	1.5	0.3	0.069	0.0046

1A	n/a	<DL	<DL	682229	Berg, BC
1B		<DL	<DL	589851	
1C		470	<DL	631444	
1D		<DL	<DL	650183	
1E		<DL	<DL	709087	
2A		<DL	<DL	690172	
2B		801	<DL	615238	
3A		<DL	<DL	602964	
3B		<DL	<DL	596734	
3C		<DL	<DL	595360	
4A		852	<DL	574325	
4B		4093	<DL	572663	
5A		1696	<DL	602292	
5B		20982	<DL	538316	
6A		968	<DL	582443	
6B		<DL	<DL	575817	
6C		<DL	<DL	659563	
6D		<DL	<DL	579340	
7A		<DL	<DL	463161	
7B		<DL	<DL	646898	
7C		<DL	<DL	589509	
7D		589	<DL	604084	
8A		2219	<DL	669494	
8B		<DL	<DL	659295	
10A		17945	<DL	510531	
10B		13600	<DL	536359	
11A		1806	<DL	574297	
12A		2823	<DL	746010	
13A		6908	<DL	509939	
9A		1299	<DL	587256	
9B		1620	<DL	577557	
15A		15952	<DL	301020	
16A		13371	11009	115888	
16B		7176	1080	75160	
17A		<DL	<DL	462237	
18A		4924	8250	472447	
18B		2061	25923	449087	
19A		6122	4454	371191	
20A		11531	4453	408041	
20B		5422	5643	432875	
14A		53140	890	494331	

14B						24772	<DL	309062	
14C						1491	7705	404651	
21-1	26362	590	12469	6576	13094	104996	1038	2882	
22-1	30000	175	6075	5332	7550	334107	1322	2600	
23	30445	6839	21700	8771	20443	45887	840	17875	
23-S	26259	11418	29051	7270	20695	105141	4658	10730	
24	24677	1536	7398	5892	8741	76361	808	66402	
24-S	25036	344	3987	5323	2579	34835	487	36836	
25-S	29325	5587	13124	13431	57991	142622	3166	304	
26-S-1	23357	295	6919	5355	6523	1219	1253	17464	
27-S-1	17763	2172	12072	5520	15156	32154	627	4290	
27-S-2	20535	721	8333	3650	12226	32349	1383	3945	
28-S-1	19125	2118	7958	3870	11682	99541	795	44	
29-S-1	20254	1734	20637	62542	18367	13059	802	2956	

Abbreviations: DL = detection limit

Table 6: XRD results (as weight percent minerals) for the Berg and Hemlo samples.

Sample ID	Location	Albite	Anorthite	Microcline	Orthoclase	Sanidine	Clinochlore	Montmorillonite	Muscovite	Barite	Calcite	Clinoclase	Dolomite	Molybdenite 2H	Pyrite	Quartz	Sylvite	Total
15	**Berg, BC**		8		21	10		10			10	3		2	1	42	1	108
16		41	9		15			5								19		89
17		8	4					30			5		9			43		99
18		37	10		23	17		5								6		98
19		11	33		8	7		12			1		1			28		101
20			3					8			2	2	3	1		77		96
21	**Hemlo, ON**			22	15		2		29		2			1	3	27		101
22		8	10						42		6			1	5	29		101
23							4		37						1	58		100
24		3	10	25	17	22			13	1	1					6		98
25		5	11	14	16	22	1		20	1	1				1	7		99
26				29	19				20						2	29		99
27			12	12	17	15	4		9	5	10			2	8	4	2	100
28		4	10	10	20	16	2		28		2				1	6		99
29		18	17	4	6	20	2		18	1	1					13		100
		Feldspar Minerals					Muscovitic Minerals											

3.5 Discussion

3.5.1 Fingerprinting deposit type using Mo isotopes

Mathur et al. (2010a) suggested that the Mo isotopic signature of molybdenite may be useful for fingerprinting the deposit type. Their study included a total 33 samples from skarn, porphyry-type, epithermal polymetallic veins and Fe oxide Cu-Au deposits. Based on the new data from this study and the δ^{98}Mo molybdenite compilation from Breillat et al. (2016), representing 420 samples in total, there is no significant relationship between δ^{98}Mo and deposit type (Figure 5). Substantial overlap in δ^{98}Mo is observed across all deposit types. This expanded compilation also indicates that porphyry deposits can have higher δ^{98}Mo compositions than previously reported. The Hemlo disseminated Au deposit is unusual, however, in having the highest known δ^{98}Mo values compared to other deposits as well as other geological materials (Kendall et al., 2017).

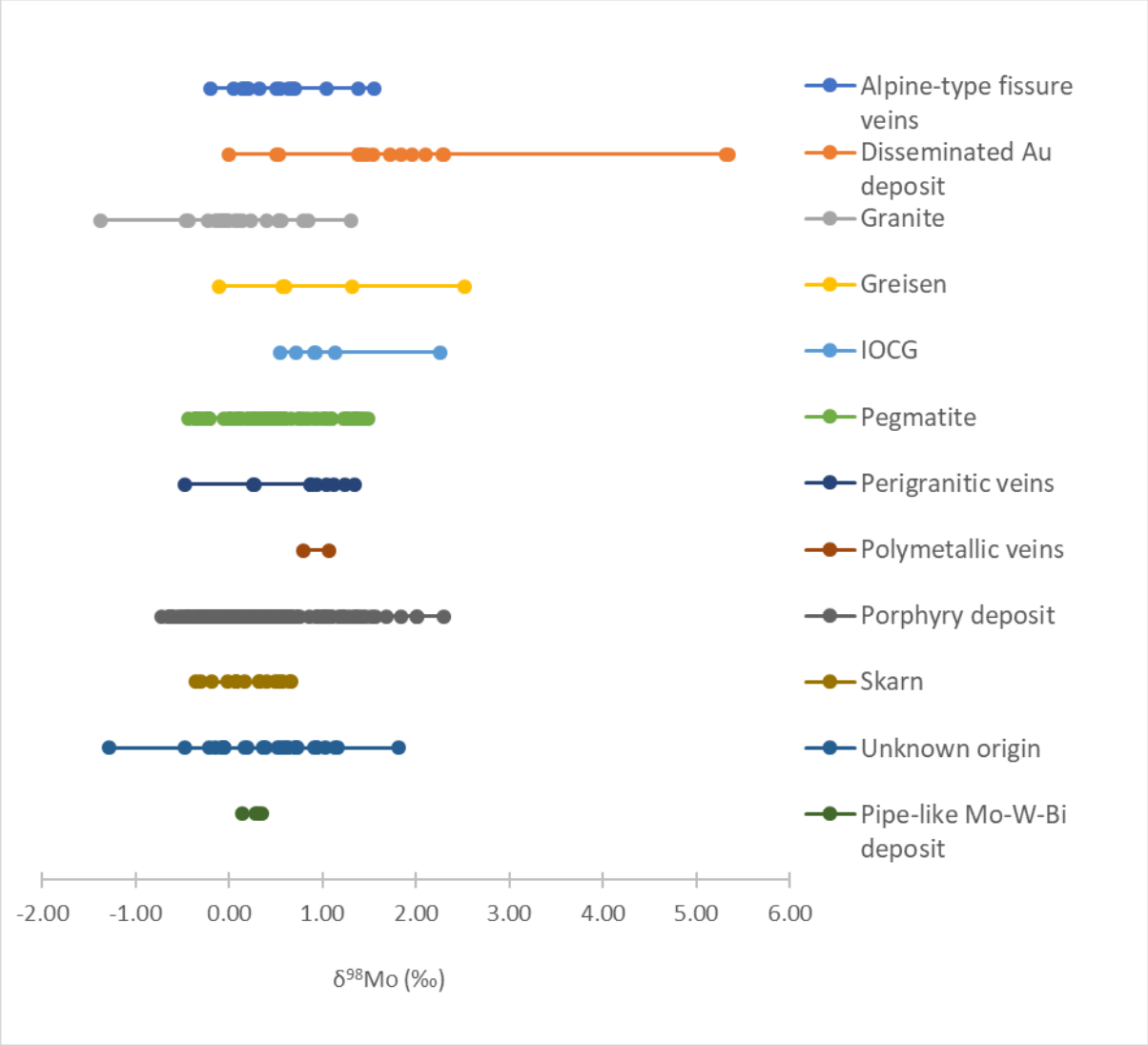

Figure 5: Compilation of Mo isotopic signatures for different deposit types (Breillat et al., 2016; Wang et al., 2016; Yao et al., 2016; this study). All data are reported relative to NIST SRM 3134 = 0.25‰.

3.5.2 Mo isotopes as an indicator for fluid temperature

Fluid temperature plays an important role in the fractionation of Mo isotopes in ore deposits (Greber et al., 2014; Shafiei et al., 2015; Breillat et al., 2016). However, there are two conflicting hypotheses for how temperature will influence Mo isotope fractionation. Greber et al. (2014) observed Mo partitioning between the fluid and crystal phases and suggested that high temperature fluids will precipitate the light Mo isotopes first. The mineralizing fluid will evolve towards a heavy Mo isotope signature as the system cools, leading to the precipitation of molybdenite with a heavier isotopic composition. The opposite trend was observed by Shafiei et al. (2015) where the Mo isotope signature of molybdenite gradually decreased with fluid evolution and decreasing temperatures. Shafiei et al. (2015) attribute the observed fractionation to fluid boiling which caused partitioning between vapour and brine phases. The data from this study and compilation correlates best with the proposal by Greber et al. (2014). In general, higher temperature systems were found to have lower average Mo isotope compositions (granite = 0.10‰, n = 25, 2SD = 1.03‰; porphyry = 0.20‰, n = 243, 2SD = 1.01‰; skarn = 0.36‰, n = 42, 2SD = 0.70‰) compared to lower temperature systems (pegmatites = 0.48‰, n = 80, 2SD = 1.05‰; perigranitic = 0.75‰, n = 10, 2SD = 1.12‰; greisen = 0.79‰, n = 6, 2SD = 1.93‰), which is consistent with conclusions from Breillat et al. (2016). Temperature is not the only control on the Mo isotope composition of molybdenite, however, and other fractionation mechanisms must also be considered.

3.5.3 Defining the average Mo isotopic signature for molybdenites

Based on the Mo isotope compilation in this study, there is no significant correlation between the Mo isotopic signature and the age of the deposit (Figure 6). Consistent with studies by Hannah et al. (2007) and Breillat et al. (2016), this observation implies that there are no major first-order temporal changes in the isotopic composition of the sources to the fluids that crystallize molybdenite as well as the isotopic composition of molybdenite sources of Mo to rivers and the oceans from oxidative weathering of the upper continental crust. The large suite of data can be used to define an average δ^{98}Mo signature for molybdenites, which is calculated to be 0.37‰ (n = 479; 2SD = 1.3‰). It is worth noting that the highest recorded

Mo isotopic composition is from the oldest (late Archean) sample. The average molybdenite δ^{98}Mo is slightly higher than the average Mo isotopic signature of approximately 0.3‰ for granites and basalts (Voegelin et al., 2014) and similar to the estimated maximum upper crustal value of 0.4‰ (Willbold and Elliott, 2017), which is consistent with predictions by Greber et al. (2014). The Mo isotopic composition of molybdenite likely represents the maximum average for both the upper continental crust and bulk continental crust because hydrothermal fluids have on average an isotopically heavier signature than their source magmas (Greber et al., 2014; Voegelin et al., 2014; Willbold and Elliott, 2017). The average crustal Mo isotope composition is useful to help constrain the Mo isotope composition of Mo inputs to rivers and oceans, which will enhance the use of Mo isotopes as a tool for estimating ocean paleoredox conditions.

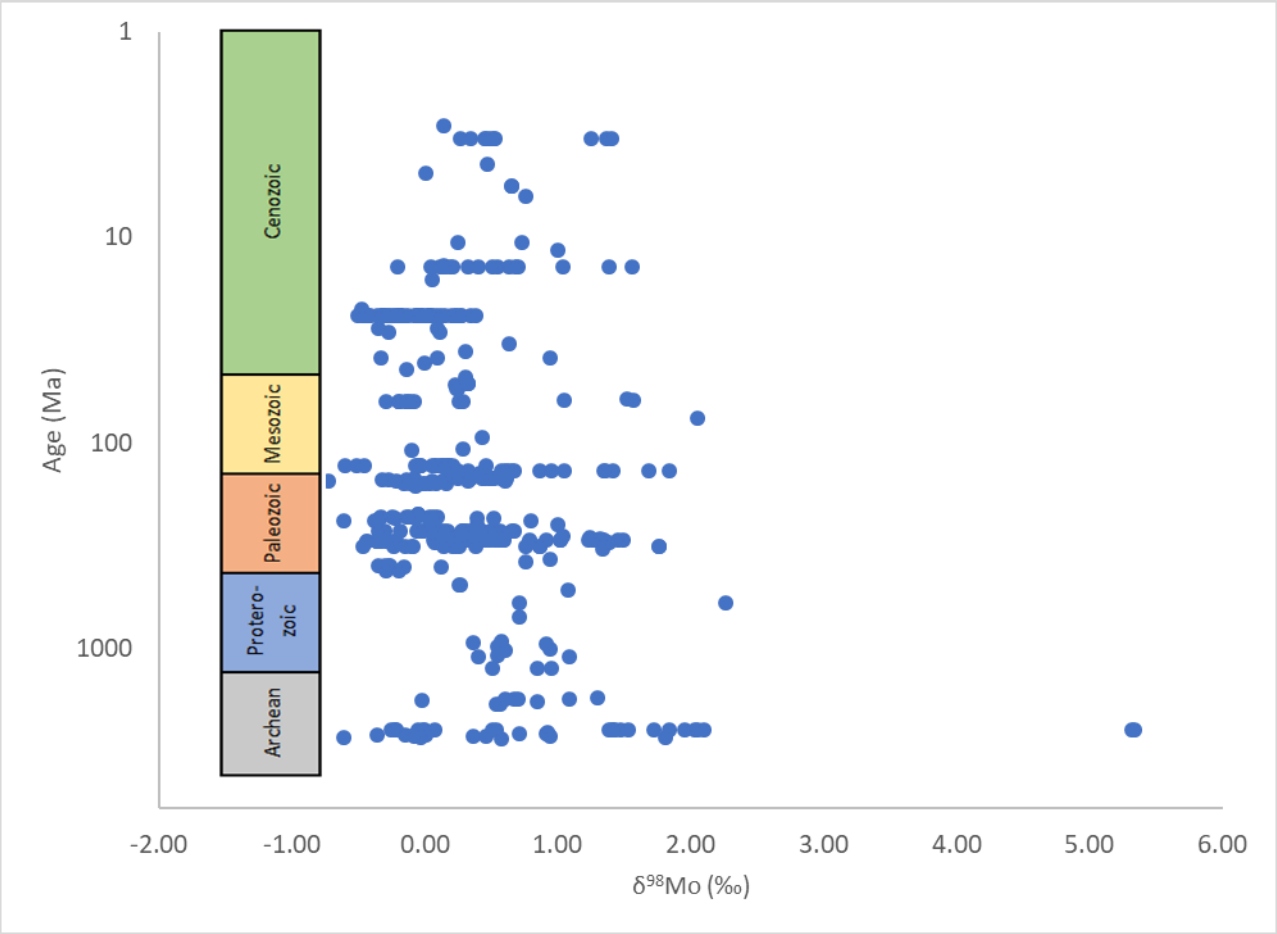

Figure 6: Relationship between deposit age and Mo isotopic composition.

3.5.4 Mo isotopes vs elemental concentrations

Previous studies have shown that the δ^{98}Mo of molybdenites generally inversely correlates with the Re concentration of molybdenites on ore-deposit and regional scales (Mathur et al., 2010a; Wang et al., 2016). This relationship may be useful for indicating the Mo isotopic composition of different fluid sources (Wang et al., 2016). Figure 7 shows the new Mo isotope data from molybdenite mineral separates in this study (excluding the Hemlo deposit) combined with the previous work of Mathur et al. (2010a) and Wang et al. (2016). From this figure, a weak inverse relationship between Re concentration and Mo isotopic composition is observed for porphyry deposits (r^2 = 0.388). The correlation is weak compared to previous studies because these samples are from multiple deposits and represent a global scale. The Re concentrations from the Berg epithermal porphyry deposit have little correlation with Mo isotopic composition, although it is noted that the range of Re concentrations and Mo isotope compositions is small (Figure 8; r^2 = 0.0346). Most impure molybdenite separates from the Hemlo disseminated Au deposit have Re concentrations very close to the detection limit but they also maintain a weak inverse relationship with Mo isotopic composition (r^2 = 0.2333).

At a regional scale, Wang et al. (2016) found that samples with a high Re concentration and a low Mo isotope signature indicate a mantle-derived source fluid, whereas samples with a low Re concentration close to zero and a high Mo isotope signature indicate a source with more crustal influence. Hybrid magmas with a mix of both crustal and mantle source fluids have a Mo isotopic signature near 0.25‰ relative to NIST SRM 3134 = 0.25‰ (Wang et al., 2016). For samples with Mo isotopic signature greater than 1.5‰, the Re concentrations are uniformly low. The variability in Figure 7 indicates mixing of the crustal and mantle-derived fluids along with further Mo isotope fractionation by mechanisms such as fluid boiling or redox conditions. The Mo isotope fractionations associated with ore-forming processes can muddle the relationship between Mo isotope composition, Re concentration, and metal source.

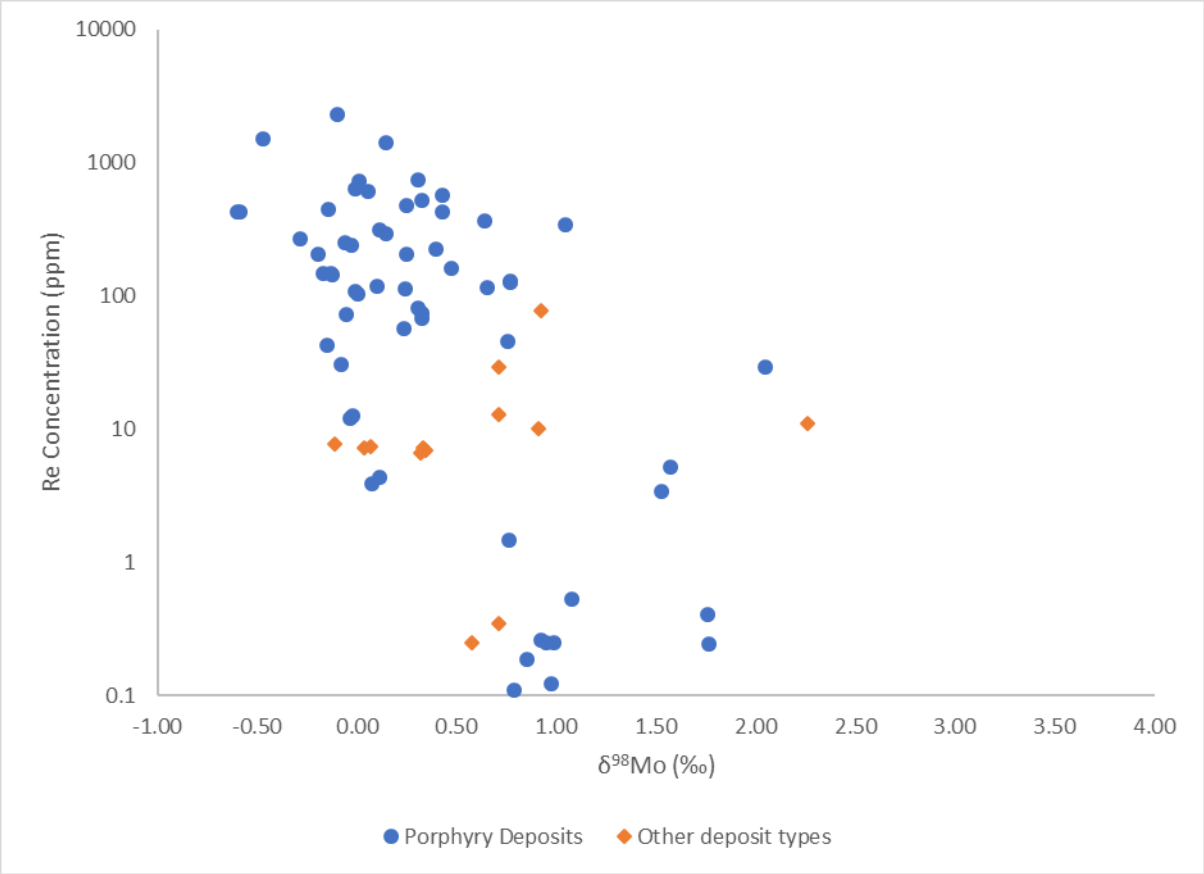

Figure 7: Re concentration vs Mo isotopic composition of pure molybdenite separates from all deposits (excluding Hemlo) from this study and compiled literature data (Mathur et al., 2010a; Wang et al., 2016).

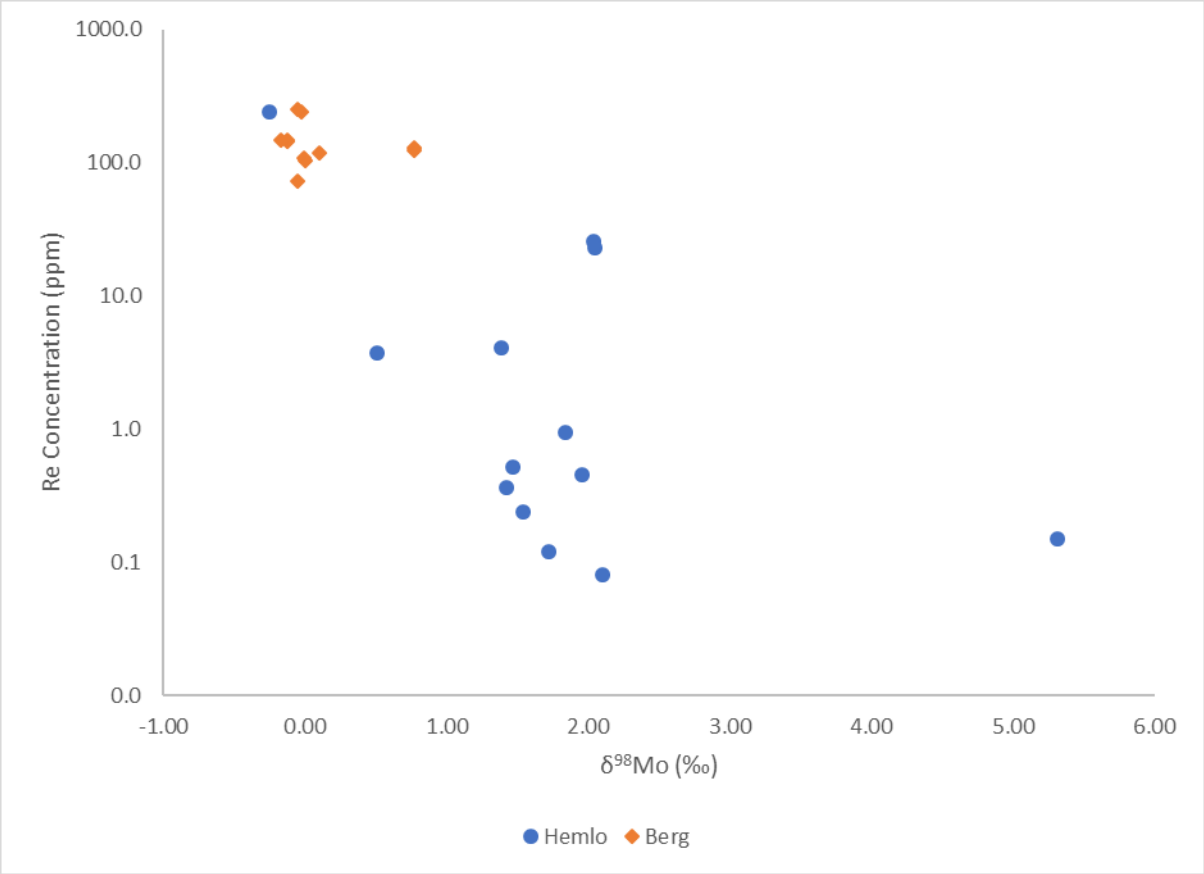

Figure 8: The Re concentration vs Mo isotopic composition of relatively pure molybdenite separates from the Berg deposit and impure mineral separates from the Hemlo deposit.

The element Fe can also be found as a trace element in molybdenite and Mo is a common trace element in pyrite that is roughly 46% Fe by weight. Although pyrite has a much lower Mo concentration than molybdenite, it is likely the primary crustal source for Mo due to the much greater abundance of pyrite in the crust compared to molybdenite (Miller et al., 2011). Molybdenite mineral separates were analyzed for their Fe concentration. Fe concentration data compared to the molybdenite isotopic composition for all deposits, excluding Hemlo, is summarized in Figure 9 and no trend was observed. Although no trend was observed, a relationship may exist for the Hemlo deposit because whole rock analysis revealed that several Hemlo samples are rich in pyrite, often exceeding the abundance of molybdenite in the whole rock. Also, initial attempts to separate molybdenite by hand were ineffective, and elemental data by Q-ICP-MS revealed that many of these samples have high concentrations of Fe. One of the Hemlo samples was observed to have approximately 33% Fe by weight, which may indicate the mineral separate contained more pyrite than molybdenite (Figure 10). Since some of the mineral separates for the Hemlo deposit likely represent pyrite and not molybdenite, the Fe concentration was compared to the Mo isotopic composition to

determine if any correlation exists. This data is summarized in Figure 10; again, no correlation was found.

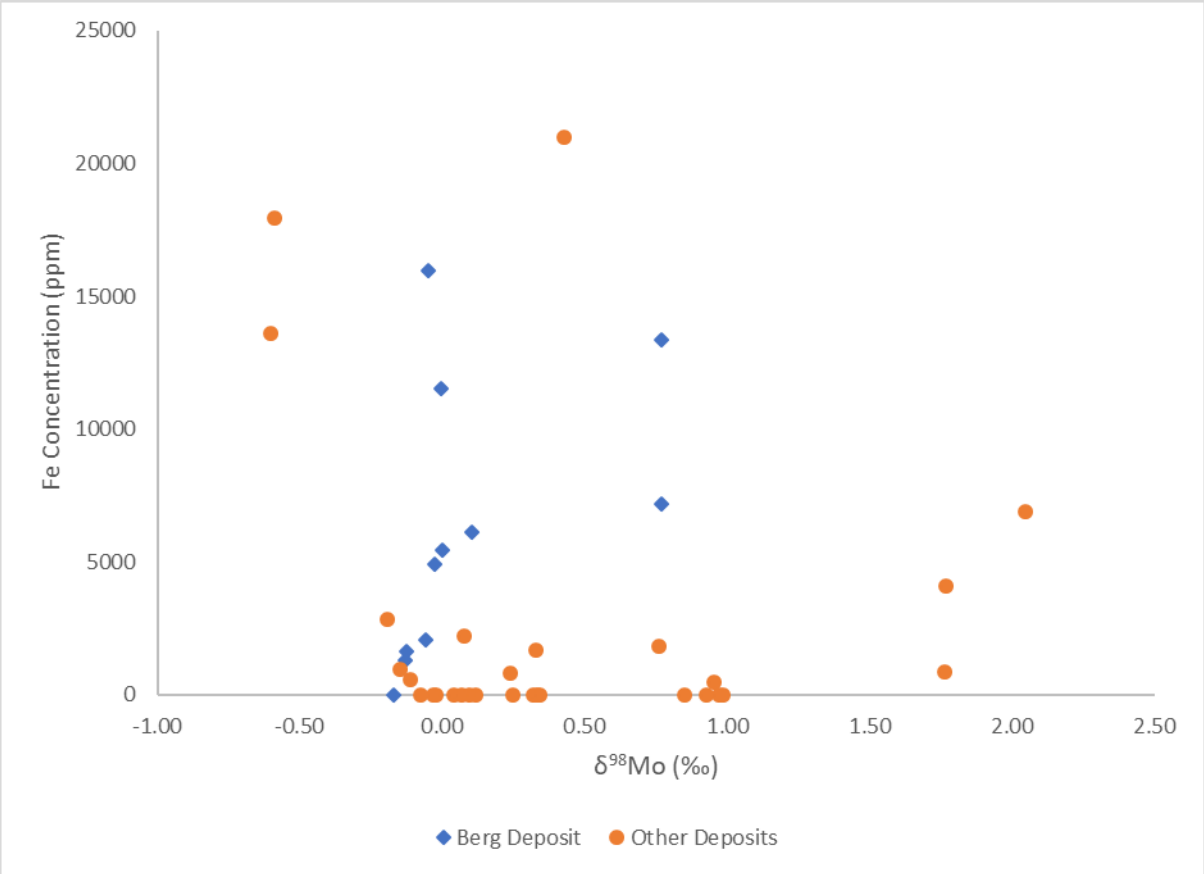

Figure 9: Fe concentration of molybdenite mineral separate for all samples (excluding Hemlo) plotted against the Mo isotopic composition.

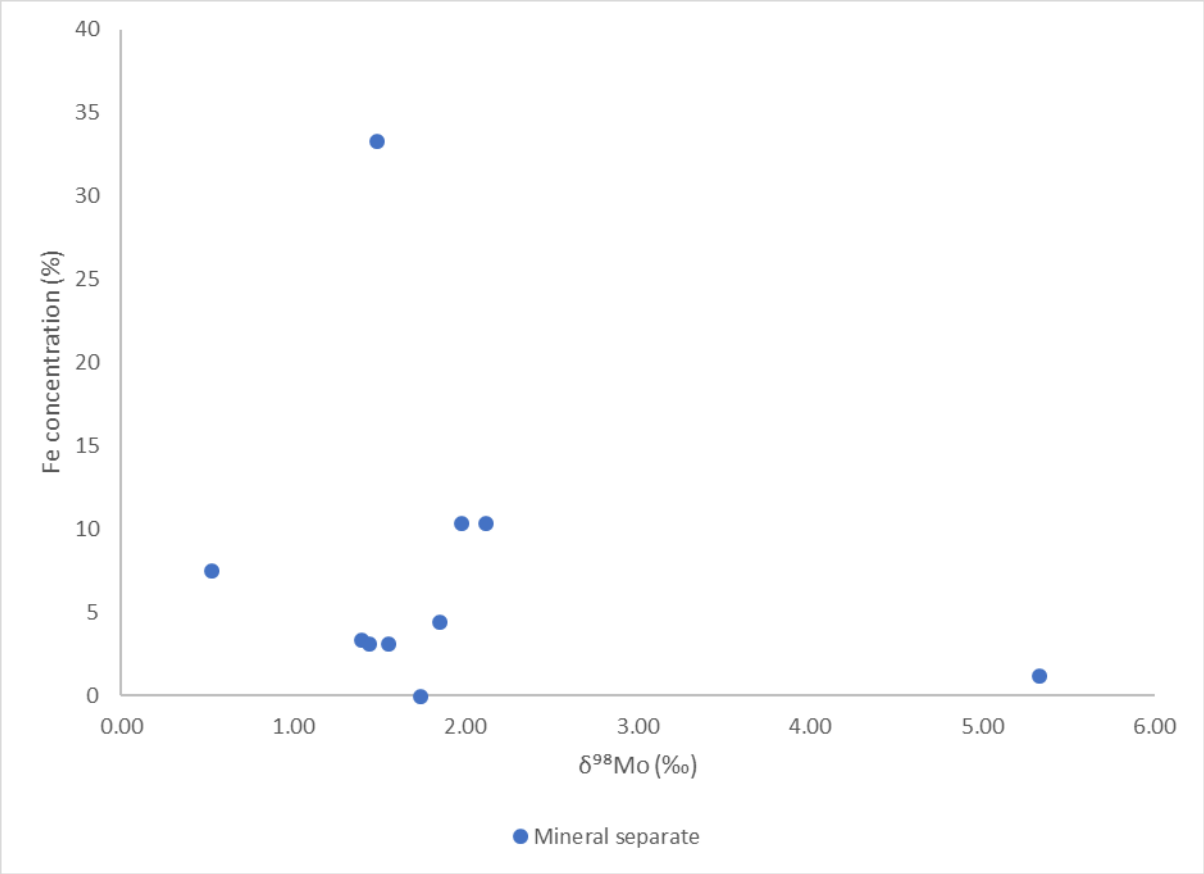

Figure 10: Fe concentration of mineral separate plotted against the Mo isotopic composition for Hemlo deposit samples.

The Mo isotopic composition can also be compared to the Mo concentration of the samples to see if a relationship exists. Many samples in this study were digested from relatively pure molybdenite separates therefore the expected Mo composition is 60% by weight. However, some samples were distinctly less than 60% by weight and hence these samples were not pure mineral separates. The Hemlo samples have Mo concentrations substantially less than 60% (from <1% to 13%) and hence required additional chemical purification to isolate the Mo for isotope analysis. The concentration of Mo does not appear to be a control on the Mo isotopic composition when comparing the entire molybdenite separates dataset (Figure 11) as well as individual deposits (Figure 12). As seen in Figure 11, the concentration of Mo for these samples is very low (<20%) and it is likely that for samples with a high Fe % by weight, the Mo isotope signature represents pyrite rather than molybdenite.

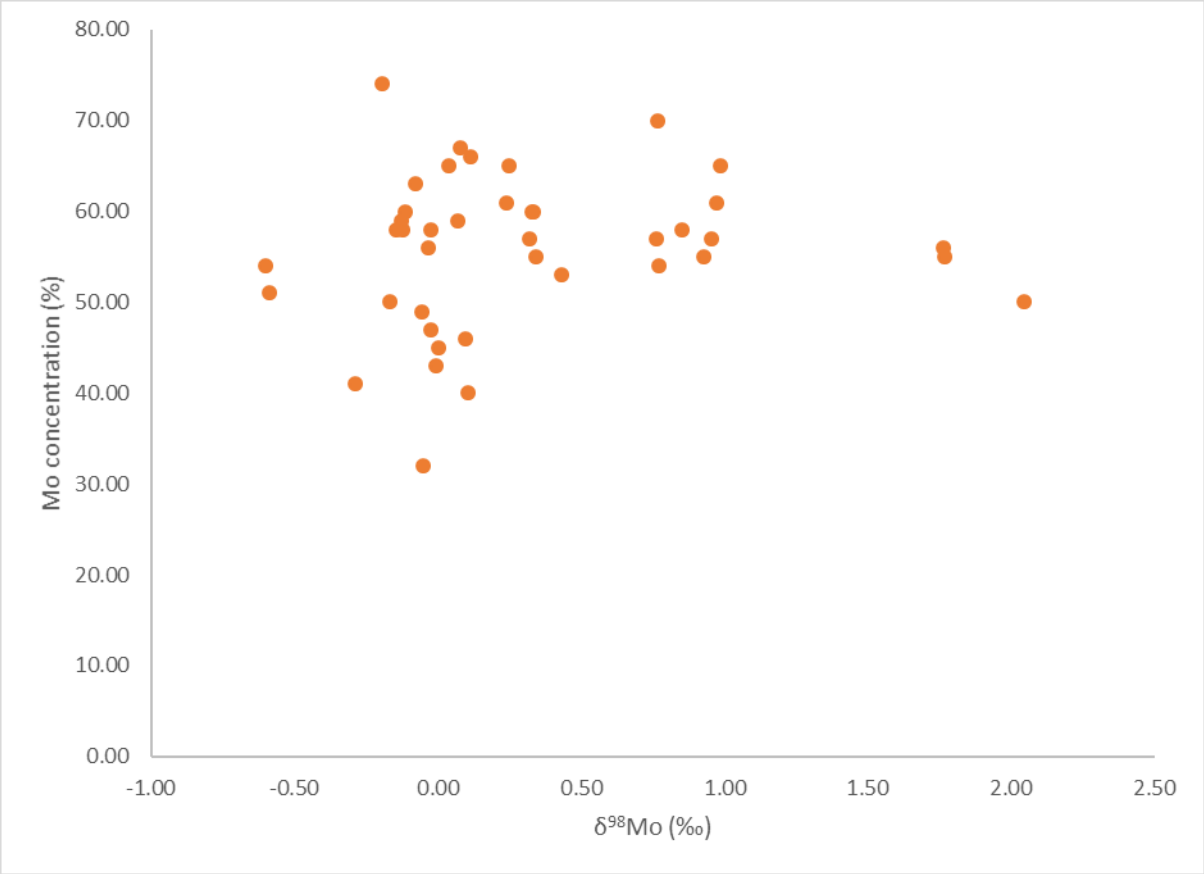

Figure 11: Mo concentration determined by MC-ICP-MS sample-double spike method compared to Mo isotopic composition for all pure molybdenite separates (all samples, excluding Hemlo).

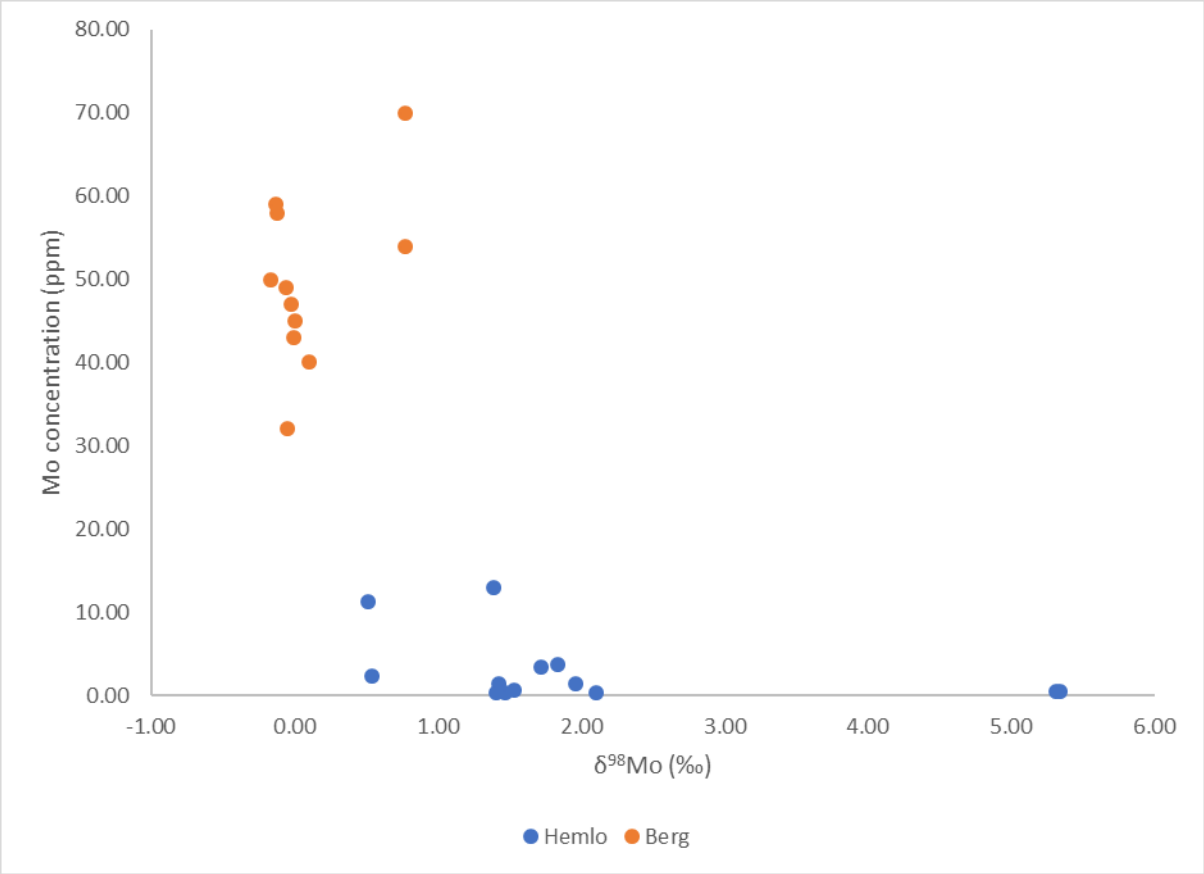

Figure 12: Mo concentration determined by the MC-ICP-MS sample-double spike method compared to Mo isotopic composition for pure molybdenite separates from the Berg deposit and impure mineral separates from the Hemlo deposit.

3.5.5 Mo isotopes vs S isotopes

Rayleigh distillation is a possible mechanism of Mo isotope fractionation in ore deposits (Hannah et al., 2007; Greber et al., 2011; Greber et al., 2014). Molybdenite is approximately 40% S by weight and S is known to experience Rayleigh distillation as a main fractionation mechanism (Hannah et al., 2007). Therefore, measuring the degree of covariation between Mo and S isotope compositions in molybdenites from a single deposit can shed light on whether Rayleigh distillation also plays an important role in Mo isotope fractionation. If a positive relationship between the two isotope systems is observed in an ore-forming system with limited Mo and S availability, then Rayleigh distillation is the main mechanism of isotope fractionation (Hannah et al., 2007). In Figure 13, the S isotopic composition is plotted against Mo isotopic composition for samples collected in this study (excluding the Hemlo deposit) and no correlation is observed. Focusing on just the Berg deposit or only porphyry-type deposits also does not yield a good correlation. It is possible that Rayleigh distillation still plays an important role in the fractionation of Mo isotopes for

some deposits, but this would be more clearly depicted on a local scale. Using a global sample suite, the variability in ore-forming conditions including the effects of multiple mineralization events, source fluid, fluid boiling, fluid mixing, water-rock interaction and late low temperature alteration may cause poor correlations with S isotope compositions.

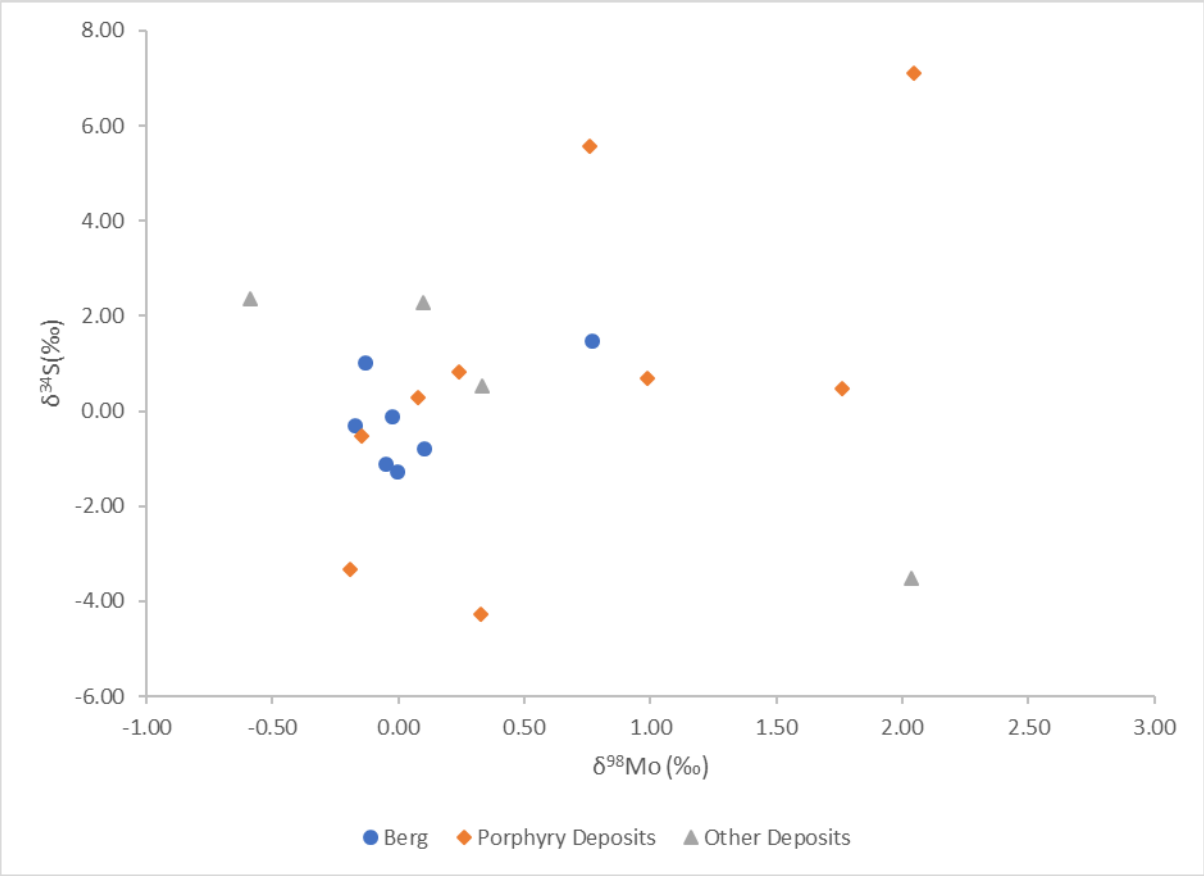

Figure 13: No clear correlation was observed between Mo and S isotopic compositions for molybdenites.

3.5.6 Mo isotope variation in a single deposit

Greber et al. (2014) found variation within a single deposit can extend to greater than 1.0‰. In this study, several hand samples were collected from the Eocene Berg epithermal-porphyry deposit and the Archean Hemlo disseminated Au deposit. The Mo isotope data from these two deposits are summarized in Figure 14. Mo isotopic variation from the Berg deposit is approximately 0.3‰ with one isotopically heavier sample expanding this range to 1‰. The range of Mo isotope variation is similar to that observed in previous studies of Mo isotope fractionation in a single porphyry deposit (Hannah et al., 2007; Mathur et al., 2010a; Greber et al., 2011, 2014; Shafiei et al., 2015; Breillat et al., 2016). By comparison, the Hemlo

deposit has a much wider range of Mo isotope variation of >5‰, ranging from -0.25‰ to 5.34‰. This range is much greater than the range of Mo isotope compositions previously recorded for any deposit type and indicates significant Mo mobility and isotope fractionation occurred at the Hemlo deposit.

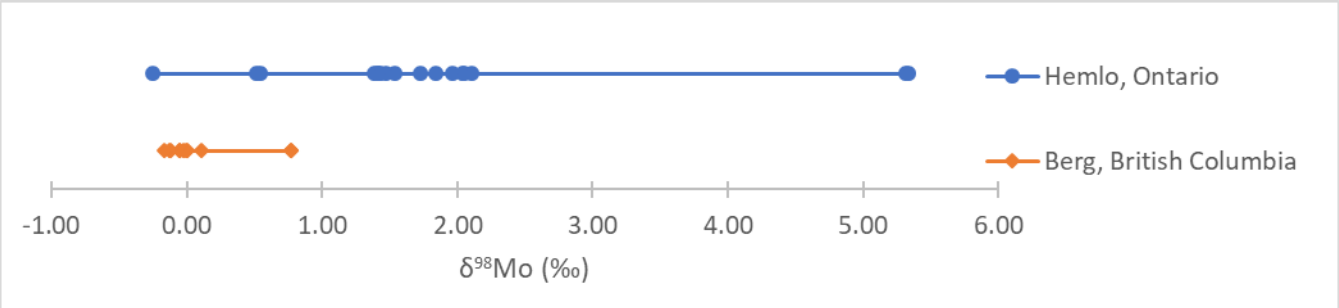

Figure 14: Range of Mo isotopic compositions observed at a single deposit.

The range of Mo isotopic compositions observed at the Hemlo disseminated Au deposit suggest that the processes responsible for Mo isotope fractionation will lead to a higher Mo isotopic composition. The Shafiei et al. (2015) model of decreasing Mo isotopic signature over time through liquid-vapour partitioning will not fit the Hemlo data because a starting isotope composition of the Mo source fluid would need to exceed 5‰. At the Hemlo disseminated Au deposit, redox conditions were likely a major control on molybdenite mineralization (Heiligmann et al., 2008; Phillips and Powell, 2010). Under reducing conditions, the first molybdenites precipitated with a lighter Mo isotope signature. As molybdenites precipitated, the residual fluid evolved to a heavier isotopic composition. Therefore, redox fractionation stemming from molybdenite crystallization in the presence of S-rich reducing fluids is a possible mechanism responsible for the high Mo isotopic signatures observed at this deposit.

At the Hemlo deposit, the feldspathic and muscovitic mineral assemblages represent two separate Mo mineralization events (Lin, 2001; Muir, 2002; Heiligmann et al., 2008). Samples with a higher percentage of muscovitic minerals had a smaller range of Mo isotopic compositions (1.42‰ to 1.96‰) compared to samples with more than 50% feldspathic minerals which span the entire range of observed Mo isotopic compositions at the Hemlo deposit. The high-grade Mo associated with the feldspar mineral assemblage was precipitated first, which may indicate secondary alteration led to further Mo isotopic fractionation up to 5‰. The amount of feldspar minerals, muscovitic minerals and/or quartz was found to have little influence on the Mo isotopic composition for samples from the Berg deposit (Figure

15B). Elemental data for the impure mineral separates from the Hemlo deposit revealed that the sample with the highest known Mo isotope signature had over 6% potassium by weight prior to Mo purification (Figure 16). Based on whole rock XRD analysis, this sample had significant amounts of K-rich feldspars and muscovite which would comprise nearly 6% K by weight. Therefore, the high K concentration observed in the mineral separate is likely another indication that initial separation of molybdenite was ineffective.

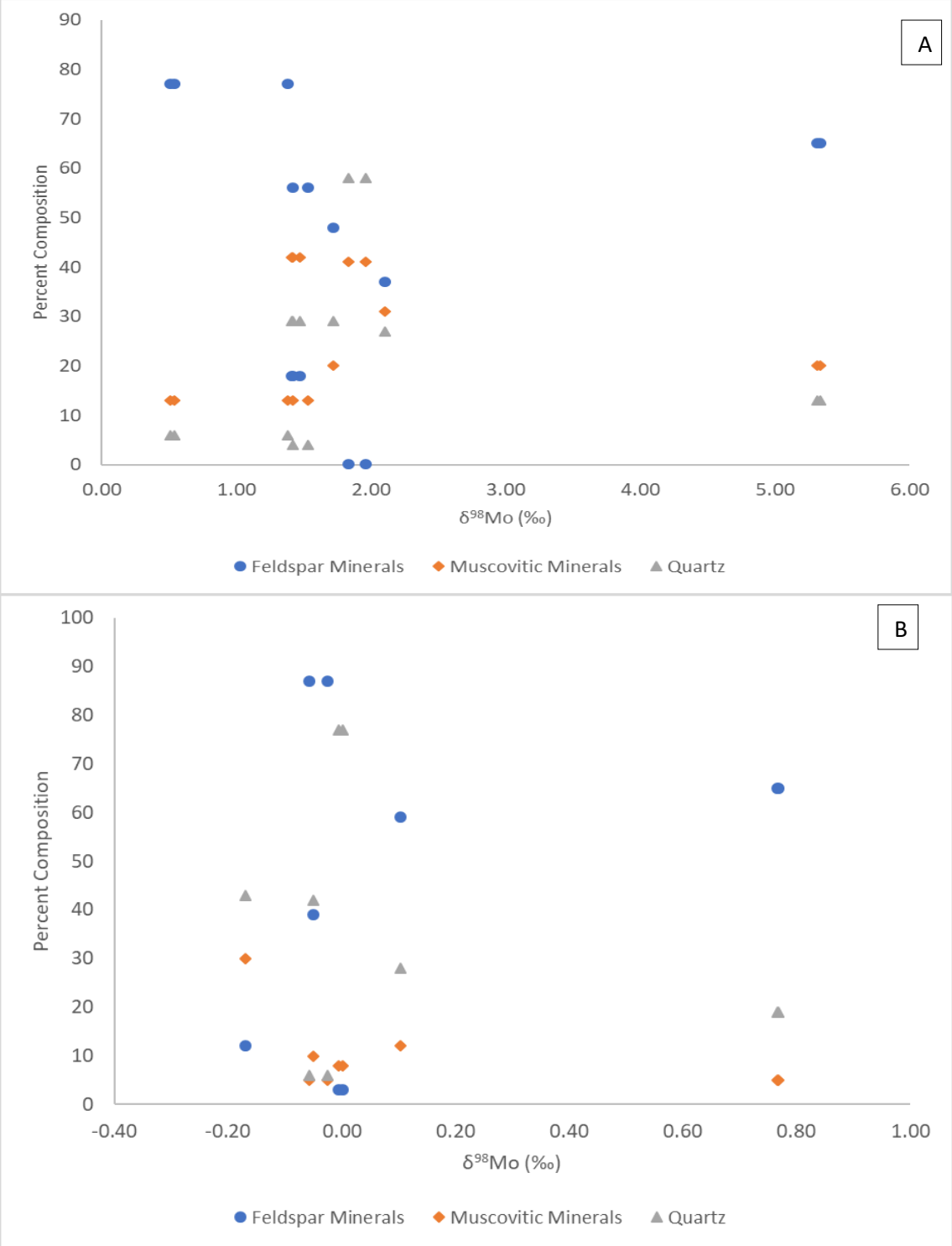

Figure 15: A: Mineral composition of the whole rock samples from the Hemlo deposit compared to the Mo isotopic composition of the isolated and purified molybdenum; B: Mineral composition of the whole rock samples from the Berg deposit compared to the Mo isotopic composition of the molybdenite separates.

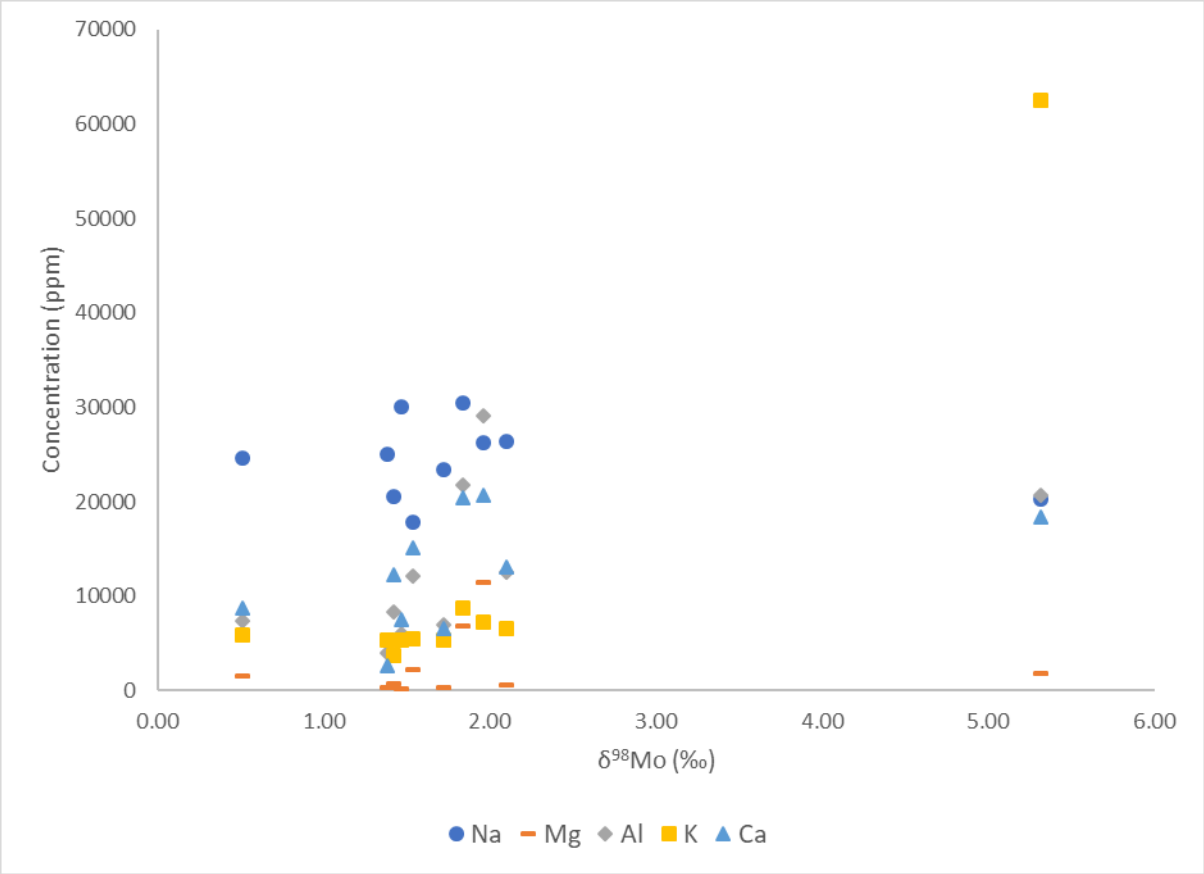

Figure 16: Hemlo sample elemental data from reverse aqua regia leaches of the impure molybdenite mineral separates compared to Mo isotopic composition after Mo purification.

3.5.7 Mo isotope variation in hand samples and single grains

Significant variability in the Mo isotope composition of molybdenites can occur for specific categories of ore deposits (> 2‰) and even within single deposits (> 1‰), including at the cm-scale (Hannah et al., 2007; Mathur et al., 2010a; Greber et al., 2011, 2014; Shafiei et al., 2015; Breillat et al., 2016). To test this hypothesis, several measurements were made for different molybdenite grains from the same hand sample for 20 hand samples from various deposit types. For most hand samples, variation did not exceed ~0.2‰. The average observed variation for δ^{98}Mo in a single hand sample is 0.06‰ (n=18), which is within the long-term analytical reproducibility of the Neptune MC-ICP-MS instrument at ASU. By contrast, significant Mo isotope fractionation at the hand sample scale was observed in 2 samples from the Hemlo disseminated Au deposit. Sample 24 (Mo = 2.4-13 weight %) yielded a range in δ^{98}Mo of 0.87‰ (n=3, 2SD = 0.99‰) and sample 14 (the best pure

molybdenite mineral separate from this deposit; Mo = 31-64 weight %) had an even wider range of 2.30‰ (n=3, 2SD = 5.3‰). These exceptions are consistent with the cm-scale variability observed by Greber et al. (2011) although the range of fractionation observed is much greater. The variation observed in the two samples could be attributed to lithological variation at the hand sample scale compared to the other samples. Remobilization of Mo at the hand-sample scale for the Hemlo deposit is another possibility but is considered less likely given that Mo isotope variability was not observed for other Hemlo samples.

Using coarse grained molybdenite, the Mo isotope variability within a single grain of molybdenite was also tested. Four large (>1 cm) molybdenite grains were selected; 2 grains from the Sach's Mine porphyry deposit in Australia, 1 grain from the Moly Hill porphyry deposit in Quebec, and one 1 large grain from the pipe-like Mo-Bi-W Wolfram deposit. These grains were cut parallel to cleavage and/or across cleavage planes. Variation in a single grain was observed to be no more than ~0.1‰ (2SD = 0.2‰), which is not readily distinguishable from the long-term analytical reproducibility. These findings agree with the SEM results of homogeneous molybdenite crystals with no zoning, and suggest limited isotopic zoning occurs in single molybdenite grains.

3.6 Conclusions

By expanding on previous data compilations of the Mo isotopic composition of molybdenites, this study has furthered understanding on Mo cycling during ore deposit formation. The range of Mo isotopic compositions was greatly expanded from -1.37‰ to 5.34‰ and the average molybdenite composition is now calculated to be 0.37‰ (n=479, 2SD = 1.3‰), which can be used to define the upper limit for the average upper crust Mo isotope composition, in agreement with the upper limit of 0.40‰ suggested recently by Willbold and Elliott (2017). It is unlikely that Mo isotopic signatures from molybdenites or reverse aqua regia digests of molybdenite-bearing rocks can be used as a tool to fingerprint deposit type or the age of the deposit (Breillat et al., 2016). There does, however, appear to be a relationship between Mo isotopic composition and temperature as well as Mo source fluid. High temperature deposits such as granites, skarns and porphyries tend to have a lower signature than relatively low temperature pegmatite or greisen deposits (Breillat et al., 2016). The slight negative correlation between Mo isotope signature and Re concentration suggests mantle fluids produce lower Mo isotopic signatures than fluids with more crustal influence (Mathur

et al, 2010a; Wang et al., 2016). However, these trends can be hidden if the deposit has experienced additional Mo isotope fractionation after the initial mineralization event.

This study also confirmed the work of Greber et al. (2014) and found some Mo isotopic variability can occur at the hand sample scale. However, little isotopic variation was observed when looking at individual molybdenite grains and no zoning was observed using SEM. The range of Mo isotopic variability in a single deposit was greatly expanded, with the Archean Hemlo disseminated Au deposit shown to exceed 5‰. The Hemlo deposit also has the highest recorded Mo isotope signature to date of 5.34‰. This high Mo isotope signature best fits the model proposed by Greber et al. (2014) where the Mo isotope signature of hydrothermal fluids gradually increases over time through removal of lighter Mo isotopes during relatively low temperature alteration.

There are many possible fractionation mechanisms for Mo isotopes in ore deposits. These include fluid-boiling, redox conditions, and Rayleigh distillation. The lack of correlation between Mo and S isotopic composition means Rayleigh distillation cannot be identified as the primary mechanism for Mo isotope fractionation. It is likely that a combination of fractionation mechanisms affect Mo cycling in the ore system. At the Hemlo deposit, redox conditions were identified as possible fractionation mechanism. The fractionation mechanism, temperature of fluids and fluid source must all be considered when interpreting the Mo isotopic signature of an ore deposit.

Chapter 4: Conclusion

4.1 Summary of Findings

This thesis began with 5 distinct objectives. In chapter 2, a detailed review of heavy metal isotope systems in ore deposits was conducted. This review focused on isotope systems that have been studied in detail, namely Cu and Zn. Other less-studied isotope systems were also reviewed including Mo, Fe, Pb and U, as well as systems still in their infancy, such as Hg, Se, Ni and Ge. By reviewing these isotope systems, patterns emerged that guided interpretation of new Mo isotope data in Chapter 3. The difference between mass dependent (eg. Cu, Zn) and volume dependent isotope fractionation (e.g., U) was explored. A variety of mass-dependent isotope fractionation mechanisms were examined including redox

conditions, Rayleigh distillation, fluid boiling, and fluid-vapor partitioning. Some systems such as Cu were observed to gradually evolve to a higher isotope signature in the mineral, whereas other isotope systems such as Zn had the opposite trend. This review provided a solid foundation for Chapter 3 and helped to build and expand on comprehension of Mo cycling in ore deposits thus satisfying objective 1.

The second objective of this study was to generate a Mo isotope data compilation for molybdenites and use this data to infer the maximum average upper crustal Mo isotope signature. A total of 479 molybdenite samples were used in this compilation by combining previous work with new data from this study. The average crustal molybdenite composition was calculated to be 0.37‰ relative to NIST SRM 3134 = 0.25‰. This average is similar to a previous estimate of the maximum Mo isotope composition for the upper continental crust (0.40‰; Willbold and Elliott, 2017). The range of Mo isotopic signatures for molybdenites has been expanded to >5‰ with several measurements exceeding 2‰ relative to NIST SRM 3134 = 0.25‰. This data was then used to disprove the hypothesis by Mathur et al. (2010a) as it was determined that the Mo isotopic composition could not be used to fingerprint the deposit type. However, data from this study did support the hypothesis by Breillat et al. (2016) that high temperature deposits have a generally lower Mo isotopic composition compared to low temperature deposits.

Using the new dataset from this study of 14 different deposits, objective 3 was accomplished by determining Mo isotopic variability at a small scale. This study found that average variation observed in most hand samples (0.06‰) was within the MC-ICP-MS instrument reproducibly. Two hand samples greatly exceeded this variation (0.87‰ and 2.30‰) which agrees with previous findings of small scale variation by Greber et al. (2014). When examining a single molybdenite grain parallel and/or perpendicular to cleavage, very little variation was observed (~0.1‰).

The fourth objective of this project involved comparing Mo isotopic composition to Re concentrations and S isotope compositions to determine if a correlation exists. First, the Mo isotopic composition was compared to the Re concentration since Re is known to substitute for Mo into the molybdenite crystal lattice. A negative correlation was observed, which agrees with studies by Mathur et al. (2010a) and Wang et al. (2016), suggesting that the Mo source fluid (mantle vs. crustal) has some influence on the resulting Mo isotope signature. Second, the Mo isotopic composition was compared to the S isotopic composition

since molybdenite is roughly 40% S by weight. If a positive correlation was observed, this would indicate that Rayleigh distillation is the main mechanism for fractionation of Mo isotopes. However, this trend was not observed at any scale. This does not mean Rayleigh distillation is not a Mo isotope fractionation mechanism, just that it is not the sole mechanism responsible for fractionation and that further low temperature fractionation mechanisms may cause decoupling of Mo and S isotope signatures.

The final objective of this project was to take a detailed look at Mo isotopic behavior in a single deposit. To achieve this, multiple hand samples were collected from the Eocene epithermal-porphyry deposit in Berg, BC as well as the Archean disseminated Au deposit in Hemlo, ON. Hand samples from the Hemlo deposit had some very unexpected results. The highest recorded Mo isotopic composition for molybdenite of 5.34‰, as well as the widest range of Mo isotopic variation in a single deposit, were measured at this late Archean deposit. This is further evidence that supports the model for increasing Mo isotope signatures in mineralizing systems with further low temperature alteration as proposed by Greber et al. (2014).

4.2 Future Work

The completion of this project has offered valuable insights into Mo cycling in ore systems. The presence of very high Mo isotope signatures, particularly at the Archean Hemlo deposit, show that further low temperature alteration is likely to result in the light Mo isotopes being preferentially incorporated into minerals, resulting in an isotopically heavy residual fluid that can impart heavy Mo isotope compositions to minerals during later-stage alteration. The dominant fractionation mechanisms for ore deposits in general are still unclear. Based on these findings, it is likely that a combination of fluid-boiling, Rayleigh distillation, fluid-vapor partitioning, and redox conditions (either through S-rich fluids or meteoric fluids) play a role in Mo isotope fractionation in ore deposits. Further work is still needed to experimentally determine Mo fractionation factors and clarify how various fractionation mechanisms influence partitioning of Mo isotopes in ore systems.

There is still a lot of work to be done before Mo isotopes can be refined into a useful exploration tool, however, the potential is there. The wide range of observed Mo isotopic compositions as well as the scope of deposit types that molybdenite is found in make continued study of this system a valuable and interesting avenue for continued geochemical

and economic geology research. The success of isotope systems such as Cu and Zn have motivated research in this field and it is clear that less studied systems such as Mo and other isotope systems mentioned in Chapter 2 also have great potential to be refined for improving ore genetic models and exploration applications.

References

Abe, M., Suzuki, T., Fujii, Y., Hada, M., & Hirao, K. (2008). An ab initio molecular orbital study of the nuclear volume effects in uranium isotope fractionations. *The Journal of chemical physics*, *129*(16), 164309

Abouchami, W., Galer, S. J. G., De Baar, H. J. W., Alderkamp, A. C., Middag, R., Laan, P., Feldmann, H., & Andreae, M. O. (2011). Modulation of the Southern Ocean cadmium isotope signature by ocean circulation and primary productivity. *Earth and Planetary Science Letters*, *305*(1), 83-91.

Albarede, F., Telouk, P., Blichert-Toft, J., Boyet, M., Agranier, A., & Nelson, B. (2004). Precise and accurate isotopic measurements using multiple-collector ICPMS1. *Geochimica et Cosmochimica Acta*, *68*(12), 2725-2744.

Anbar, A. D. (2004). Molybdenum stable isotopes: observations, interpretations and directions. *Reviews in Mineralogy and Geochemistry*, *55*(1), 429-454.

Anbar, A. D., Jarzecki, A. A., & Spiro, T. G. (2005). Theoretical investigation of iron isotope fractionation between Fe (H 2 O) 6 3+ and Fe (H 2 O) 6 2+: implications for iron stable isotope geochemistry. *Geochimica et Cosmochimica Acta*, *69*(4), 825-837.

Asadi, S., Mathur, R., Moore, F., & Zarasvandi, A. (2015). Copper isotope fractionation in the Meiduk porphyry copper deposit, Northwest of Kerman Cenozoic magmatic arc, Iran. *Terra Nova*, *27*(1), 36-41.

Asael, D., Matthews, A., Bar-Matthews, M., & Halicz, L. (2007). Copper isotope fractionation in sedimentary copper mineralization (Timna Valley, Israel). *Chemical Geology*, *243*(3-4), 238-254.

Asael, D., Matthews, A., Oszczepalski, S., Bar-Matthews, M., & Halicz, L. (2009). Fluid speciation controls of low temperature copper isotope fractionation applied to the Kupferschiefer and Timna ore deposits. *Chemical Geology*, *262*(3-4), 147-158.

Barling, J., Arnold, G. L., & Anbar, A. D. (2001). Natural mass-dependent variations in the isotopic composition of molybdenum. *Earth and Planetary Science Letters*, *193*(3), 447-457.

Beard BL, Johnson CM, Skulan JL, Nealson KH, Cox L, Sun H (2002) Application of Fe isotopes to tracing the geochemical and biological cycling of Fe. Chem Geol 195: 87–117

Berkenbosch, H. A., de Ronde, C. E. J., Paul, B. T., & Gemmell, J. B. (2015). Characteristics of Cu isotopes from chalcopyrite-rich black smoker chimneys at Brothers volcano, Kermadec arc, and Niuatahi volcano, Lau basin. Mineralium Deposita, 50(7), 811-824.

Braxton D, Mathur R (2011) Exploration applications of copper isotopes in the supergene environment: A case study of the Bayugo porphyry copper-gold deposit, Southern Philippines. Econ Geol 106: 1447-1463

Breillat, N., Guerrot, C., Marcoux, E., & Négrel, P. (2016). A new global database of δ 98 Mo in molybdenites: a literature review and new data. *Journal of Geochemical Exploration*, *161*, 1-15.

Brennecka, G. A., Weyer, S., Wadhwa, M., Janney, P. E., Zipfel, J., & Anbar, A. D. (2010). 238U/235U variations in meteorites: Extant 247Cm and implications for Pb-Pb

dating. *science*, *327*(5964), 449-451.
Candela, P. A., & Holland, H. D. (1984). The partitioning of copper and molybdenum between silicate melts and aqueous fluids. *Geochimica et Cosmochimica Acta*, *48*(2), 373-380.
Cao, X. (1989). Solubility of molybdenite and the transport of molybdenum in hydrothermal solutions.
Carruzzo, S., Kontak, D. J., Clarke, D. B., & Kyser, T. K. (2004). An integrated fluid–mineral stable-isotope study of the granite-hosted mineral deposits of the New Ross area, south mountain batholith, Nova Scotia, Canada: evidence for multiple reservoirs. *The Canadian Mineralogist*, *42*(5), 1425-1441.
Cavallo, A., Bigioggero, B., Colombo, A., & Tunesi, A. (2004). The Beola: a dimension stone from the Ossola Valley (NW Italy). *Periodico di Mineralogia*, *73*(3), 85-97.
Chen, J. B., Gaillardet, J., Dessert, C., Villemant, B., Louvat, P., Crispi, O., & Wang, Y. N. (2014). Zn isotope compositions of the thermal spring waters of La Soufrière volcano, Guadeloupe Island. *Geochimica et Cosmochimica Acta*, *127*, 67-82.
Debret, B., Millet, M. A., Pons, M. L., Bouilhol, P., Inglis, E., & Williams, H. (2016). Isotopic evidence for iron mobility during subduction. Geology, 44(3), 215-218.
Dekov, V. M., Rouxel, O., Asael, D., Hålenius, U., & Munnik, F. (2013). Native Cu from the oceanic crust: Isotopic insights into native metal origin. *Chemical Geology*, *359*, 136-149.
Duan, X., Weinstock-Guttman, B., Wang, H., Bang, E., Li, J., Ramanathan, M., & Qu, J. (2010). Ultrasensitive quantification of serum vitamin D metabolites using selective solid-phase extraction coupled to microflow liquid chromatography and isotope-dilution mass spectrometry. *Analytical chemistry*, *82*(6), 2488-2497.
Duan, J., Tang, J., & Lin, B. (2016). Zinc and lead isotope signatures of the Zhaxikang PbZn deposit, South Tibet: Implications for the source of the ore-forming metals. *Ore Geology Reviews*, *78*, 58-68.
Ducher, M., Blanchard, M., & Balan, E. (2016). Equilibrium zinc isotope fractionation in Zn-bearing minerals from first-principles calculations. *Chemical Geology*, *443*, 87-96.
Ehrlich, S., Butler, I., Halicz, L., Rickard, D., Oldroyd, A., & Matthews, A. (2004). Experimental study of the copper isotope fractionation between aqueous Cu (II) and covellite, CuS. *Chemical Geology*, *209*(3-4), 259-269.
Elliott, T., & Steele, R. C. (2017). The isotope geochemistry of Ni. *Reviews in Mineralogy and Geochemistry*, *82*(1), 511-542.
Escoube, R., Rouxel, O. J., Luais, B., Ponzevera, E., & Donard, O. F. (2012). An intercomparison study of the germanium isotope composition of geological reference materials. *Geostandards and Geoanalytical Research*, *36*(2), 149-159.
Farges, F., Siewert, R., Brown, G. E., Guesdon, A., & Morin, G. (2006). Structural environments around molybdenum in silicate glasses and melts. I. Influence of composition and oxygen fugacity on the local structure of molybdenum. *The Canadian Mineralogist*, *44*(3), 731-753.
Faure G., and T. Mensing, 2005. Isotopes: Principles and Applications. 3rd Ed. John Wiley.
Fujii, T., Moynier, F., Pons, M. L., & Albarède, F. (2011). The origin of Zn isotope fractionation in sulfides. *Geochimica et Cosmochimica Acta*, *75*(23), 7632-7643.

Gagnevin, D., Boyce, A. J., Barrie, C. D., Menuge, J. F., & Blakeman, R. J. (2012). Zn, Fe and S isotope fractionation in a large hydrothermal system. *Geochimica et Cosmochimica Acta*, *88*, 183-198.

Goldberg, T., Gordon, G., Izon, G., Archer, C., Pearce, C. R., McManus, J., Anbar, A. D., & Rehkämper, M. (2013). Resolution of inter-laboratory discrepancies in Mo isotope data: an intercalibration. *Journal of Analytical Atomic Spectrometry*, *28*(5), 724-735.

Golden, J., McMillan, M., Downs, R. T., Hystad, G., Goldstein, I., Stein, H. J., Zimmerman, A., Sverjensky, D. A., Armstrong, J. T., & Hazen, R. M. (2013). Rhenium variations in molybdenite (MoS2): Evidence for progressive subsurface oxidation. *Earth and Planetary Science Letters*, *366*, 1-5.

Graham, S., Pearson, N., Jackson, S., Griffin, W., & O'reilly, S. Y. (2004). Tracing Cu and Fe from source to porphyry: in situ determination of Cu and Fe isotope ratios in sulfides from the Grasberg Cu–Au deposit. *Chemical Geology*, *207*(3-4), 147-169.

Greber, N. D., Hofmann, B. A., Voegelin, A. R., Villa, I. M., & Nägler, T. F. (2011). Mo isotope composition in Mo-rich high-and low-T hydrothermal systems from the Swiss Alps. *Geochimica et cosmochimica acta*, *75*(21), 6600-6609.

Greber, N. D., Pettke, T., & Nägler, T. F. (2014). Magmatic–hydrothermal molybdenum isotope fractionation and its relevance to the igneous crustal signature. *Lithos*, *190*, 104-110.

Gueguen, B., Rouxel, O., Ponzevera, E., Bekker, A., & Fouquet, Y. (2013). Nickel Isotope Variations in Terrestrial Silicate Rocks and Geological Reference Materials Measured by MC-ICP-MS. *Geostandards and Geoanalytical Research*, *37*(3), 297-317.

Haest, M., Muchez, P., Petit, J. C., & Vanhaecke, F. (2009). Cu isotope ratio variations in the Dikulushi Cu-Ag deposit, DRC: Of primary origin or induced by supergene reworking?. *Economic Geology*, *104*(7), 1055-1064.

Halliday A.N., Lee D.C., Christensen J.N., Rehkamper M., Yi W., Luo X., Hall C.M., Ballentine C.J., Pettke T., Stirling C. (2000) Multiple-Collector Inductively Coupled Plasma Mass Spectrometry. Inorganic Mass Spectrometry: Fundamentals and Applications, Marcel Dekker Inc., p. 292-307.

Hannah, J. L., Stein, H. J., Wieser, M. E., De Laeter, J. R., & Varner, M. D. (2007). Molybdenum isotope variations in molybdenite: Vapor transport and Rayleigh fractionation of Mo. *Geology*, *35*(8), 703-706.

Heberlein, D. R., Fletcher, W. K., & Godwin, C. I. (1983). Lithogeochemistry of hypogene, supergene and leached cap samples, Berg Porphyry Copper Deposit, British Columbia. *Journal of Geochemical Exploration*, *19*(1-3), 595-609.

Heiligmann, M., Williams-Jones, A. E., & Clark, J. R. (2008). The role of sulfate-sulfide-oxide-silicate equilibria in the metamorphism of hydrothermal alteration at the Hemlo gold deposit, Ontario. *Economic Geology*, *103*(2), 335-351.

Hess, F. L. (1924). *Molybdenum deposits*. Washington: Government Printing Office.

Hoffmann, U., Breitkreuz, C., Breiter, K., Sergeev, S., Stanek, K., & Tichomirowa, M. (2013). Carboniferous–Permian volcanic evolution in Central Europe—U/Pb ages of volcanic rocks in Saxony (Germany) and northern Bohemia (Czech Republic). *International Journal of Earth Sciences*, *102*(1), 73-99.

Hofmann, A., Bekker, A., Dirks, P., Gueguen, B., Rumble, D., & Rouxel, O. J. (2014).

Comparing orthomagmatic and hydrothermal mineralization models for komatiite-hosted nickel deposits in Zimbabwe using multiple-sulfur, iron, and nickel isotope data. *Mineralium Deposita*, *49*(1), 75-100.

Hou, K., Li, Y., Gao, J., Liu, F., & Qin, Y. (2014). Geochemistry and Si–O–Fe isotope constraints on the origin of banded iron formations of the Yuanjiacun Formation, Lvliang Group, Shanxi, China. *Ore Geology Reviews*, *57*, 288-298.

Housh, T. B., & Çiftçi, E. (2008). Cu isotope geochemistry of volcanogenic massive sulphide deposits of the eastern Pontides, Turkey. In *IOP Conference Series: Earth and Environmental Science* (Vol. 2, No. 1, p. 012025). IOP Publishing.

Huang, J. H., Huang, F., Evans, L., & Glasauer, S. (2015). Vanadium: Global (bio) geochemistry. Chemical Geology, 417, 68-89.

Huemann, K. G., Gallus, S. M., Rädlinger, G., & Vogl, J. (1998). Precision and accuracy in isotope ratio measurements by plasma source mass spectrometry. *Journal of Analytical Atomic Spectrometry*, *13*(9), 1001-1008.

Ikehata, K., & Hirata, T. (2012). Copper isotope characteristics of copper-rich minerals from the Horoman peridotite complex, Hokkaido, northern Japan. *Economic Geology*, *107*(7), 1489-1497.

Jamieson-Hanes, J. H., Shrimpton, H. K., Veeramani, H., Ptacek, C. J., Lanzirotti, A., Newville, M., & Blowes, D. W. (2017). Evaluating zinc isotope fractionation under sulfate reducing conditions using a flow-through cell and in situ XAS analysis. *Geochimica et Cosmochimica Acta*, *203*, 1-14.

John, S. G., Rouxel, O. J., Craddock, P. R., Engwall, A. M., & Boyle, E. A. (2008). Zinc stable isotopes in seafloor hydrothermal vent fluids and chimneys. *Earth and Planetary Science Letters*, *269*(1-2), 17-28.

Johnson, C. M., Beard, B. L., Roden, E. E., Newman, D. K., & Nealson, K. H. (2004). Isotopic constraints on biogeochemical cycling of Fe. *Reviews in mineralogy and geochemistry*, *55*(1), 359-408.

Johnson, T. M., & Bullen, T. D. (2004). Mass-dependent fractionation of selenium and chromium isotopes in low-temperature environments. *Reviews in mineralogy and geochemistry*, *55*(1), 289-317.

Kelley, K. D., Wilkinson, J. J., Chapman, J. B., Crowther, H. L., & Weiss, D. J. (2009). Zinc isotopes in sphalerite from base metal deposits in the Red Dog district, Northern Alaska. *Economic Geology*, *104*(6), 767-773.

Kendall, B., Brennecka, G. A., Weyer, S., & Anbar, A. D. (2013). Uranium isotope fractionation suggests oxidative uranium mobilization at 2.50 Ga. *Chemical Geology*, *362*, 105-114.

Kendall, B., Komiya, T., Lyons, T. W., Bates, S. M., Gordon, G. W., Romaniello, S. J., Jiang, G., Creaser, R. A., Xiao, S., McFadden, K., Sawaki, Y., Tahata, M., Shu, D., Han, J., Li, Y., Chu, X., & Anbar A. D. (2015). Uranium and molybdenum isotope evidence for an episode of widespread ocean oxygenation during the late Ediacaran Period. *Geochimica et Cosmochimica Acta*, *156*, 173-193.

Kendall, B., Dahl, T. W., & Anbar, A. D. (2017). The stable isotope geochemistry of molybdenum. *Reviews in Mineralogy and Geochemistry*, *82*(1), 683-732.

King, B. (2004). Minerals explained 39: Molybdenite. *Geology Today*, *20*(1), 34-37.

Klemm, L. M., Pettke, T., & Heinrich, C. A. (2008). Fluid and source magma evolution of the Questa porphyry Mo deposit, New Mexico, USA. *Mineralium Deposita*, *43*(5), 533.

Larson, P. B., Maher, K., Ramos, F. C., Chang, Z., Gaspar, M., & Meinert, L. D. (2003). Copper isotope ratios in magmatic and hydrothermal ore-forming environments. *Chemical Geology*, *201*(3-4), 337-350.

Layton-Matthews, D., Leybourne, M. I., Peter, J. M., Scott, S. D., Cousens, B., & Eglington, B. M. (2013). Multiple sources of selenium in ancient seafloor hydrothermal systems: Compositional and Se, S, and Pb isotopic evidence from volcanic-hosted and volcanic-sediment-hosted massive sulfide deposits of the Finlayson Lake District, Yukon, Canada. *Geochimica et Cosmochimica Acta*, *117*, 313-331.

Leonard, P. R. R., Lentz, D. R., & Poujol, M. (2006). Petrology, geochemistry, and U-Pb (zircon) age of the quartz-feldspar porphyry dyke at the Lake George antimony mine, New Brunswick: implications for origin, emplacement process, and mineralization.

Li, W., Jackson, S. E., Pearson, N. J., Alard, O., & Chappell, B. W. (2009). The Cu isotopic signature of granites from the Lachlan Fold Belt, SE Australia. *Chemical Geology*, *258*(1-2), 38-49.

Lin, S. (2001). Stratigraphic and structural setting of the Hemlo gold deposit, Ontario, Canada. *Economic Geology*, *96*(3), 477-507.

Mahan, B., Siebert, J., Pringle, E. A., & Moynier, F. (2017). Elemental partitioning and isotopic fractionation of Zn between metal and silicate and geochemical estimation of the S content of the Earth's core. *Geochimica et Cosmochimica Acta*, *196*, 252-270.

Maher, K. C., & Larson, P. B. (2007). Variation in copper isotope ratios and controls on fractionation in hypogene skarn mineralization at Coroccohuayco and Tintaya, Peru. *economic geology*, *102*(2), 225-237.

Maher, K. C., Jackson, S., & Mountain, B. (2011). Experimental evaluation of the fluid–mineral fractionation of Cu isotopes at 250° C and 300° C. *Chemical Geology*, *286*(3-4), 229-239.

Malinovsky, D., Rodushkin, I., Baxter, D. C., Ingri, J., & Öhlander, B. (2005). Molybdenum isotope ratio measurements on geological samples by MC-ICPMS. *International Journal of Mass Spectrometry*, *245*(1-3), 94-107.

Malinovsky, D., Hammarlund, D., Ilyashuk, B., Martinsson, O., & Gelting, J. (2007). Variations in the isotopic composition of molybdenum in freshwater lake systems. *Chemical Geology*, *236*(3-4), 181-198.

Mao, J., Zhaochong, Z., Zuoheng, Z., & Andao, D. (1999). Re-Os isotopic dating of molybdenites in the Xiaoliugou W (Mo) deposit in the northern Qilian mountains and its geological significance. *Geochimica et Cosmochimica Acta*, *63*(11-12), 1815-1818.

Markl, G., Von Blanckenburg, F., & Wagner, T. (2006). Iron isotope fractionation during hydrothermal ore deposition and alteration. *Geochimica et Cosmochimica Acta*, *70*(12), 3011-3030.

Mason, T. F., Weiss, D. J., Chapman, J. B., Wilkinson, J. J., Tessalina, S. G., Spiro, B., Horstwood, M. S. A., Spratt, J., & Coles, B. J. (2005). Zn and Cu isotopic variability in the Alexandrinka volcanic-hosted massive sulphide (VHMS) ore deposit, Urals, Russia. *Chemical Geology*, *221*(3-4), 170-187.

Mathur, R., Ruiz, J., Titley, S., Liermann, L., Buss, H., & Brantley, S. (2005). Cu isotopic fractionation in the supergene environment with and without bacteria. *Geochimica et Cosmochimica Acta*, *69*(22), 5233-5246.

Mathur, R., Titley, S., Barra, F., Brantley, S., Wilson, M., Phillips, A., Munizaga, F., Maksaev, V., Vervoort, J., & Hart, G. (2009). Exploration potential of Cu isotope fractionation in porphyry copper deposits. *Journal of Geochemical Exploration*, *102*(1), 1-6.

Mathur, R., Brantley, S., Anbar, A., Munizaga, F., Maksaev, V., Newberry, R., Vervoort, J., & Hart, G. (2010a). Variation of Mo isotopes from molybdenite in high-temperature hydrothermal ore deposits. *Mineralium Deposita*, *45*(1), 43-50.

Mathur, R., Dendas, M., Titley, S., & Phillips, A. (2010b). Patterns in the copper isotope composition of minerals in porphyry copper deposits in southwestern United States. *Economic Geology*, *105*(8), 1457-1467.

Mathur, R., Ruiz, J., Casselman, M. J., Megaw, P., & van Egmond, R. (2012). Use of Cu isotopes to distinguish primary and secondary Cu mineralization in the Cañariaco Norte porphyry copper deposit, Northern Peru. *Mineralium Deposita*, *47*(7), 755-762.

Mayer, A. J., & Wieser, M. E. (2014). The absolute isotopic composition and atomic weight of molybdenum in SRM 3134 using an isotopic double-spike. *Journal of Analytical Atomic Spectrometry*, *29*(1), 85-94.

Mikulski, S. Z., & Stein, H. J. (2005). The Re-Os age for molybdenite from the Variscan Strzegom-Sobótka massif, SW Poland. In *Mineral deposit research: meeting the global challenge* (pp. 789-792). Springer, Berlin, Heidelberg.

Miller, C. A., Peucker-Ehrenbrink, B., & Ball, L. (2009). Precise determination of rhenium isotope composition by multi-collector inductively-coupled plasma mass spectrometry. *Journal of Analytical Atomic Spectrometry*, *24*(8), 1069-1078.

Miller, C. A., Peucker-Ehrenbrink, B., Walker, B. D., & Marcantonio, F. (2011). Re-assessing the surface cycling of molybdenum and rhenium. *Geochimica et Cosmochimica Acta*, *75*(22), 7146-7179.

Miller, C. A., Peucker-Ehrenbrink, B., & Schauble, E. A. (2015). Theoretical modeling of rhenium isotope fractionation, natural variations across a black shale weathering profile, and potential as a paleoredox proxy. *Earth and Planetary Science Letters*, *430*, 339-348.

Mirnejad, H., Mathur, R., Einali, M., Dendas, M., & Alirezaei, S. (2010). A comparative copper isotope study of porphyry copper deposits in Iran. *Geochemistry: Exploration, Environment, Analysis*, *10*(4), 413-418.

Morrison, J., Fallick, T., Donelly, T., Leossen, M., St. Jean, G. and Drimmie, R. J. (1996). δ^{34}S Measurements of Standards from Several Laboratories by Continuous Flow isotope Ratio Mass Spectrometry (CF-IRMS). Micromass UK Ltd. Technical Note TN 309, April 1996

Muir, T. L. (2002). The Hemlo gold deposit, Ontario, Canada: principal deposit characteristics and constraints on mineralization. *Ore Geology Reviews*, *21*(1-2), 1-66.

Mulja, T., Williams-Jones, A. E., Wood, S. A., & Boily, M. (1995). The rare-element-enriched monzogranite-pegmatite-quartz vein systems in the Preissac-Lacorne Batholith, Quebec; I, Geology and mineralogy. *The Canadian Mineralogist*, *33*(4),

793-815.
Muntyan, B. L. (2012). Amethyst Scepters from the Santo Nino Mine, Santa Cruz County, Arizona. *Rocks & Minerals*, *87*(2), 126-133.
Murphy, M. J., Stirling, C. H., Kaltenbach, A., Turner, S. P., & Schaefer, B. F. (2014). Fractionation of 238U/235U by reduction during low temperature uranium mineralization processes. *Earth and Planetary Science Letters*, *388*, 306-317.
Nägler, T. F., Anbar, A. D., Archer, C., Goldberg, T., Gordon, G. W., Greber, N. D., Siebert, C., Sohrin, Y., & Vance, D. (2014). Proposal for an international molybdenum isotope measurement standard and data representation. *Geostandards and Geoanalytical Research*, *38*(2), 149-151.
Nielsen, S. G., Wasylenki, L. E., Rehkämper, M., Peacock, C. L., Xue, Z., & Moon, E. M. (2013). Towards an understanding of thallium isotope fractionation during adsorption to manganese oxides. Geochimica et Cosmochimica Acta, 117, 252-265.
Nielsen, S. G., Rehkämper, M., & Prytulak, J. (2017). Investigation and application of thallium isotope fractionation. Reviews in Mineralogy and Geochemistry, 82(1), 759-798.
Palacios, C., Rouxel, O., Reich, M., Cameron, E. M., & Leybourne, M. I. (2011). Pleistocene recycling of copper at a porphyry system, Atacama Desert, Chile: Cu isotope evidence. *Mineralium Deposita*, *46*(1), 1-7.
Panteleyev, A., Lefebure, D. V., & Ray, G. E. (1995). Porphyry Cu+/-Mo+/-Au. *Selected British Columbia mineral deposit profiles*, *1*, 1995-20.
Pašava, J., Tornos, F., & Chrastný, V. (2014). Zinc and sulfur isotope variation in sphalerite from carbonate-hosted zinc deposits, Cantabria, Spain. *Mineralium Deposita*, *49*(7), 797-807.
Phillips, G. N., & Powell, R. (2010). Formation of gold deposits: a metamorphic devolatilization model. *Journal of Metamorphic Geology*, *28*(6), 689-718.
Placzek, C. J., Heikoop, J. M., House, B., Linhoff, B. S., & Pelizza, M. (2016). Uranium isotope composition of waters from South Texas uranium ore deposits. *Chemical Geology*, *437*, 44-55.
Plimer, I. R. (1974). Pipe-like molybdenite-wolframite-bismuth deposits of wolfram camp, North Queensland, Australia. *Mineralium Deposita*, *9*(2), 95-104.
Prytulak, J., Nielsen, S. G., Ionov, D. A., Halliday, A. N., Harvey, J., Kelley, K. A., Niu, Y. L., Peate, D. W., Shimizu, K., & Sims, K. W. W. (2013). The stable vanadium isotope composition of the mantle and mafic lavas. *Earth and Planetary Science Letters*, *365*, 177-189.
Prytulak, J., Brett, A., Webb, M., Plank, T., Rehkämper, M., Savage, P. S., & Woodhead, J. (2017). Thallium elemental behavior and stable isotope fractionation during magmatic processes. Chemical Geology, 448, 71-83.
Pons, M. L., Fujii, T., Rosing, M., Quitté, G., Télouk, P., & Albarède, F. (2013). A Zn isotope perspective on the rise of continents. Geobiology, 11(3), 201-214.Rakovan, J. (2007). Greisen. *Rocks and Minerals*, *82*(2), 157.
Rees, C. E. (1984). The isotopic analysis of sulphur. McMaster University. Isotopic, *Nuclear and Geochemical Studies Group*, Contribution No. 139.
Rehkämper, M., Schönbächler, M. and Stirling, C. H. (2001). Multiple Collector ICP-MS:

Introduction to Instrumentation, Measurement Techniques and Analytical Capabilities. Geostandards Newsletter, 25: 23–40. doi: 10.1111/j.1751-908X.2001.tb00785.x

Rehkämper, M., Wombacher, F., Horner, T. J., & Xue, Z. (2012). Natural and anthropogenic Cd isotope variations. In *Handbook of Environmental Isotope Geochemistry* (pp. 125-154). Springer, Berlin, Heidelberg.

Rempel, K. U., Migdisov, A. A., & Williams-Jones, A. E. (2006). The solubility and speciation of molybdenum in water vapour at elevated temperatures and pressures: Implications for ore genesis. *Geochimica et Cosmochimica Acta*, *70*(3), 687-696.

Rempel, K. U., Williams-Jones, A. E., & Migdisov, A. A. (2009). The partitioning of molybdenum (VI) between aqueous liquid and vapour at temperatures up to 370 C. *Geochimica et Cosmochimica Acta*, *73*(11), 3381-3392.

Ripley, E. M., Dong, S., Li, C., & Wasylenki, L. E. (2015). Cu isotope variations between conduit and sheet-style Ni–Cu–PGE sulfide mineralization in the Midcontinent Rift System, North America. *Chemical Geology*, *414*, 59-68.

Ripperger, S., Rehkämper, M., Porcelli, D., & Halliday, A. N. (2007). Cadmium isotope fractionation in seawater—A signature of biological activity. *Earth and Planetary Science Letters*, *261*(3-4), 670-684.

Romer, R. L., Thomas, R., Stein, H. J., & Rhede, D. (2007). Dating multiply overprinted Sn-mineralized granites—examples from the Erzgebirge, Germany. *Mineralium Deposita*, *42*(4), 337-359.

Rouxel, O., Fouquet, Y., & Ludden, J. N. (2004). Subsurface processes at the lucky strike hydrothermal field, Mid-Atlantic ridge: evidence from sulfur, selenium, and iron isotopes 1. *Geochimica et Cosmochimica Acta*, *68*(10), 2295-2311.

Rouxel, O. J., & Luais, B. (2017). Germanium isotope geochemistry. *Reviews in Mineralogy and Geochemistry*, *82*(1), 601-656.

Rudge, J. F., Reynolds, B. C., & Bourdon, B. (2009). The double spike toolbox. *Chemical Geology*, *265*(3-4), 420-431.

Schauble, E. A. (2007). Role of nuclear volume in driving equilibrium stable isotope fractionation of mercury, thallium, and other very heavy elements. *Geochimica et Cosmochimica Acta*, *71*(9), 2170-2189.

Seo, J. H., Lee, S. K., & Lee, I. (2007). Quantum chemical calculations of equilibrium copper (I) isotope fractionations in ore-forming fluids. *Chemical Geology*, *243*(3-4), 225-237.

Shafiei, B., Shamanian, G., Mathur, R., & Mirnejad, H. (2015). Mo isotope fractionation during hydrothermal evolution of porphyry Cu systems. *Mineralium Deposita*, *50*(3), 281-291.

Sherman, L. S., Blum, J. D., Nordstrom, D. K., McCleskey, R. B., Barkay, T., & Vetriani, C. (2009). Mercury isotopic composition of hydrothermal systems in the Yellowstone Plateau volcanic field and Guaymas Basin sea-floor rift. *Earth and Planetary Science Letters*, *279*(1-2), 86-96.

Siebert, C., Nägler, T. F., & Kramers, J. D. (2001). Determination of molybdenum isotope fractionation by double-spike multicollector inductively coupled plasma mass spectrometry. *Geochemistry, Geophysics, Geosystems*, *2*(7).

Siebert, C., McManus, J., Bice, A., Poulson, R., & Berelson, W. M. (2006). Molybdenum

isotope signatures in continental margin marine sediments. *Earth and Planetary Science Letters*, *241*(3-4), 723-733.

Sinclair, W.D. (2007). Porphyry deposits, in Goodfellow, W.D., ed., Mineral Deposits of Canada: A Synthesis of Major Deposit-Types, District Metallogeny, the Evolution of Geological Provinces, and Exploration Methods: Geological Association of Canada, Mineral Deposits Division, Special Publication No. 5, 223-243

Skulan, J. L., Beard, B. L., & Johnson, C. M. (2002). Kinetic and equilibrium Fe isotope fractionation between aqueous Fe (III) and hematite. *Geochimica et Cosmochimica Acta*, *66*(17), 2995-3015.

Smith, D. K., Johnson, G. G., Scheible, A., Wims, A. M., Johnson, J. L., & Ullmann, G. (1987). Quantitative X-ray powder diffraction method using the full diffraction pattern. *Powder Diffraction*, *2*(2), 73-77.

Smith, D. H. (2000). Thermal ionization mass spectrometry. *PRACTICAL SPECTROSCOPY SERIES*, *23*, 1-30.

Smith, C. N., Kesler, S. E., Klaue, B., & Blum, J. D. (2005). Mercury isotope fractionation in fossil hydrothermal systems. *Geology*, *33*(10), 825-828.

Smith, C. N., Kesler, S. E., Blum, J. D., & Rytuba, J. J. (2008). Isotope geochemistry of mercury in source rocks, mineral deposits and spring deposits of the California Coast Ranges, USA. *Earth and Planetary Science Letters*, *269*(3-4), 399-407.

Song, S., Hu, K., Wen, H., Zhang, Y., Li, K., & Fan, H. (2011). Molybdenum isotopic composition as a tracer for low-medium temperature hydrothermal ore-forming systems: A case study on the Dajiangping pyrite deposit, western Guangdong Province, China. *Chinese science bulletin*, *56*(21), 2221-2228.

Stein, H. J., & Hannah, J. L. (1985). Movement and origin of ore fluids in Climax-type systems. Geology, 13(7), 469-474.

Stein, H. J., Markey, R. J., Morgan, J. W., Hannah, J. L., & Scherstén, A. (2001). The remarkable Re–Os chronometer in molybdenite: how and why it works. *Terra Nova*, *13*(6), 479-486.

Stirling, C. H., Andersen, M. B., Potter, E. K., & Halliday, A. N. (2007). Low-temperature isotopic fractionation of uranium. *Earth and Planetary Science Letters*, *264*(1-2), 208-225.

Taner, H., Williams-Jones, A. E., & Wood, S. A. (1998). The nature, origin and physicochemical controls of hydrothermal Mo-Bi mineralization in the Cadillac deposit, Quebec, Canada. *Mineralium Deposita*, *33*(6), 579-590.

Thode, H. G. (1991). Sulphur Isotopes in Nature and the Environment: An Overview. Stable Isotopes in the Assessment of Natural and Anthropogenic Sulphur in the Environment SCOPE, John Wiley and Sons Ltd., 2-26

Tomkins, A. G., Pattison, D. R., & Zaleski, E. (2004). The Hemlo gold deposit, Ontario: An example of melting and mobilization of a precious metal-sulfosalt assemblage during amphibolite facies metamorphism and deformation. *Economic Geology*, *99*(6), 1063-1084.

Tossell, J. A. (2005). Calculating the partitioning of the isotopes of Mo between oxidic and sulfidic species in aqueous solution. Geochimica et Cosmochimica Acta, 69(12), 2981-2993.

Uvarova, Y. A., Kyser, T. K., Geagea, M. L., & Chipley, D. (2014). Variations in the uranium isotopic compositions of uranium ores from different types of uranium deposits. *Geochimica et Cosmochimica Acta*, *146*, 1-17.

Veeramani, H., Eagling, J., Jamieson-Hanes, J. H., Kong, L., Ptacek, C. J., & Blowes, D. W. (2015). Zinc isotope fractionation as an indicator of geochemical attenuation processes. *Environmental Science & Technology Letters*, *2*(11), 314-319.

Voegelin, A. R., Pettke, T., Greber, N. D., von Niederhäusern, B., & Nägler, T. F. (2014). Magma differentiation fractionates Mo isotope ratios: evidence from the Kos Plateau Tuff (Aegean Arc). *Lithos*, *190*, 440-448.

Wang, Y., Zhu, X. K., Mao, J. W., Li, Z. H., & Cheng, Y. B. (2011). Iron isotope fractionation during skarn-type metallogeny: a case study of Xinqiao Cu–S–Fe–Au deposit in the Middle–Lower Yangtze valley. *Ore Geology Reviews*, *43*(1), 194-202.

Wang, Y., Zhou, L., Gao, S., Li, J. W., Hu, Z. F., Yang, L., & Hu, Z. C. (2016). Variation of molybdenum isotopes in molybdenite from porphyry and vein Mo deposits in the Gangdese metallogenic belt, Tibetan plateau and its implications. *Mineralium Deposita*, *51*(2), 201-210.

Wang, Z., Chen, J., & Zhang, T. (2017). Cu Isotopic Composition in Surface Environments and in Biological Systems: A Critical Review. International journal of environmental research and public health, 14(5), 538.

Weber, C. R., Paterson, I. B. L., & Townsend, D. J. (1978). *Molybdenum in New South Wales* (Vol. 43). Geological Survey of New South Wales.

Welch, S. A., Beard, B. L., Johnson, C. M., & Braterman, P. S. (2003). Kinetic and equilibrium Fe isotope fractionation between aqueous Fe (II) and Fe (III). *Geochimica et Cosmochimica Acta*, *67*(22), 4231-4250.

Wen, H., Carignan, J., Hu, R., Fan, H., Chang, B., & Yang, G. (2007). Large selenium isotopic variations and its implication in the Yutangba Se deposit, Hubei Province, China. *Chinese Science Bulletin*, *52*(17), 2443-2447.

Wen, H., & Carignan, J. (2011). Selenium isotopes trace the source and redox processes in the black shale-hosted Se-rich deposits in China. *Geochimica et Cosmochimica Acta*, *75*(6), 1411-1427.

Wiesli, R. A., Beard, B. L., & Johnson, C. M. (2004). Experimental determination of Fe isotope fractionation between aqueous Fe (II), siderite and “green rust” in abiotic systems. *Chemical Geology*, *211*(3-4), 343-362.

Wieser, M., Schwieters, J. and Douthitt, C. (2012). Multi-Collector Inductively Coupled Plasma Mass Spectrometry, in Isotopic Analysis: Fundamentals and Applications Using ICP-MS (eds F. Vanhaecke and P. Degryse), Wiley-VCH Verlag GmbH & Co. KGaA, Weinheim, Germany. doi: 10.1002/9783527650484.ch3

Wieser, M. E., & de Laeter, J. R. (2003). A preliminary study of isotope fractionation in molybdenites. *International Journal of Mass Spectrometry*, *225*(2), 177-183.

Wieser, M. E., & Schwieters, J. B. (2005). The development of multiple collector mass spectrometry for isotope ratio measurements. *International Journal of Mass Spectrometry*, *242*(2-3), 97-115.

Wilkinson, J. J., Weiss, D. J., Mason, T. F. D., & Coles, B. J. (2005). Zinc isotope variation in hydrothermal systems: preliminary evidence from the Irish Midlands ore field.

Economic Geology, *100*(3), 583-590.
Willbold, M., & Elliott, T. (2017). Molybdenum isotope variations in magmatic rocks. Chemical Geology, 449, 253-268.
Wilt, J. C., & Keith, S. B. (1980). Molybdenum in Arizona. *Fieldnotes from the State of Arizona Bureau of Geology and Mineral Technology*, *10*(3), 1-12.
Wu, F., Qi, Y., Yu, H., Tian, S., Hou, Z., & Huang, F. (2016). Vanadium isotope measurement by MC-ICP-MS. *Chemical Geology*, *421*, 17-25.
Xie, Q., Lu, S., Evans, D., Dillon, P., & Hintelmann, H. (2005). High precision Hg isotope analysis of environmental samples using gold trap-MC-ICP-MS. *Journal of Analytical Atomic Spectrometry*, *20*(6), 515-522.
Yang, L. (2009). Accurate and precise determination of isotopic ratios by MC-ICP-MS: A review. *Mass spectrometry reviews*, *28*(6), 990-1011.
Yang, X. M. (2012). Calculation of Rare Earth Element Patterns in Magmatic Fluids: Evidence for Origin of the Lake George Sb-Au-W-Mo Ore Deposit, New Brunswick, Canada. *Open Geol. J*, *6*, 19-24.
Yao, J., Mathur, R., Sun, W., Song, W., Chen, H., Mutti, L., Xiang, X., & Luo, X. (2016). Fractionation of Cu and Mo isotopes caused by vapor-liquid partitioning, evidence from the Dahutang W-Cu-Mo ore field. *Geochemistry, Geophysics, Geosystems*, *17*(5), 1725-1739.
Zajacz, Z., Candela, P. A., & Piccoli, P. M. (2017). The partitioning of Cu, Au and Mo between liquid and vapor at magmatic temperatures and its implications for the genesis of magmatic-hydrothermal ore deposits. *Geochimica et Cosmochimica Acta*, *207*, 81-101.
Zhang, L., Audétat, A., & Dolejš, D. (2012). Solubility of molybdenite (MoS2) in aqueous fluids at 600–800° C, 200 MPa: A synthetic fluid inclusion study. *Geochimica et Cosmochimica Acta*, *77*, 175-185.
Zhou, J. X., Huang, Z. L., Zhou, M. F., Zhu, X. K., & Muchez, P. (2014). Zinc, sulfur and lead isotopic variations in carbonate-hosted Pb–Zn sulfide deposits, southwest China. *Ore Geology Reviews*, *58*, 41-54.
Zhu, C., Wen, H., Zhang, Y., & Fan, H. (2016). Cadmium and sulfur isotopic compositions of the Tianbaoshan Zn–Pb–Cd deposit, Sichuan Province, China. *Ore Geology Reviews*, *76*, 152-162.
Zhu, X. K., Guo, Y., Williams, R. J. P., O'nions, R. K., Matthews, A., Belshaw, N. S., Canters, G. W., de Waal, E. C., Weser, U., Burgess, B. K., & Salvato, B. (2002). Mass fractionation processes of transition metal isotopes. *Earth and Planetary Science Letters*, *200*(1-2), 47-62.